# Geological Survey of Finland

## Bulletin 381

**Lead isotope characteristics of epigenetic gold mineralization in the Palaeoproterozoic Lapland greenstone belt, northern Finland**

by Irmeli Mänttäri

Geological Survey of Finland
Espoo 1995

Geological Survey of Finland, Bulletin 381

# LEAD ISOTOPE CHARACTERISTICS OF EPIGENETIC GOLD MINERALIZATION IN THE PALAEOPROTEROZOIC LAPLAND GREENSTONE BELT, NORTHERN FINLAND

by
IRMELI MÄNTTÄRI

with 26 figures, 8 tables and 6 appendices

GEOLOGICAL SURVEY OF FINLAND
ESPOO 1995

**Mänttäri, Irmeli 1995.** Lead isotope characteristics of epigenetic gold mineralization in the Palaeoproterozoic Lapland greenstone belt, northern Finland. *Geological Survey of Finland, Bulletin 381.* 70 pages, 26 figures, 8 tables, and 6 appendices.

Epigenetic gold deposits occur in diverse geological settings in the Lapland greenstone belt, which forms part of a NW-SE trending Palaeoproterozoic terrain in the northern Fennoscandian Shield. The Svecokarelian orogeny resulted in compressive deformation and greenschist facies metamorphism throughout the belt at ca. 1.9 Ga.

Sulfide and country rock lead isotope compositions of ten gold deposits have been determined in order to evaluate the lead isotope characteristics and the ages and the sources of gold mineralization. For comparison, sulfides from stratabound base metal deposits and unmineralized volcanics of the Upper Lapponian Group in central Lapland have also been analysed. In addition, several sulfur isotope analyses, suggesting an ultimately magmatic source for the sulfur in the sulfides, were performed.

On the basis of their sulfide lead isotope characteristics the gold occurrences can be divided into relatively nonradiogenic deposits and economically more important, radiogenic deposits. In the nonradiogenic group, the Soretiavuoma, Kiistala, and Kuotko deposits (Soretiavuoma group) show relatively lead rich sulfides with homogeneous lead compositions, resulting from orogenic mixing of mantle and upper crustal material. In the Kuotko area, another gold mineralizing phase involving mantle derived lead is apparent. In the radiogenic group (Saattopora, Hangaslampi, Pahtavaara, Bidjovagge) the sulfide lead isotope compositions form linear trends and exhibit low Th/U and high U/Pb. The similar lead isotope characteristics suggest a common genesis for the gold mineralization in these deposits, and the occurrence of uranium rich inclusions in the sulfides is interpreted as recording crystallization from a relatively oxidized fluid.

Relative timing with respect to intrusive ages of the syn- and postorogenic granites (1900-1880 and 1780 Ma, respectively) permits recognition of the following hydrothermal stages, of which the earliest appear to have been significant for gold mineralization: 1) mineralization of the Soretiavuoma group, associated with the (early- to) synorogenic phase, 2) the Saattopora gold mineralization, which took place during the synorogenic phase, 3) a separate gold mineralizing phase at Kuotko, 4) (syn- to) late orogenic metamorphic resetting of the U-Pb systems in the middle and lower unit volcanics of the Upper Lapponi Group, and a distinct late orogenic regional hydrothermal event apparent at Pahtavaara, Hangaslampi, and Bidjovagge, possibly implying related and roughly contemporaneous processes, 5) thucolite and monazite formation at Saattopora coeval with the postorogenic granites, 6) an anorogenic disturbance (ca. 1700 Ma) of the U-Pb system in the Saattopora wall rocks, and 7) Phanerozoic separation of Svecokarelian lead with the formation of radiogenic sulfides in the Bidjovagge ore and locally in the Kittilä area.

Key words (Georef Thesaurus, AGI): isotope ratios, Pb-206/Pb-204, Pb-207/Pb-204, Pb-208/Pb-204, lead, uranium, thorium, sulfides, gold ores, greenstone belts, metavolcanic rocks, hydrothermal processes, absolute age, Proterozoic, Paleoproterozoic, Kuusamo, Lapland, Finland, Norway

*Irmeli Mänttäri, Geological Survey of Finland, FIN-02150 ESPOO, FINLAND*

ISBN 951-690-593-5
ISSN 0367-522X

Vammalan Kirjapaino Oy, Vammala 1995

## CONTENTS

## INTRODUCTION

In recent years Archaean greenstone belts of the Fennoscandian Shield have shown great potential for gold mineralization (see Nurmi & Sorjonen-Ward, 1993), while at the same time, there has been considerable exploration activity in the Palaeoproterozoic Lapland greenstone belt. As a result of this, the Bidjovagge and Saattopora gold-copper mines were developed, and it is expected that mining operations at the Pahtavaara gold deposit will commence in the near future.

Investigations on and around the gold prospects in Lapland have focussed mainly on host-rock alteration (Korkiakoski et al., 1989; Hulkki, 1990; Nurmi et al., 1991; Pankka et al., 1991; Korkiakoski, 1992; Pankka & Vanhanen, 1992; Eilu, 1994), geological and structural setting (Ward et al., 1989; Gaál & Ward, 1990; Ward et al., 1992), mineralogy (Korkiakoski, 1987; Kojonen & Johanson, 1989), and fluid inclusions (Ettner et al., 1993 and 1994). Carbon and oxygen stable isotope analyses on carbonates have been undertaken for the Saattopora (Korkiakoski, 1992 ref. Tamminen in prep.) and Pahtavaara gold deposits (Korkiakoski, 1992). Moreover, stable isotopes have been analysed from the Bidjovagge mine (Ettner et al., 1994). Radiogenic isotopes have been used to date different lithological units (e.g. Meriläinen, 1976; Hiltunen, 1982; Lehtonen, 1984; Silvennoinen, 1991) and to provide information on the petrogenesis of the rocks (e.g. Patchett et al. 1981; Huhma, 1986). Sulfur isotope data from base metal deposits, such as Saattopora, Pahtavuoma, and Riikonkoski in central Lapland, were published by Mäkelä and Tammenmaa (1978).

This study concentrates on the application of lead isotopes as an exploration method. The fundamentals of lead isotope geology are linked to the formation of the Earth about 4.55 Ga ago. Since then, the primordial lead composition has been changed by the radioactive decay of $^{238}U$, $^{235}U$, and $^{232}Th$ to produce the daughter elements, $^{206}Pb$, $^{207}Pb$, and $^{208}Pb$, respectively. The fourth lead isotope, $^{204}Pb$, is however practically stable. Lead thus has the advantage of providing three isotopes that record information about geological processes. Moreover, lead isotopes do not show significant fractionation by processes that affect the isotopes of lighter elements.

In ore geology, lead isotopes are normally used to estimate metal sources and mineralization ages, but other applications, related to the evaluation of mineral prospects, also exist. Some of the oldest publications concerning lead isotopes in mineral exploration are Cannon et al. (1958 and 1961), Cannon and Pierce (1967 and 1969), Doe & Stacey (1974), and Stacey et al. (1968). More recently, Gulson (1986) collated a wide number of case histories in order to assess the potential of lead isotope analyses as an aid to exploration. However, genetic investigations and applications used in mineral exploration go hand in hand, because neither deposit scale nor regional exploration can be carried out effectively without a thorough understanding of ore forming processes.

Some of the earliest work using lead isotopes in Finland was done by Walter Wahl (1940 and 1941) and traditionally lead isotopes have been used to delineate different geotectonic provinces and to identify the

presence of older crustal components in crust forming processes (e.g. Kouvo, 1958; Vinogradov et al. 1959; Kouvo & Kulp, 1961; Rickard, 1978; Vaasjoki, 1981; Huhma, 1986; Vaasjoki, in press). Studies concerning lead isotope characteristics and evaluation of the mineralization ages and metal sources of mineral deposits in Finland have been published by Vaasjoki (1989), Vaasjoki and Kontoniemi (1991), and Vaasjoki et al. (1993).

The aim of this study was to determine the lead isotope characteristics and systematics of epigenetic gold mineralization within the Palaeoproterozoic Lapland greenstone belt, and to evaluate respective sources of lead and the mineralization ages for each deposit. Emphasis was given to gold occurrences located in the central part of Lapland. As reference material, synvolcanic stratabound base metal deposits (Inkinen, 1979) and unmineralized volcanic rocks of the Upper Lapponi Group in central Lapland (Lehtonen et al., 1992) were also investigated. In addition, samples were included from the Hangaslampi gold deposit of the Kuusamo schist belt in northeastern Finland and from the Bidjovagge ore deposit in Norway, which is located within a northern extension of the Central Lapland greenstone belt.

As gold is the most valuable element in these deposits, genetic aspects of gold mineralization are a matter of general importance. However, gold and lead might have different sources, and therefore the use of lead isotope data from sulfides and gold samples in explaining genetic aspects of gold mineralization could be problematic.

## GEOLOGY OF THE CENTRAL LAPLAND GREENSTONE BELT

### Introduction

The Palaeoproterozoic Central Lapland greenstone belt lies in the northern part of the Fennoscandian Shield (Fig. 1) and forms part of a wide SE to NW trending granitoid-greenstone association extending from Lake Onega in Russia to northern Norway (e.g. Gaál & Gorbatschev, 1987; Lehtonen et al., 1992). This belt comprises volcanic-sedimentary rocks deposited on the Archaean basement ca. 2.5-1.8 Ga ago.

The growth of the greenstone belt was controlled by an intracratonic rift-system (Lehtonen et al., 1985; Gaál & Gorbatschev, 1987; Ward et al., 1989; Gaál, 1990; Gaál & Ward, 1990; Laajoki, 1990; Manninen, 1991). Widespread and locally intense regional albite and carbonate alteration is considered to be synvolcanic (Eilu, 1994), and thus it predates compressive deformation, as does also the mineralization of the synvolcanic base metal deposits, such as Pahtavuoma and Riikonkoski (Inkinen, 1979; Puustinen, 1985) in Finland, and Pahtohavare and Viscaria in Sweden (Carlson et al., 1988; Carlson, 1991). At approximately 1.9 Ga the Svecokarelian orogeny caused compressive deformation and metamorphism under greenschist facies conditions.

Fig. 1. Generalized geological map of northern Finland (upper map), simplified after the Geological Map of the Northern Fennoscandia (1987) and the maps by Kulikov et al. (1980) and Lehtonen et al. (1992). Lithostratigraphic map of the Central Lapland area (lower map), simplified after the map of Lehtonen et al. (1992). Names identify the formations referred to in the text and numbers indicate the locations of mineralizations (★) included in the study. *Stratabound base metal deposits:* Riikonkoski and Hormakumpu (1), Pahtavuoma (2). *Epigenetic gold deposits*: Soretiavuoma (3), Kuotko (4), Suurikuusikko and Kiistala (5), Pahtavaara (6), Lammasvuoma (7), Saattopora (8), Hangaslampi (9), Meurastuksenaho (10), Bidjovagge (11).

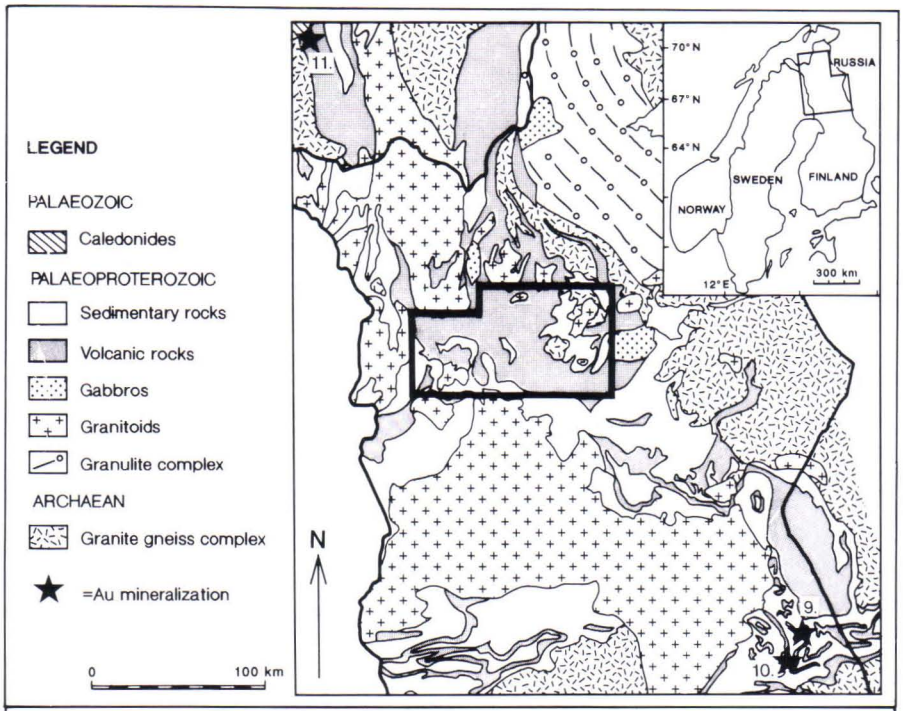
LEGEND
PALAEOZOIC
Caledonides
PALAEOPROTEROZOIC
Sedimentary rocks
Volcanic rocks
Gabbros
Granitoids
Granulite complex
ARCHAEAN
Granite gneiss complex
=Au mineralization
0
100 km
N
11.
9.
10.
70° N
67° N
64° N
12° E
RUSSIA
SWEDEN
FINLAND
NORWAY
300 km

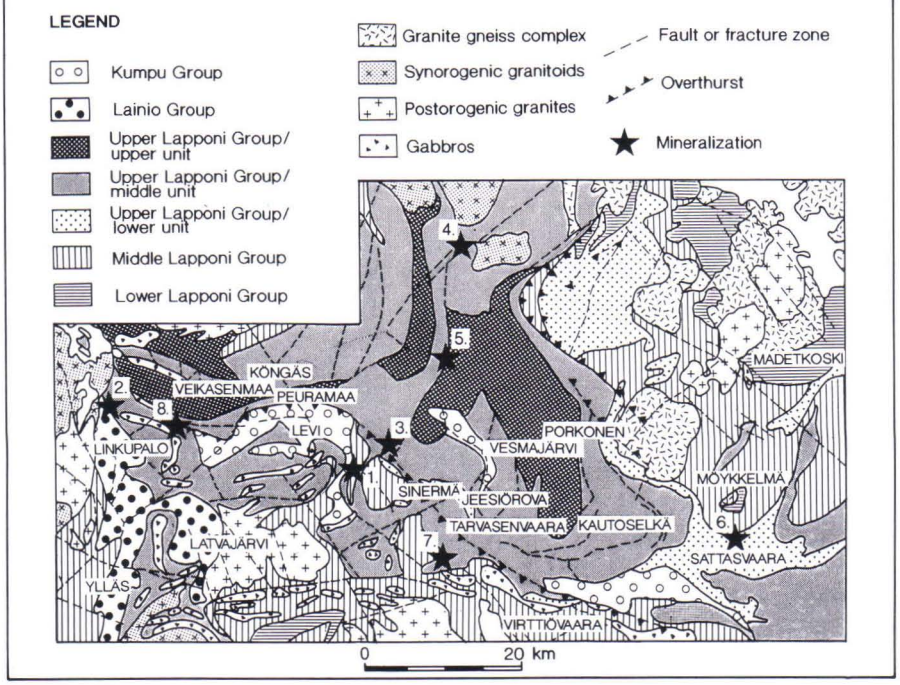
LEGEND
Kumpu Group
Lainio Group
Upper Lapponi Group/ upper unit
Upper Lapponi Group/ middle unit
Upper Lapponi Group/ lower unit
Middle Lapponi Group
Lower Lapponi Group
Granite gneiss complex
Synorogenic granitoids
Postorogenic granites
Gabbros
Fault or fracture zone
Overthurst
Mineralization
KONGAS
VEIKASENMAA
PEURAMAA
LEVI
LINKUPALO
SINERMÄ
JEESIÖROVA
TARVASENVAARA
KAUTOSELKÄ
PORKONEN
VESMAJÄRVI
MADETKOSKI
MOYKKELMÄ
SATTASVAARA
LATVAJÄRVI
YLLÄS
VIRTTIÖVAARA
1.
2.
3.
4.
5.
6.
7.
8.
0
20 km

## Regional geological setting

A geological map (1:400 000) of central Lapland and the accompanying explanatory notes were published by Mikkola (1941). More recently, a geological map at a scale of 1:200 000 and an explanatory report were published by Lehtonen et al. (1984 and 1985). Stratigraphic interpretations have been demonstrated by, amongst others Mäkelä (1968), Paakkola (1971), Rastas (1980), Silvennoinen et al. (1980), Silvennoinen (1985), and Manninen et al. (1987). The stratigraphic classification used in this work is based on the current interpretations and nomenclature of central Lapland lithostratigraphy (Table 1) provided by Lehtonen et al. (1992).

The basement to the greenstone sequence in central Lapland (Fig. 1 and Table 1) comprises 2765-3100 Ma (Kröner et al., 1981; Kröner & Compston, 1990) Archaean gneisses (Lehtonen et al., 1992). The Palaeoproterozoic supracrustal rocks have been subdivided into the Lower, Middle, and Upper Lapponi Groups (Lehtonen et al., 1992). Coarse clastic quartzites and conglomerates of the Lainio and Kumpu Groups rest unconformably on the Lapponi Group supracrustals at the southern edge of the greenstone belt (Lehtonen et al., 1992).

The Lower Lapponian ultramafic to felsic lavas and pyroclastics occur in the eastern parts of the Central Lapland greenstone belt. The 2526±46 Ma (Pihlaja & Manninen, 1988) felsic volcanics of the Madetkoski Formation form the topmost part of the Lower Lapponi Group. The Middle Lapponian sedimentary rocks surround the Upper Lapponian volcanics in the east, south, and south-west. Geochronologically, the Middle Lapponi Group

Table 1. Lithostratigraphy of the Central Lapland greenstone belt according to Lehtonen et al. 1992 (modified after Table 1, p. 2).

| GROUP | | TYPE FORMATION | AGE (approx.) Ma/zircon U-Pb | MAIN LITHOLOGIES |
|---|---|---|---|---|
| KUMPU | | Levi | <1913-2060 | quartzites, conglomerates |
| LAINIO | | Vesikkovaara<br>Latvajärvi<br>Ylläs | ca. 1883 | quartzites, conglomerates<br>intermediate to felsic volcanics<br>quartzites, conglomerates |
| UPPER LAPPONI | *Upper unit* | Vesmajärvi<br>Porkonen | 2012±3;(>1920) | mafic tholeiites<br>BIF |
| | *Middle unit* | Kautoselkä | >2050 | mafic tholeiites |
| | *Lower unit* | Sattasvaara | | picrites, komatiites |
| MIDDLE LAPPONI | | Virttiövaara | >2210 | sedimentary rocks |
| LOWER LAPPONI | | Möykkelmä<br>Madetkoski | ca. 2435<br>ca. 2526 | mafic tholeiites, komatiites<br>mafic to felsic tholeiites |
| ARCHAEAN BASEMENT COMPLEX | | | 2765-3100 | |

lies between 2435 and 2210 Ma, the higher age limit being constrained by the age of the Koitelainen gabbro (Puustinen, 1977; Mutanen, 1989), which seems not to cut the Middle Lapponian rocks. The lower age limit is determined by the age of albite diabases which intrude the Middle Lapponian metasediments (Lehtonen et al., 1992).

The majority of the greenstone belt volcanics erupted between 2.2 and 1.9 Ga. These Upper Lapponian volcanics are divided into three stratigraphical units: the lower, the middle, and the upper unit (Lehtonen et al., 1992) (Table 1). Komatiitic pillow lavas and pyroclastics of the lower unit are mainly found in the eastern part of the Central Lapland greenstone belt. The middle unit consists of a thick tholeiitic sequence interbedded with epiclastic sediments and black schists. Geochemical analyses of the middle unit tholeiites show a sialic crustal component, and thus they may be connected with an early phase of rift formation (Manninen et al., 1987). A minimum age of ca. 2050 Ma for the middle unit volcanism is provided by the zircon U-Pb-ages of the cutting dikes, e.g. the Sätkänävaara albite diabase and Riikonkoski albite gabbro (Lehtonen et al., 1992). The Porkonen-Pahtavaara Iron Formation separates the tholeiitic upper unit from the middle unit. An age range between 2015-1920 Ma for the upper unit is indicated by zircon U-Pb age determinations from the Veikasenmaa felsic porphyry and a quartz porphyry cutting the Nyssäkoski mafic volcanics (Lehtonen et al., 1992).

The rocks of the Lainio Group were deformed by the main phases of the Svecokarelian orogeny, whereas the sediments of the Kumpu Group were deposited during the late stages of deformation. The U-Pb-zircon age of the felsic volcanism in the Latvajärvi Formation, within the Lainio Group, is 1883±5 Ma (Lehtonen et al., 1992). Approximately the same age has been reported for the Kiruna porphyries in northern Sweden (Skiöld, 1986 and 1987).

The volcanic-sedimentary sequence in central Lapland is intruded by postorogenic granites (1760-1790 Ma) and synkinematic quartz-monzonitic to quartz-dioritic granitoids with ages ca. 1880-1899 Ma (Lehtonen et al., 1984 and 1985). In the northern and north-western parts of the belt granodioritic to tonalitic gneisses occur. The U-Pb data from these so-called Hetta granites (Appendix 1) exhibit heterogeneous zircon populations including inherited Archaean zircons, with the smallest zircons being Palaeoproterozoic in age. The negative $\varepsilon_{Nd}$ values obtained for these granites also indicate that they represent reactivation of basement gneisses during the early and synorogenic stages of the Svecokarelian orogeny (Huhma, 1986).

## EPIGENETIC GOLD AND BASE METAL DEPOSITS IN NORTHERN FENNOSCANDIA

### Gold deposits

The gold deposits of the Fennoscandian Shield were classified by Nurmi (1991) into three tectonostratigraphic groups: 1) the Late Archaean (2.9-2.7 Ga) greenstone hosted deposits in eastern Finland, 2) the Palaeoproterozoic (2.5-1.9 Ga) greenstone hosted deposits of Lapland, in the northern part of the shield, 3) the deposits hosted by the Palaeoproterozoic Svecofennian complex (2.0-1.75 Ga) in southern Finland and Central Sweden. All deposits included in this study lie within the Palaeoproterozoic Lapland greenstone belt (Fig. 1).

In Finnish Lapland, the greenstone hosted

gold deposits lie within the Kittilä and Sodankylä rural municipalities in central Lapland and in the Kuusamo area in southeastern Lapland (Fig. 1). The host rocks to the gold deposits were metamorphosed under greenschist facies conditions. Although the deposits are spatially connected with synvolcanic albite-carbonate alteration, they show clear evidence of superimposed epigenetic mineralizing processes. The gold-mineralizing hydrothermal fluids, channeled by shear and fracture zones, are considered to be of metamorphic origin, and the mineralization is supposed to have taken place after the main phase of deformation and the peak of metamorphism (Ward et al., 1989; Nurmi et al., 1991; Ward et al., 1992). It appears that the previously hydrothermally altered lithologies in the area were compositionally and structurally favourable for fluid flow.

The gold deposits occur in and around tectonic shear and fracture zones in a variety of geological environments (Ward et al., 1989) including: 1) altered mafic to ultramafic lithologies (Saattopora, Soretiavuoma, Pahtavaara, Lammasvuoma), 2) the vicinity of granitoids and altered porphyry dikes (Kuotko), and 3) strongly altered metasediments (Kuusamo deposits). Gold mineralization in central Lapland is typically associated with quartz-carbonate veins and breccias, although disseminated types are also present. Dominant sulfides are pyrite, pyrrhotite, chalcopyrite, and arsenopyrite. In the Kuusamo area, disseminated Au-Co-U-deposits occur in intensely altered albite-carbonate-sericite rocks (Pankka et al., 1991).

Following the opinion of many writers (e.g. Kerrich & Fyfe, 1981; Groves & Phillips, 1987; Cameron, 1988; Colvine et al., 1988), Korkiakoski (1992) connected the origin of the Pahtavaara gold deposit with a wider cratonization process, in which both the magmatic processes taking place in the crust and devolatilization caused by metamorphism were important in the concentration of gold. However, an alternative interpretation was given by Hulkki (1990), who proposed that the Pahtavaara gold mineralization was primarily connected with fumarolic activity during rifting, with further remobilization and concentration of gold during subsequent compressional deformation. The mineralization of the Kuusamo gold occurrences is considered to have taken place after the peak of metamorphism of the Svecokarelian orogeny (1.9-1.8 Ga) (Pankka & Vanhanen, 1992) and the associated mineralizing fluids are considered to have been metamorphic and/or magmatic in origin (Pankka et al., 1991).

In northern Norway, the Bidjovagge gold-copper ore in the north-western part of the Palaeoproterozoic Kautokeino greenstone belt (2.0-2.1 Ga: Krill et al., 1985; Olsen & Nilsen, 1985) is shear zone related and occurs within a zone of sodium and carbonate metasomatism (Bjørlykke et al., 1993). An epigenetic origin for the mineralization and a deep crustal or mantle source for the gold has been suggested by Gjelsvik (1958), Padget (1959), Bjørlykke et al. (1987 and 1990), Nilsen and Bjørlykke (1991), and by Bjørlykke et al. (1993).

In northern Sweden, the economically most important part of the Pahtohavare Cu-Au ore is regarded as epigenetic (Söderholm & Nixon, 1988; Martinsson, 1992), but syngenetic mineralizations such as Viscaria are also present. According to Martinsson (1992), the tectonic system controlling the site of the Pahtohavare gold deposit is younger than the folding phase seen in the greenstones. Presumably, the mineralizing hydrothermal fluid is metamorphic in origin, in which the devolatilization of sulfatic evaporite bearing beds might have played an important role (Martinsson, 1992). Nevertheless, the influence of magmatic fluids can not be excluded.

## Base metal deposits

Many of the gold deposits showing epigenetic structural characteristics are spatially associated with base metal concentrations, usually related to albite alteration zones with variable mineralizing styles and metal (Cu, Zn, Fe) contents. These deposits include Pahtavuoma, Riikonkoski, and Sirkka, and the Saattopora copper mineralization (Inkinen, 1979 and 1985; Puustinen, 1985) in central Lapland, and the Viscaria copper ore and a part of the Pahtohavare deposit (Carlson, 1991; Martinsson, 1991 and 1992) in the Kiruna greenstone belt (2200-1930 Ma: Skiöld & Cliff, 1984; Skiöld, 1986), northern Sweden. Genetically these deposits and the regional hydrothermal albite alteration represent syngenetic processes associated with the extensional phase of the greenstone belt formation (Inkinen, 1979 and 1985; Ward et al., 1989; Martinsson, 1992).

## Previous lead isotope results

In northern Sweden and Norway the sulfide lead isotope compositions of both the syngenetic base metal deposits and the epigenetic gold deposits have typically been modified by the Palaeozoic Caledonian orogeny (ca. 420 Ma). Reactivation of the Proterozoic basement during the orogeny caused remobilization of the lead, which is now commonly reflected in the radiogenic lead isotope compositions of the sulfides (e.g. Rickard, 1978; Johansson, 1983; Johansson & Rickard, 1984; Bjørlykke et al., 1987; Romer & Boundy, 1988; Romer, 1989a, 1989b and 1989c; Bjørlykke et al., 1990; Romer 1990, 1991 and 1993; Romer & Wright, 1993). This type of radiogenic sulfide lead has been detected in an area extending nearly 100 km to east of the present boundary of the Caledonian allochthon.

In northern Sweden undisturbed Proterozoic sulfide lead isotope compositions have been obtained for instance from the Huornaisenvuoma skarn iron ore at Lannavaara (Frietsch, 1991), from the Kiuri Rassåive, Pallemvaratji, and Askelluokta syngenetic Cu-Zn-Pb deposits at Tjåmotis (Sundblad & Rostholt, 1986; Sundblad, 1991), from the aplite related Munka Mo-deposit in the Rappen district (Romer, 1993), and from the stratabound Kopparåsen Cu-Zn-U deposit (Romer & Boundy, 1988). The lead isotope composition of the Huornaisenvuoma samples represents the most primitive composition in the area, and is similar to the Outokumpu galena from Finland (Vaasjoki, 1981). The least radiogenic lead isotope compositions of the Tjåmotis and Kopparåsen deposits lie close to the trend of the Svecokarelian orogenic leads as defined by Vaasjoki (1981). This trend illustrates orogenic mixing of upper crustal and mantle material at ca. 1900 Ma.

Lead isotope and U-Pb age results from the Bidjovagge gold-copper ore have been published by Bjørlykke et al. (1987 and 1990) and Cumming et al. (1993), according to which the sulfide leads are radiogenic with $^{206}Pb/^{204}Pb$ ratios between ca. 22 and 158. On the $^{206}Pb/^{204}Pb$ vs. $^{207}Pb/^{204}Pb$ diagram, the data plot on a linear trend from which the least radiogenic samples give a slope of 0.1338. This trend has been interpreted with a two-stage model (Bjørlykke et al., 1990) in which a source age of lead is fixed at ca. 1875 Ma and subsequent lead mobilization and mineralization occurred during peneplain formation at the Cambrian-Precambrian boundary. A U-Pb age of 1837±8 Ma has been obtained from the Bidjovagge uraninite (Cumming et al., 1993), and occurrence of gold as an inclusion in uraninite is considered to be evidence of simultaneous precipitation of gold and uraninite from a common fluid (Cumming et al., 1993).

## DESCRIPTIONS OF THE MINERAL DEPOSITS STUDIED

### Base metal deposits

Several samples from the Pahtavuoma, Riikonkoski, and Hormakumpu base metal deposits in central Lapland were included in the study; locations of these deposits are shown on a lithological map in Figure 1.

In the Pahtavuoma Cu-Zn-U deposit, four separate, mainly phyllite-hosted copper deposits occur near the contact with volcanic rocks. No wall rock alteration has been observed in proximity to the sulfide deposits. The mineralization is typically associated with quartz-carbonate fracture fillings in breccias and with stratiform disseminations. In addition, six zinc and three uranium showings have been found in the Pahtavuoma area (Inkinen, 1979). The zinc showings occur at the margins of the copper deposits, although independent zinc-ore bodies also occur. The U-showings are connected with the copper mineralization, in which carbonate and uranium bearing minerals fill the youngest fractures, which cut across primary sedimentary structures (Inkinen, 1979).

The Riikonkoski and Hormakumpu copper mineralization is associated with albite-quartz-carbonate breccias, and the deposits are mainly hosted by phyllite or sericite schist. The main ore minerals are chalcopyrite and pyrrhotite, with pyrite being rare (Puustinen, 1985).

### Gold deposits

Samples from ten gold deposits and occurrences were included in the study. The Soretiavuoma, Kuotko, Suurikuusikko, Kiistala, Pahtavaara, Lammasvuoma, and Saattopora prospects are located in central Lapland, the Hangaslampi and Meurastuksenaho in the Kuusamo district, and Bidjovagge in northern Norway (Fig. 1). In addition to these there are a large number of gold prospects in the region that will not be considered in this context.

#### Soretiavuoma

The Soretiavuoma gold occurrence is hosted by altered komatiitic volcanics. Gold occurs prefentially in the transitional zones between the intensely carbonated inner section with sulfide rich quartz-carbonate-albite-tourmaline vein networks and the surrounding talc-chlorite alteration zone (Keinänen, 1987; Keinänen et al., 1988). Undeformed, barren quartz veins cut the deformed sulfide rich and gold bearing veins, in which the most common ore minerals are pyrite, chalcopyrite, pyrrhotite, and arsenopyrite (Suoperä, 1988). Gold occurs both as separate grains and inclusions in pyrite and along grain boundaries (Suoperä, 1988).

#### Kuotko

The predominant lithologies in the vicinity of the Kuotko gold deposits are Upper Lapponian mafic pyroclastics and tuffaceous rocks, and synorogenic granitoids (ca. 1.9 Ga) connected with altered porphyritic felsic dykes (Härkönen & Keinänen, 1989). The locations of the Au-deposits are controlled by a wide shear zone between the granitoids. The occurrence of lamprophyres in the area indicates the presence of fracture zones penetrating into the mantle.

Three types of mineralization can be distinguished in the Kuotko area (Härkönen & Keinänen, 1989): 1) pyrite and arsenopyrite containing quartz-carbonate vein networks that

brecciate felsic dykes, 2) narrow quartz-carbonate-sulfide veins around felsic dykes, and 3) separate massive pyrite, pyrrhotite, and arsenopyrite veins containing quartz and carbonate. Native gold is associated with sulfide minerals.

### Suurikuusikko and Kiistala

Suurikuusikko gold occurrence was discovered during follow-up investigations subsequent to the finding of the gold-rich lense at Kiistala (Härkönen, 1992). The mineralization is represented by a shear zone hosted pyrite and arsenopyrite rich breccia, at the contact between mafic volcanics and a graphite-rich schists (Härkönen & Keinänen, 1989). Gold occurs as tiny inclusions in arsenopyrite and pyrite.

In the Kiistala carbonate-arsenopyrite-galena vein, visible gold occurs predominantly in galena and sideritic carbonate (Härkönen & Karvinen, 1987). The vein is hosted by graphite schist and chlorite rich tuffite with interbeds of intermediate lava. Further drillings in the vein surroundings indicated only narrow veins with colourless carbonate occasionally containing arsenopyrite (Härkönen & Karvinen, 1987).

### Pahtavaara

The Pahtavaara gold deposit lies in the most intensely altered eastern part of a long discontinuous hydrothermally altered zone that follows the northern edge of the Sattasvaara komatiite complex (Korkiakoski, 1987; Korkiakoski et al., 1989; Hulkki, 1990; Korkiakoski, 1992).

Elevated gold contents are associated with talc-carbonate-pyrite veins in biotite schists and with quartz-barite lenses or veins in amphibole rocks. Magnetite is abundant, and pyrite is the most common sulfide. Gold occurs with pyrite and at the margins of the quartz-barite lenses (Korkiakoski, 1992).

### Lammasvuoma

At the Lammasvuoma gold prospect, sulfides occur as disseminated, replacement, and breccia types. The mineralization is variably hosted, for example by albite-carbonate rocks, similar to those hosting the Saattopora gold deposit.

### Saattopora

Mining of the Saattopora gold-copper ore by Outokumpu Finnmines Oy commenced at the end of 1988, and the mine currently consists of three open pits, namely the A-, B-, and C-ore.

At the northern edge of the ore belt tuffitic rocks are common, while albitic phyllites and mica schists occur in the south (Anttonen et al., 1989). Ultramafic rocks also occur between the ore zones hosted by albite-carbonate schist (albitic felsite). The highest gold contents have been obtained from quartz-carbonate-sulfide veins that cut the albitic felsite. Anomalous gold contents have also been measured from the host rocks adjacent to these veins. In the A- and B-ores the main sulfides are chalcopyrite and pyrrhotite, while the B-ore also contains minor amounts of pyrite and arsenopyrite. The C-ore, with the lowest Au/Cu ratio, is richest in arsenopyrite (Hugg, oral com., 1991).

The Saattopora copper mineralization is located at the contact zone between sedimentary and volcanic rocks. It is hosted predominantly by phyllite, yet part of the mineralization occurs in albitic felsite. The principal ore minerals, chalcopyrite and pyrrhotite, are either disseminated or associated with breccias and quartz-carbonate veins. Minor amounts of sphalerite occur in the copper mineralization, which contrasts with the gold ore at Saattopora. Elevated gold contents have been analysed from the albitic felsite hosting part of the copper mineralization (Inkinen, oral com., 1991).

### Hangaslampi and Meurastuksenaho

In the Kuusamo area, the Au-Co-U deposits occur mainly in the upper part of the Sericite Quartzite Formation (>2200 Ma; Silvennoinen, 1991) and the lower part of the Siltstone Formation (>2078±8 Ma; Silvennoinen, 1991) (Pankka et al., 1991). These deposits can be subdivided into two end-members according to the type of mineralization (Pankka et al., 1991; Pankka & Vanhanen, 1992): 1) replacement deposits within ductile deformation zones, and 2) breccia-type deposits within brittle deformation zones. The schistose and flattened replacement deposits are associated with zones of sericitization and chloritization and are continuous in the shear zone direction. The breccia-type deposits are related to hydrothermal pipes with brecciating carbonate and quartz. The Hangaslampi deposit represents the first type and Meurastuksenaho is an intermediate type between the two end-members.

The Hangaslampi deposit is hosted principally by hydrothermally altered albite rocks and sericitic schists. Elevated gold contents have been recorded from the quartz-sericite and biotite-sericite rocks with pyrite, pyrrhotite, and minor chalcopyrite. The distributions of gold and uraninite have a strong positive mutual correlation (Pankka, 1989; Pankka et al., 1991).

The mineralization at the Meurastuksenaho Au-Co-U-deposit is associated with albite-quartz-carbonate and chlorite-amphibole rocks of the Sericite Quartzite Formation (Pankka et al., 1991). The principal ore minerals, pyrrhotite and pyrite, together with minor chalcopyrite and cobaltite, exhibit both disseminated and more massive habits. Gold also shows a tendency to correlate positively with Co-rich parts of the deposit.

### Bidjovagge

Copper mining activity at Bidjovagge commenced in the beginning of 1970's but in 1985 Outokumpu Finnmines Oy reopened the mine, producing gold as well as copper.

In the Kautokeino area in northern Norway, Archaean gneisses and amphibolites are separated by three N-S trending Palaeoproterozoic greenstone belts. The Bidjovagge ore lies in the westernmost belt, which consists of shallow marine sediments and mafic to ultramafic volcanics intruded by diabase dykes and granitoids. In the mine area, both sediments and diabases are albitized, this process having taken place before mineralization (Söderholm & Nixon, 1988).

The ore can be divided into copper and gold ore types on the basis of their metal contents (Nilsen & Bjørlykke, 1991; Bjørlykke et al., 1993). A different type of classification was proposed by Lamberg and Toikkanen (1991), who distinguished between Cu-Au, Au-Te, and Au rich ore types. Generally, the ore is shear zone related and hosted by albitic felsite, metadiabase, and black schist. The mineralization is associated with carbonate veins, vein networks, and disseminations in brecciated zones (Bjørlykke et al., 1990). Principal ore minerals are chalcopyrite, pyrite, pyrrhotite, and hematite. A positive correlation exists between the gold content and radioactivity, which is mostly generated by davidite (Bjørlykke et al., 1987).

# SAMPLING AND ANALYTICAL METHODS

## Sample material

The study targets were chosen so as to represent various geological environments. The majority of the sample material was taken from drill cores stored by Outokumpu Finnmines Oy and the Geological Survey of Finland, Rovaniemi, although some samples were obtained from geologists working on the gold prospects and the geology of the greenstone belt in central Lapland. Sulfide samples were selected from drill core sections with elevated gold contents, and adjacent wall rock samples were also collected. The length of drill core sampled was normally about 10 cm. Polished thin sections were prepared from the majority of the mineralized samples and also from a few wall rock samples.

The locations of the studied mineral deposits and occurrences are shown on the lithological map in Figure 1, while explanations to the abbreviations used in the figures are given in Appendix 2. Some background information concerning the sample material and mineral separates is presented in Appendices 3 and 4, and petrographical descriptions of the samples are given in Appendix 5.

## Analytical procedures

### Sample preparation and chemical separation

Milling of the whole rock samples, and crushing and separation of the mineralized samples were done at the Mineralogical Laboratory of the Geological Survey of Finland at Espoo. Heavy liquids and a Frantz isodynamic magnetic separator were used in mineral separation. Finally, the separated mineral concentrates were hand-picked under a binocular microscope. As many sulfide fractions as possible were analysed from each sample and in addition, various size fractions for some minerals were analysed.

In addition to the sulfide samples, several relatively pure carbonate fractions were also obtained. If the carbonates contained sulfide and magnetite inclusions, the trace lead in carbonate was leached using an extremely weak (<0.5 N) hydrochloric acid. In this procedure, the leachable component is mainly $CaCO_3$. Conventional minerals, such as monazite, rutile, and uraninite, used for U-Pb age determination, were found only from the Saattopora and Bidjovagge samples. Total dissolutions (WR) and acid leaches (LE) of the whole-rock powders were analysed from the wall rock samples taken from the vicinity of the mineralized sections. The acid leaches were intended to represent the lead isotope composition of the readily soluble phases, such as sulfides and carbonates.

Apart from some extremely lead rich minerals such as galena, and the lead poor Pahtavaara sulfides, the weight of the analysed sulfide fraction was normally ca. 200 mg. The sulfides were washed with ca. 1.2 N HCl in an ultrasonic bath to remove surface contamination. The weight of the whole-rock samples was usually about 200 mg. However, the wall rocks immediately adjacent to the mineralizations were occasionally so poor in lead that sample weights of up to ca. 400 mg were required.

The washed sulfide fractions and whole-rock leaches were first dissolved in an 1:1 $HCl-HNO_3$ acid mixture. The total dissolutions of the whole-rock powders were carried out in Savillex® teflon beakers in a $HF-HNO_3$

acid mixture. After evaporation, the samples were redissolved into 1N HBr. Lead was extracted from other elements using anion-exchange chromatography, and lead purification was completed with anodic electrodeposition (Gulson & Mizon, 1979). Since only a few measurements of lead concentrations were done, the colour of the anode deposit was used to estimate the relative lead contents of the sulfides (Appendix 4).

Native gold was washed with an HF-$HNO_3$-acid mixture and dissolved in aqua regia. The lead was extracted with anion-exchange chromatography following the procedure described in Saarnisto et al. (1991, p. 312-313).

For U-Pb-dating, depending on the mineral involved, a 2-30 mg sample was dissolved in a steel-jacketed teflon crucible with an HF-$HNO_3$ acid mixture, following the conventional procedure described by Krogh (1973). The sample was spiked with $^{235}U$ and $^{206}Pb$ or mixed $^{235}U+^{208}Pb$ tracers. Uranium and lead were extracted using anion-exchange chromatography. If required, uranium was further purified by extraction with ammonium nitrate and methylisobuthylketone.

## Mass spectrometry and data processing

Lead was loaded on a Re-filament with a phosphoric acid-silica gel mixture and uranium with phosphoric acid on a Ta-side filament in a triple filament system. The analyses were performed with a VG Sector 54 thermal ionization multicollector mass spectrometer, with a filament temperature of ca. 1200 °C for lead. The 2σ-error estimates based on multiple analyses on standard are less than 0.20%, 0.20%, and 0.25% for the $^{206}Pb/^{204}Pb$, $^{207}Pb/^{204}Pb$, and $^{208}Pb/^{204}Pb$ ratios, respectively. The measured lead isotope ratios were normalized according to the analysed ratios of SRM 981-standard (Gulson et al., 1984), with correction coefficients of +0.09 to +0.13% per a.m.u. or with specific correction factors for the $^{206}Pb/^{204}Pb$, $^{207}Pb/^{204}Pb$, and $^{208}Pb/^{204}Pb$ ratios. The blank for the sulfide lead process was less than 2 ng, which is considered to be insignificant. The Pb-blank of the U-Pb-procedure was 0.5 ng. In addition, a very high measured $^{206}Pb/^{204}Pb$ ratio of about 40000, with a total $^{204}Pb$ content lower than that expected for the blank, indicates an even lower blank level for at least that sample preparation. The corrected lead isotope data are listed in Appendices 3 and 4.

The linear regressions used for the lead isotope data presentations have been fitted using two methods (Ludwig 1990, pp. 11-12). York's original algorithm (1969) is used when the only causes of scatter are the assigned errors. However, high MSWD (mean square of weighted deviates) values indicate that the scatter frequently exceeds analytical errors. In these cases the regression fittings assign equal weights to the data points and zero error-correlations for the X,Y pairs.

The calculated Pb-Pb-model ages of the least radiogenic samples are based on the two-stage evolution model of Stacey and Kramers (1975). The concordia intercepts and associated uncertainties of the linear regressions are calculated according to the model of Ludwig (1980). All ages have been calculated using the decay constants recommended by the I.U.G.S. Subcommission on Geochronology (Steiger & Jäger, 1977 ref. Jaffey et al., 1971).

## Other analyses

U, Th, and Pb concentrations of selected sulfides were measured at the Geological Survey of Finland, Espoo. Th and U were analysed with an inductively coupled plasma (ICP) mass spectrometer and Pb with an atomic absorption spectrophotometer (AAS).

Sulfur isotopes were analysed at the Department of Isotope Geology of the Dionýz Štúr

Institute of Geology, Bratislava, Slovakia, according to the method of Ustinov and Grinenko (1965). In summary, the powdered sulfide sample was purified by heating it for 30 minutes at a maximum temperature of 320°C. The oxidation of sulfide to $SO_2$ was performed using CuO at a temperature of 770°C (30 minutes). The released $SO_2$ was collected into glass ampoules and analysed with a Finnigan MAT 250 mass spectrometer. Although recent measurements of international standards have not been done, the results are considered to be representative enough for this study, as previous analyses on standards have given reliable results.

## Lead evolution reference models

When low radiogenic data are presented on a $^{206}Pb/^{204}Pb$ vs. $^{207}Pb/^{204}Pb$ or $^{206}Pb/^{204}Pb$ vs. $^{208}Pb/^{204}Pb$ diagram, it is customary to include a reference lead evolution curve. These should be considered as model trajectories, which may approximate but do not necessarily represent the true course of lead evolution in the area concerned.

The Stacey and Kramers (1975) two-stage model for average crustal lead growth is the most commonly used. This assumes that terrestial lead evolved initially from a primordial composition, which is considered to be the same as that of the Canyon Diablo troilite at 4.57 Ga. At ca. 3.7 Ga, U-Th-Pb differentiation processes led to a change in conditions, described by the second-stage of lead evolution. The average $^{238}U/^{204}Pb$, $^{232}Th/^{204}Pb$, and $^{232}Th/^{238}U$ values at the end of this second stage are assumed to be 9.74, 36.84, and 3.78, respectively.

If the data points fall significantly below the Stacey and Kramers (1975) curve on a $^{206}Pb/^{204}Pb$ vs. $^{207}Pb/^{204}Pb$ diagram, the mantle growth curve of Zartman and Doe (1981) is considered. This model is based on the geochemical behaviour of Th, U, and Pb within varying terrestrial reservoirs, i.e. upper crust, lower crust, and mantle, which by repeated recycling (orogeny) produce different lead evolutions for each reservoir. The evolution of mantle lead commenced at 4.0 Ga, and the $^{238}U/^{204}Pb$, $^{232}Th/^{204}Pb$, and $^{232}Th/^{238}U$ values have been changing as a result of each subsequent orogenic event. The present day values are 8.35, 29.39, and 3.52 respectively.

## SULFUR ISOTOPE RESULTS AND DISCUSSION

Sulfur isotopes were analysed from several sulfide samples occurring in association with gold mineralization and results are presented in Table 2. Based on the equilibrium fractionation geothermometry of cogenetic sulfur-bearing compounds (Sakai, 1957 and 1968; Tatsumi, 1965; Bachinski, 1969) the sulfur isotope data can be used to estimate the formation temperatures of the sulfides. However, in most of the present cases the $\delta^{34}S$ values of the analysed sulfide pairs failed to follow the predicted course of the equilibrium fractionation. This may be attributed to fluctuating sulfide crystallization conditions, such as changes in T, pH, and $f_{O_2}$. Nonetheless, a pyrite-pyrrhotite pair from the Saattopora B-ore gave a temperature estimate of 382°C and that for the pyrite-chalcopyrite pair from Bidjovagge is 269°C ($\Delta^{34}S=A \times 10^6/T^2$; A=0.30/pyrite-pyrrhotite pair, A=0.45/pyrite-chalcopyrite pair; Kajiwara & Krouse, 1971).

The $\delta^{34}S$ range for sulfides from gold deposits in central Lapland is 3.5‰, with a mean of +3.79‰. This narrow range may indicate regionally similar sulfur sources and depositional conditions. Ohmoto and Rye (1979) suggest that $\delta^{34}S$ values centered around 0‰ (-4 - +4‰) indicate a magmatic source for the

sulfur, although primary magmatic and sulfur extracted from magmatic minerals can not be distinguished. At Bidjovagge, the negative sulfur isotope values for sulfides occurring in black schist might indicate the existence of two separate sulfur sources, or the fractionation of sulfur isotopes during sulfide crystallization.

In general, $\delta^{34}S$ values similar to those of the central Lapland deposits have been reported from shear zone related gold-quartz vein sulfides in the Barberton greenstone belt, South-Africa (+1 - +4‰; deRonde et al., 1992) and the Proterozoic greenstone-hosted Flin Flon gold occurrences at Saskatchewan, Canada (+2.8 - +5.5‰; Ansdell & Kyser, 1992). Moreover, the results for central Lapland agree with the $\delta^{34}S$ values of +1 to +4‰ (Lambert et al., 1984) obtained from many Australian Archaean discordant gold deposit hosted pyrites. These values have been explained as representing sulfur derived from fluid-induced metamorphic remobilization of the greenstone sulfides.

Table 2. Sulfur isotope results for some sulfides from gold deposit in Lapland.

| DEPOSIT | SAMPLE | MINERAL | $\delta^{34}S$(‰) |
|---|---|---|---|
| Kuotko | R436/76.40 | PY | +3.32 |
| Kuotko | R305/7.95 | ASPY | +3.62 |
| Soretiavuoma | R307/48.70 | PY | +4.46 |
| Soretiavuoma | R307/48.45 | CP | +5.73 |
| Saattopora/A | A1205 | PO | +3.93 |
| Saattopora/A | A1205 | CP | +4.08 |
| Saattopora/B | R208/124.45 | PY | +2.93 |
| Saattopora/B | R208/124.45 | PO | +2.23 |
| Bidjovagge | S154B/124.65 | PY | −2.07 |
| Bidjoavgge | S154B/124.65 | CP | −1.90 |
| Bidjovagge | N20E/203.55 | PY | +6.12 |
| Bidjovagge | N20E/203.55 | CP | +6.14 |
| Bidjovagge | N95F/46.70 | PY | +1.26 |
| Bidjovagge | N95F/46.70 | CP | +1.23 |
| Bidjovagge | N95F/59.45 | PY | +2.76 |

ASPY = arsenopyrite; CP = chalcopyrite; PO = pyrrhotite; PY = pyrite.

$$\delta^{34}S_i(‰) = \frac{(^{34}S/^{32}S)_i - (^{34}S/^{32}S)_{std}}{(^{34}S/^{32}S)_{std}} \times 1000;$$

i = mineral; std = standard

## U-Pb AGE DETERMINATIONS AND RADIOGENIC $^{207}Pb/^{206}Pb$ AGES

The U-Pb analytical results from the Lapland greenstone hosted gold mineralizations are presented in Table 3. Because the number of conventional minerals used in U-Pb dating is low in the sample material, the common lead corrected radiogenic $^{207}Pb/^{206}Pb$ ages of the highly radiogenic sulfides and wall rocks were used as minimum estimates (Table 4) for the closure ages of the U-Pb systems.

### Saattopora area

A thucolite (Fig. 2) from a carbonate-sulfide vein at Saattopora (SP(A)-R257/61.40) shows a discordant age, the $^{207}Pb/^{206}Pb$ age being around 1765 Ma (Table 3). Idiomorphic coarse grained monazite from the Saattopora ore concentrate shows an almost concordant U-Pb age of ca. 1780 Ma (Table 3) and is, within error limits, almost the same as the $^{207}Pb/^{206}Pb$ age of the thucolite. Thin section examination of the vein sample suggests that monazite belongs to the wall rock paragenesis.

On the concordia diagram (Fig. 3), the analytical data for thucolite and monazite plot on a linear trend with an upper intersection at 1781±18 Ma (Fig. 3). A previously analysed

Table 3. U-Pb analytical data from the Saattopora, Hangaslampi, and Bidjovagge gold deposits. Selected analyses of uranium rich minerals from Lapland, are also included.

| DEPOSIT | Concentrations | | Atomic abundances* | | | | Atomic ratios** | | | | Age(Ma) | |
|---|---|---|---|---|---|---|---|---|---|---|---|---|
| Analysed | (ppm) | | Measured | $^{206}Pb = 100$ | | | $\frac{^{206}Pb}{^{238}U}$ | $\frac{^{207}Pb}{^{235}U}$ | $\frac{^{207}Pb}{^{206}Pb}$ | $\frac{^{206}Pb}{^{238}U}$ | $\frac{^{207}Pb}{^{235}U}$ | $\frac{^{207}Pb}{^{206}Pb}$ |
| mineral | $^{238}U$ | $^{206}Pb$ | $^{206}Pb/^{204}Pb$ | $^{204}Pb$ | $^{207}Pb$ | $^{208}Pb$ | | | | | | |
| SAATTOPORA | | | | | | | | | | | | |
| G443/concentrate | | | | | | | | | | | | |
| MONAZITE | 571.4 | 156.0 | 1869 | 0.0359 | 11.39 | 24.77 | 0.3155 | 4.744 | 0.1091 | 1767±16 | 1775±9 | 1784±11 |
| A-R257/74.60 | | | | | | | | | | | | |
| RUTILE | 4.115 | 1.065 | 155.7 | 0.6165 | 18.77 | 24.56 | 0.2992 | 4.254 | 0.1031 | 1687±9 | 1684±5 | 1681±20 |
| A-R257/61.40/THUCOLITE | | | | | | | | | | | | |
| A/aliquot 1 | 23840 | 5731 | 33560 | 0.0001 | 10.81 | 0.0314 | 0.2778 | 4.141 | 0.1081 | 1580±8 | 1662±5 | 1767±1 |
| A/aliquot 2 | 25904 | 6562 | 36013 | 0.0010 | 10.80 | 0.0231 | 0.2928 | 4.360 | 0.1080 | 1655±8 | 1704±4 | 1766±2 |
| B/aliquot 1 | 24027 | 5939 | 41110 | 0.0005 | 10.77 | 0.0459 | 0.2857 | 4.237 | 0.1076 | 1619±7 | 1681±5 | 1759±2 |
| B/aliquot 2 | 24015 | 5930 | 44427 | 0.0005 | 10.79 | 0.0419 | 0.2854 | 4.243 | 0.1078 | 1618±8 | 1682±5 | 1763±1 |
| HANGASLAMPI | | | | | | | | | | | | |
| R388/41.20 | | | | | | | | | | | | |
| PYRITE (brannerite inclusions) | 8.364 | 2.537 | 1044 | 0.0941 | 12.56 | 4.248 | 0.3505 | 5.459 | 0.1130 | 1936±9 | 1894±5 | 1847±1 |
| R388/66.85 | | | | | | | | | | | | |
| PYRRHOTITE (brannerite inclusions) | 488.8 | 139.3 | 15551 | 0.0064 | 11.23 | 0.8881 | 0.3294 | 5.059 | 0.1114 | 1835±9 | 1829±5 | 1822±0 |
| BIDJOVAGGE | | | | | | | | | | | | |
| R154B/102.45 | | | | | | | | | | | | |
| RUTILE | 9.863 | 2.254 | 143.7 | 0.6828 | 19.36 | 46.31 | 0.2642 | 3.615 | 0.0993 | 1511±8 | 1552±4 | 1610±12 |
| N95F/59.45 | | | | | | | | | | | | |
| TITANITE | 162.1 | 31.70 | 1312 | 0.0695 | 10.78 | 27.02 | 0.2259 | 3.058 | 0.0982 | 1313±8 | 1422±5 | 1589±4 |
| PALKISKURU, Enontekiö***1) | | | | | | | | | | | | |
| DAVIDITE A61 | | | | | | | | | | | | |
| A | 57699 | 14479 | 3050 | 0.0327 | 11.18 | 1.498 | 0.2900 | 4.291 | 0.1073 | 1641±7 | 1691±4 | 1754±2 |
| B | 51084 | 12528 | 2898 | 0.0343 | 11.19 | 1.668 | 0.2834 | 4.189 | 0.1072 | 1608±7 | 1671±9 | 1752±19 |
| LAAVIVUOMA, Kittilä***2) | | | | | | | | | | | | |
| URANINITE | 56.5% | 14.6% | 185505 | 0.0005 | 10.92 | 0.0149 | 0.3038 | 4.572 | 0.1091 | 1710±10 | 1744±6 | 1785±2 |
| KESÄNKI, Kolari***3) | | | | | | | | | | | | |
| V-Fe-OXIDE 9249 | | | | | | | | | | | | |
| aliquot 1 | 27902 | 7091 | 80882 | 0.0000 | 10.69 | 0.0665 | 0.2937 | 4.328 | 0.1069 | 1660±4 | 1698±2 | 1747±5 |
| aliquot 2 | 27988 | 7095 | 80882 | 0.0000 | 10.69 | 0.0647 | 0.2930 | 4.318 | 0.1069 | 1656±3 | 1696±2 | 1747±4 |

* = Blank corrected values; ** = Corrected for blank and age related common lead (Stacey and Kramers 1975);
*** = Analyses by Olavi Kouvo.

1): Davidite from shear zone in granodiorite. Source of sample: Kari Pääkkönen, GSF.

2): Uraninite from amphibole-sulfide vein cutting a mica schist. GSF, M52.5/2741/84/R307/76.20-76.40, Laavivuoma (Pääkkönen, 1988); Source of sample: Kari Pääkkönen, GSF.

3): Uranium bearing V-Fe-oxide from sericite quartzite. Outokumpu Oy, 2732 05, Kol/Kes-22, Kesänki, Kolari; Source of sample: Risto Sarikkola, Outokumpu Oy.

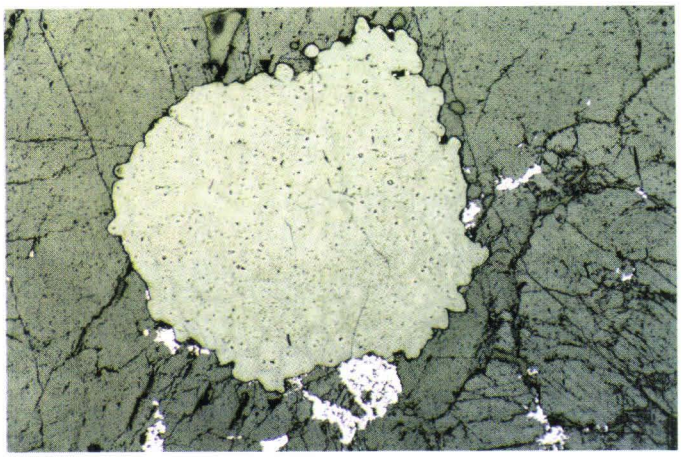

Fig. 2. Thucolite grain from a carbonate-sulfide vein, Saattopora A-ore (SP(A)-R257/61.40). Width of view is 3.70 mm, reflected and plane polarized light.

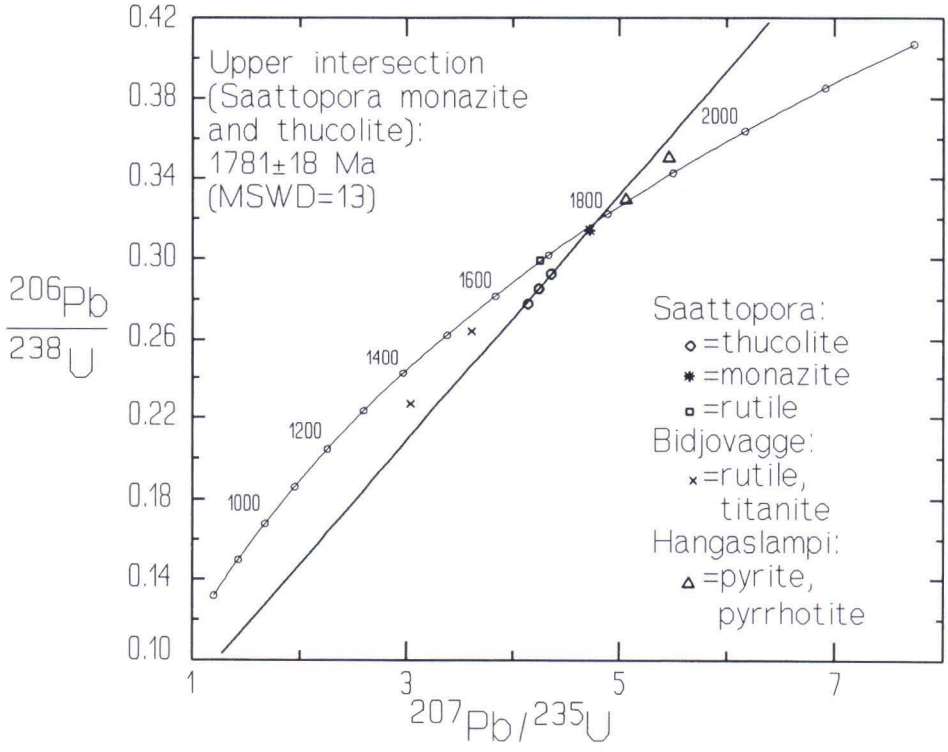


Fig. 3. Concordia plot of U-Pb data.

uraninite (A766) from a granitic vein cutting the Pahtavuoma copper mineralization has a similar Pb-Pb age of ca. 1780 Ma (Vaasjoki, oral com., 1993). In addition, Olavi Kouvo has analysed a uranium-bearing V-Fe-oxide (Kesänki), a uraninite (Laavivuoma), and a davidite (Palkiskuru) from Lapland, all of which yielded approximately the same age as the Saattopora thucolite (see Table 3 for further information concerning these samples).

An almost concordant U-Pb age of ca. 1685 Ma (Table 3 and Fig. 3) was obtained for rutile (Fig. 4) from a fine grained albite-carbonate rock brecciated by sulfide-tourmaline veins (SP(A)-R257/74.60). In thin section narrow sulfide-filled fractures were sometimes observed to be overgrown by rutile, although the reverse relationship was also recorded. Thus, rutile formation both postdates and predates minor sulfide mobilization. This exceptionally young age cannot be attributed to a low closure temperature for rutile, which according to Mezger et al. (1989) varies between 350-450°C, depending on the grain size. However, if the cooling rate is slow enough, the diffusion of the radiogenic lead may continue long after the estimated closure temperature is attained (Dodson, 1973, 1976 and 1981). On the other hand, the formation of hydrothermal rutile could be connected with the breakdown reactions of previously formed Ti-rich minerals, which can take place readily even at low temperatures (Van Baalen 1993).

Analyses of monazite and rutile from the albite-carbonate rock hosting the Saattopora copper mineralization gave common lead corrected $^{207}Pb/^{206}Pb$ ages of 1773 and 1672 Ma (Table 4), respectively. These are approximately the same as those obtained for the Saattopora gold ore (Tables 3 and 4). Sulfides associated with the copper mineralization show homogeneous $^{207}Pb/^{206}Pb$ ages around 2.0 Ga (Table 4), which contrast with the widely scattered results from sulfides within the Saattopora gold ore (Table 4).

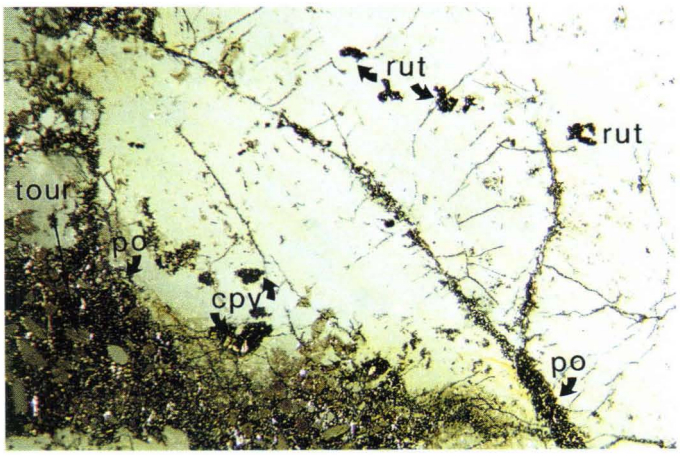


Fig. 4. Rutile (rut) from an albite-carbonate rock, which is brecciated by pyrrhotite (po) and tourmaline (tour), with minor chalcopyrite (cpy), Saattopora A-ore (SP(A)-R257/74.60). Width of view is 11.0 mm, reflected light.

Table 4. $^{207}Pb/^{206}Pb$ ages for the highly radiogenic samples.

| DEPOSIT/SAMPLE | $^{206}Pb/^{204}Pb$ | $^{207}Pb/^{204}Pb$ | $(^{207}Pb/^{206}Pb)$* | AGE(Ma) |
|---|---|---|---|---|
| SAATTOPORA GOLD ORE | | | | |
| A1205-PYRRHOTITE | 1149 | 147 | 0.1162 | 1899 |
| A1205-PYRRHOTITE | 1490 | 172 | 0.1063 | 1737 |
| A1205-RUTILE/abraded | 386 | 51.3 | 0.0972 | 1572 |
| A-R257/74.60-RUTILE^ | 156 | 29.9 | 0.1041 | 1698 |
| A-R257/82.20-PYRRHOTITE | 308 | 51.3 | 0.1237 | 2010 |
| A-R257/82.20-CHALCOPYRITE | 234 | 43.4 | 0.1288 | 2081 |
| A-R257/61.40-THUCOLITE^ | ca.40000 | ca.4000 | ca.0.108 | 1765 |
| G443-MONAZITE#1^ | 1869 | 218 | 0.1092 | 1785 |
| G443-MONAZITE#2 | 7122 | 789 | 0.1089 | 1781 |
| concentrate-GOLD/fine | 550 | 79.3 | 0.1198 | 1953 |
| concentrate-GOLD/coarse | 492 | 73.4 | 0.1220 | 1985 |
| concentrate-GOLD/magnetic | 435 | 64.3 | 0.1169 | 1907 |
| A-R257/70.60-LE | 2102 | 238 | 0.1066 | 1743 |
| A-R257/70.60-WR | 1668 | 188 | 0.1043 | 1703 |
| B-R208/120.80-LE | 260 | 42.3 | 0.1104 | 1806 |
| B-R208/120.80-WR | 213 | 35.5 | 0.1022 | 1664 |
| SAATTOPORA Cu-MINERALIZATION | | | | |
| ab-crb rock-CHALCOPYRITE | 473 | 72.7 | 0.1256 | 2038 |
| ab-crb rock-PYRITE | 498 | 74.6 | 0.1230 | 2001 |
| ab-crb rock-PYRRHOTITE#1 | 765 | 107 | 0.1226 | 1995 |
| ab-crb rock-PYRRHOTITE#2 | 894 | 123 | 0.1227 | 1996 |
| ab-crb rock-PYRITE | 559 | 81.9 | 0.1227 | 1996 |
| ab-crb rock-RUTILE | 1093 | 126 | 0.1026 | 1672 |
| ab-crb rock-MONAZITE | 13685 | 1497 | 0.1084 | 1773 |
| phyllite-LE | 276 | 40.6 | 0.0969 | 1566 |
| phyllite-WR | 286 | 40.3 | 0.0922 | 1471 |
| HANGASLAMPI | | | | |
| R388/41.20-PYRITE#1 | 1208 | 148 | 0.1114 | 1822 |
| R388/41.20-PYRITE#2^ | 1044 | 131 | 0.1129 | 1847 |
| R388/41.20-PYRITE#3 | 808 | 104 | 0.1125 | 1840 |
| R388/66.85-PYRRHOTITE#1 | 2893 | 344 | 0.1142 | 1867 |
| R388/66.85-PYRRHOTITE#2^ | 15551 | 1746 | 0.1114 | 1822 |
| R388/57.90-LE | 452 | 65.3 | 0.1147 | 1875 |
| R388/57.90-WR | 541 | 72.1 | 0.1083 | 1770 |
| MEURASTUKSENAHO | | | | |
| R332/179.60-PYRRHOTITE | 166 | 32.1 | 0.1112 | 1819 |
| BIDJOVAGGE | | | | |
| N95F/21.80-LE | 341 | 39.7 | 0.0746 | 1059 |
| N95F/21.80-WR | 254 | 33.2 | 0.0746 | 1056 |
| N95F/45.30-CHALCOPYRITE | 189 | 34.7 | 0.1122 | 1835 |
| N95F/59.45-PYRITE | 781 | 112 | 0.1264 | 2049 |
| S154B/102.40-RUTILE | 144 | 28.2 | 0.1003 | 1630 |

* = Corrected for age related common lead (Stacey and Kramers 1975).
^ = including the U-Pb-analysis.
LE = acid leach of whole rock powder, WR = total dissolution of whole rock powder.

## Hangaslampi

Two highly radiogenic sulfides from the Hangaslampi deposit, namely pyrite (HL-R388/41.20) and pyrrhotite (HL-R388/66.85) (Figs. 5 and 6), were analysed for their U contents and Pb isotope ratios (Table 3). The pyrite analysis plots on the upper side of the concordia curve (Fig. 3), most probably indicating some episodic uranium loss. The pyrrhotite is extremely rich in uranium and shows good concordancy with a U-Pb age of ca. 1830 Ma. The $^{207}Pb/^{206}Pb$ age estimates (Table 4) for the Hangaslampi and Meurastuksenaho sulfides have ages similar to that of the concordant pyrrhotite, and the mean age of the six samples is ca. 1836 Ma.

High uranium contents and $^{206}Pb/^{204}Pb$ ratios in sulfides are unusual, and must have originated from some uranium rich mineral. Accordingly, two grains of a mineral resembling uraninite in appearance (Figs. 7a and 7b) were identified from the Hangaslampi sample (HL-R388/66.85) using the Cameca SX 50 microprobe at the Geological Survey of Finland, Espoo. One grain (Fig. 7a) is clearly

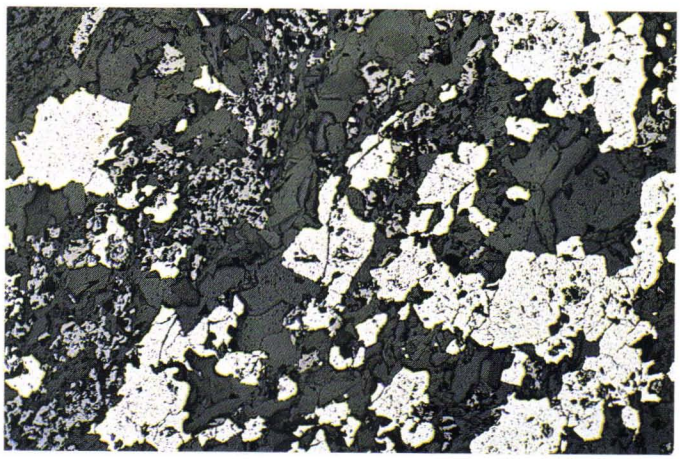

Fig. 5. Pyrite from a sericite-quartz schist, Hangaslampi (HL-R388/41.20). Width of view is 1.50 mm, reflected and plane-polarized light.

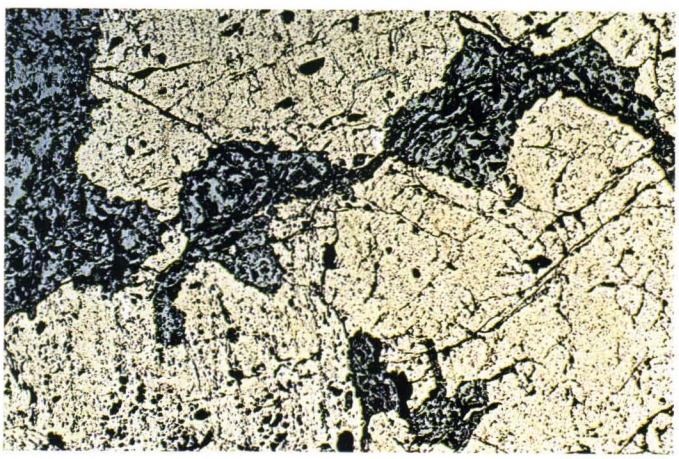

Fig. 6. Pyrrhotite grains poikilitically in magnetite, Hangaslampi (HL-R388/66.85). Width of view is 3.70 mm, reflected and plane polarized light.

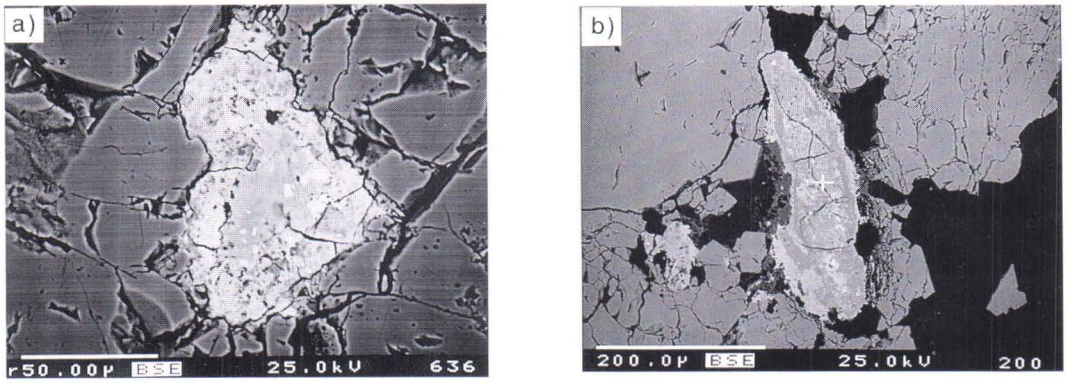


Fig. 7. Back scattered electron images (a and b) of the U-Ti mineral (brannerite) in pyrrhotite, Hangaslampi (HL-R388/66.85). In these images, the small bright white spots are galena and the portions of the U-Ti-mineral richest in uranium appear as white areas. Width of view is a) 0.18 mm and b) 0.57 mm.

an inclusion in pyrrhotite, and possesses high $U_2O_3$ and $TiO_2$ contents, varying from ca. 20 to 70 % and 20 to 52 %, respectively. The other grain (Fig. 7b), occupying the fractured contact zone of carbonate against pyrrhotite and magnetite, was more heterogeneous, with distinct uranium and titanium rich domains and some cerium rich parts containing no uranium. The composition of this U-Ti mineral could correspond to that of brannerite ($UTi_2O_6$). Although the sulfides from the Saattopora ore also have radiogenic characteristics, with high uranium contents, no uranium rich inclusions were found during probing of the Saattopora sample SP(A)-R257/61.40.

Small grains of galena were found in brannerite (Figs. 7a and 7b); these represent mobilized and concentrated radiogenic lead, formed as a result of radioactive decay of uranium.

## Bidjovagge

Black to brown roundish rutile from a metadiabase hosting the Bidjovagge ore (BV-S154B/102.45) (Fig. 8) shows discordancy with a $^{207}Pb/^{206}Pb$ age of ca. 1610 Ma (Table 3 and Fig. 3). Microscopically, the rutile seems to be younger than chalcopyrite (Fig. 8), and therefore the rutile formation is attributed to a hydrothermal phase postdating the major sulfide crystallization.

Titanite having a brown to light brown colour and sometimes a dull appearance (BV-N95F/59.45) (Fig. 9a) has a $^{207}Pb/^{206}Pb$ age of 1589±4 Ma (Table 3 and Fig. 3). Microscopical studies indicate that the titanites were the last minerals to crystallize in the wall rocks (Fig. 9a). In some cases titanite encloses rutile and ilmenite grains (Fig. 9b), and hence the formation of titanite can be attributed to retrograde metamorphic reactions from the rutile and ilmenite (Force, 1991, p. 12). However, the ages for the rutile and titanite are highly discordant and are considered to give only a lower age approximation for the closure of the U-Pb systems in minerals.

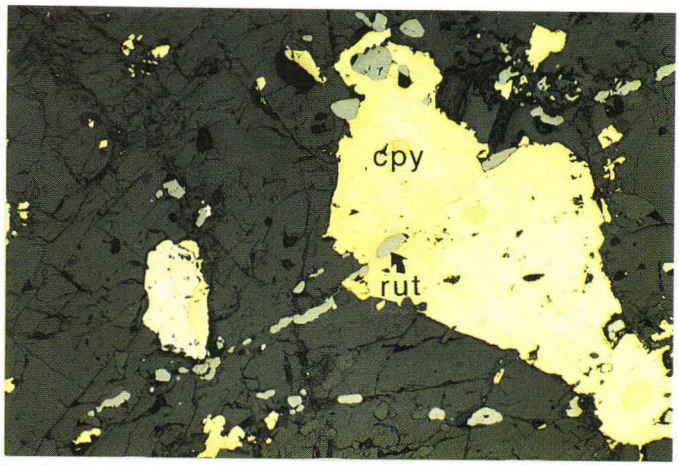


Fig. 8. Metadiabase hosted rutile (rut), which is younger than chalcopyrite (cpy), Bidjovagge (BV-S154B/102.45). Width of view is 1.50 mm, reflected and plane-polarized light.

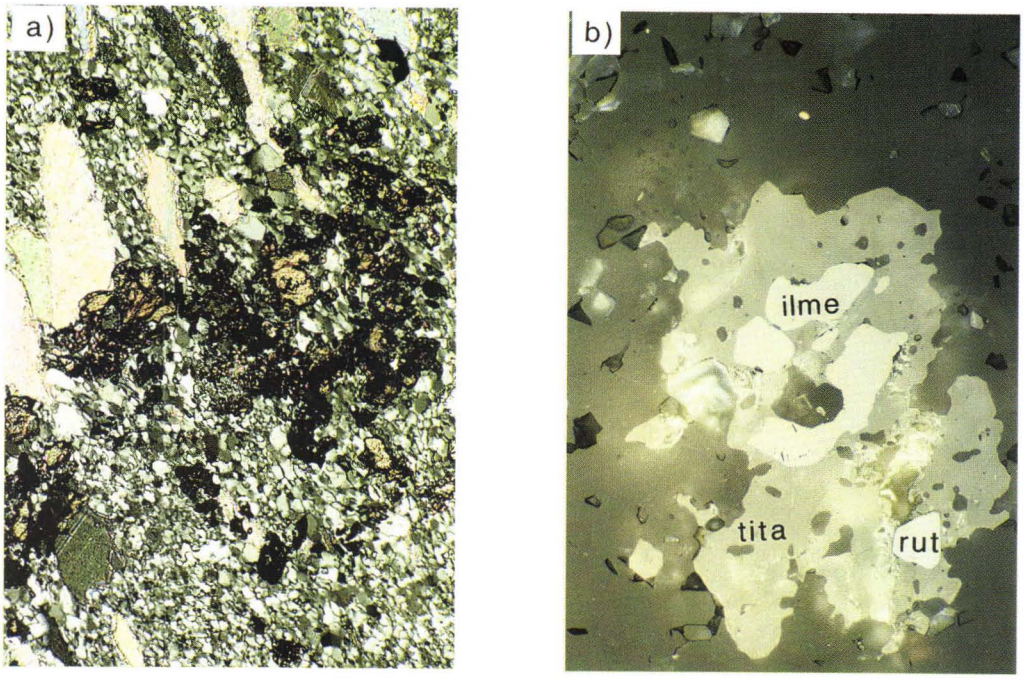


Fig. 9. a) Titanites from an albite-carbonate rock. b) Occasionally titanite (tita) encloses ilmenite (ilme) and rutile (rut), Bidjovagge (BV-N95F/59.45). Width of view is a) 1.01 mm, transmitted and cross-polarized light and b) 0.21 mm, transmitted and plane-polarized light.

### Wall rock samples

Wall rock samples (WR) rich in radiogenic lead from the vicinity of the Saattopora mine yield $^{207}Pb/^{206}Pb$ age estimates (Table 4) considerably younger than those of the sulfides. An acid leach and total dissolution of a wall rock sample from the Bidjovagge area give a $^{207}Pb/^{206}Pb$ age estimate of ca. 1000 Ma, and a sample from the Hangaslampi area ca. 1770 Ma. However, if the sample sizes were too small to have maintained the actual equilibrium volume of the lead and uranium in the rock (see e.g. Roddick & Compston, 1977), these single results might be irrelevant, although the Hangaslampi result could reflect the effect of nearby postorogenic granites.

## LEAD ISOTOPE RESULTS

### Upper Lapponian volcanics, central Lapland

#### Samples

Lead isotopes for whole rock samples from central Lapland volcanics are given in Appendix 3. According to Lehtonen et al. (1992), the samples from the different formations represent the following Upper Lapponian stratigraphical units (see Fig. 1): Vesmajärvi and Veikasenmaa (upper unit); Tarvasenvaara, Linkupalo, Köngäs, Sinermä, and Kautoselkä (middle unit); Jeesiörova, Peuramaa, and Sattasvaara (lower unit).

#### Results

Most of the samples having the lowest $^{206}Pb/^{204}Pb$ ratios of the Upper Lapponi group were collected from the lower unit. The least radiogenic lead isotope composition, plotting close to the mantle evolution curve of Zartman and Doe (1981) (Fig. 10), was recorded from the Vesmajärvi Formation, which belongs to the upper unit.

On the $^{206}Pb/^{204}Pb$ vs. $^{207}Pb/^{204}Pb$ diagram (Fig. 11), all the whole-rock lead isotope compositions measured from the three different Upper Lapponian units conform to a linear trend with a slope corresponding to an age of ca. 1835 Ma. This may be an artifact caused by the mixing of lead from different sources, as the analyses belonging to the different units have slightly deviating slopes (Table 5). Nevertheless, the separate slope ages determined from the linear trends of the lower (1869±30 Ma) and middle (1837±48 Ma) units do coincide within error limits. The linear trend of the upper unit samples corresponds to an older age.

The somewhat high MSWD-values (see Table 5) calculated from the regressions either reflect some incompleteness in the homogenization process, or the effect of geological processes postdating the homogenization. On the $^{206}Pb/^{204}Pb$ vs. $^{208}Pb/^{204}Pb$ diagram (Fig. 11), the lead isotope data fall into separate sublinear compositional trends indicating differences in the Th/U ratios.

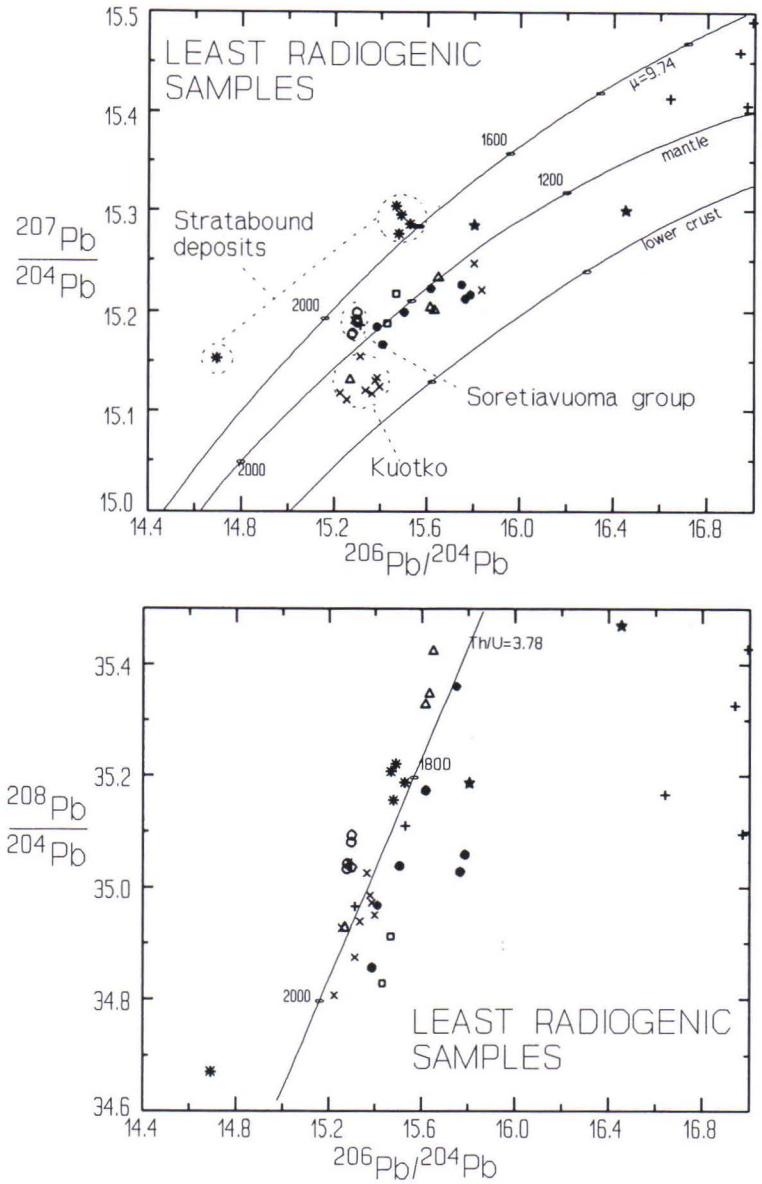


Fig. 10. $^{206}Pb/^{204}Pb$ vs. $^{207}Pb/^{204}Pb$ (upper diagram) and $^{206}Pb/^{204}Pb$ vs. $^{208}Pb/^{204}Pb$ (lower diagram) plots of the least radiogenic sulfides, carbonates, and Upper Lapponian volcanics. For reference the Stacey and Kramers (1975) lead evolution curve and the mantle lead evolution curve of Zartman and Doe (1981) (upper diagram only) are also presented. *Sulfides:* ○=Soretiavuoma; x=Kuotko; Δ=Kuotko/lamprophyre; +=Suurikuusikko and Kiistala; ⁎=Pahtavuoma and Riikonkoski. *Carbonates:* ★ =Saattopora/A-ore; □ =Pahtavaara. *Whole-rocks*: • =Upper Lapponian volcanics.

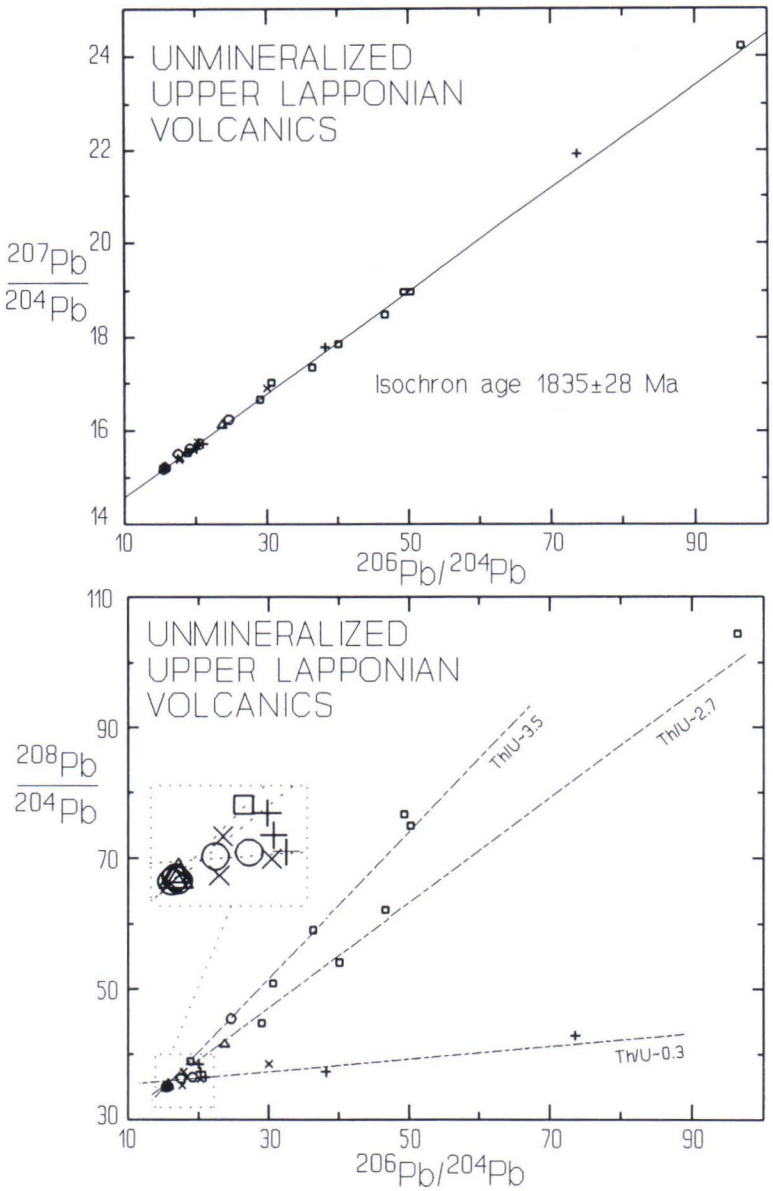


Fig. 11. $^{206}Pb/^{204}Pb$ vs. $^{207}Pb/^{204}Pb$ (upper diagram) and $^{206}Pb/^{204}Pb$ vs. $^{208}Pb/^{204}Pb$ (lower diagram) plots of the whole-rock lead isotope data from the Upper Lapponian volcanics, Central Lapland greenstone belt. *Upper unit:* +=Veikasenmaa (n=5); x=Vesmajärvi (n=5). *Middle unit:* □ =Linkupalo (n=3), Köngäs (n=2), Sinermä (n=2), Tarvasenvaara (n=1), and Kautoselkä (n=1). *Lower unit:* Δ =Peuramaa (n=2) and Jeesiörova (n=2); ○ =Sattasvaara (n=6).

Table 5. Slopes, corresponding age estimates, and MSWD-values of the regressional fittings for most of the lead isotope data of the Upper Lapponian volcanics.

| Upper Lapponian units (n) Formations (n) | Slope | AGE ± 2σ/Ma | MSWD |
|---|---|---|---|
| Lower unit (9) | 0.1143 | 1869 ± 30 | 1.3 |
| Peuramaa and Jeesiörova (4) | | 1851 ± 46 | 0.7 |
| Sattasvaara (5) | | 1883 ± 94 | 2.2 |
| Middle unit (8) | 0.1123 | 1837 ± 48 | 51 |
| Upper unit (10) | 0.1166 | 1904 ± 32 | 22 |
| Veikasenmaa (5) | | 1914 ± 50 | 22 |
| Vesmajärvi (3) | | 1901 ± 30 | 0.01 |
| All samples (29) | 0.1122 | 1835 ± 28 | 63 |

MSWD = mean square of weighted deviates.

## Lead isotope characteristics of the three Upper Lapponian volcanic units

The differences between the lead isotope characteristics of the Upper Lapponian volcanics can, to some extent, be used to classify the volcanics into the three volcanic units of the Upper Lapponian Group. The middle unit samples are usually radiogenic and show the highest Th/U ratios (2.7-3.5); the Linkupalo samples form the steepest Th/U trend, whereas the upper unit samples show varying radiogenic patterns, and the amount of thorogenic lead is low in most of the radiogenic samples. Weakly radiogenic uranogenic lead isotopic compositions are typical of the lower unit samples, some of which (Jeesiörova samples and most of the Sattasvaara samples) form the least radiogenic compositional group among all the analysed volcanics. Features comparable with the geochemical results include the higher Th contents in the middle unit in comparison with the upper unit (Lehtonen et al., 1992).

In the lower unit, the lead isotope characteristics of the Mikkuurova and Peuramaa samples differ from the other samples (Appendix 3). This is seen in the relatively high $^{208}Pb/^{204}Pb$ ratios of the picrites from the Peuramaa Formation and the Mikkuurova Mg-basalt from the Sattasvaara Formation. In addition, the other Peuramaa sample and the Mikkuurova sample have high $^{206}Pb/^{204}Pb$ ratios.

## Resetting of the U-Pb systems

The uranogenic lead isotope compositional trends (Table 5) of the middle and lower unit volcanics of the Upper Lapponi Group slope too gently to illustrate the uranogenic lead growth from the volcanism to the present, but could be explained by a nearly synchronous resetting of the U-Pb systems in both units. The age estimate (ca. 1870-1840 Ma) for the resetting, and its wide areal extent would imply that it was caused by metamorphic and tectonic processes related to the Svecokarelian orogeny.

The separate trends seen on the $^{206}Pb/^{204}Pb$ vs. $^{208}Pb/^{204}Pb$ diagram (Fig. 11) could reflect primary compositional differences in Th/U ratios. However, another possible reason for the seemingly low Th/U ratios, at least for the upper unit samples, could be fractionation of uranium and thorium (enrichment of uranium or loss of thorium) due to metamorphic processes. This might be connected with the allochtonous emplacement of the granulite belt at ca. 1.91 Ga (Bernard-Griffiths et al. 1984; Sorjonen-Ward et al., 1994), as the Pb-Pb isochron age (Table 5) for the volcanics of the upper unit apparently coincides with this age.

## Base metal deposits

### Samples

A few samples from the Pahtavuoma, Riikonkoski, Hormakumpu, and Alakylä deposits, representing synvolcanic stratabound base metal mineralization, were analysed (Appendix 4). These samples mainly consisted of galenas hosted by black schist and albite-sericite schist.

### Results

The uranogenic lead isotope compositions of the Pahtavuoma Cu-Zn-U deposit form a relatively homogeneous group on the upper side of the Stacey and Kramers (1975) lead evolution curve (Fig. 12). The fairly high μ-value of about 10 (Table 6) for the Pahtavuoma galena most likely indicates some involvement of an upper crustal lead component.

The uranogenic lead isotope compositions of the Riikonkoski galenas show two clearly separate compositions (Fig. 12). The least radiogenic sample, lying on the upper side of the Stacey and Kramers (1975) lead evolution curve, has a model age of ca. 2354 Ma and a μ-value of 10.6, which is the highest value in the present data set (Table 6). The other Riikonkoski galena shows a distinctly radiogenic composition, with a $^{206}Pb/^{204}Pb$ ratio of about 24.4 (Appendix 4 and Fig. 12). The lead isotope compositions of the Hormakumpu and Alakylä samples (Appendix 4 and Fig. 12) fall into a single, relatively homogeneous, radiogenic lead compositional group.

### Discussion

In the Riikonkoski area, the least radiogenic lead composition apparently represents the initial lead composition of the mineralization. The high μ-value (Table 6) clearly indicates the involvement of an Archaean crustal lead component in the galena. The existence of another, radiogenic composition indicates a secondary origin for that galena.

The slope of the two-point trend constructed between the least radiogenic and radiogenic galenas is 0.1357 (R), corresponding to an apparent age of ca. 2170 Ma. However, because the U/Pb ratio in galena is typically low, the addition of in situ formed radiogenic lead does not alter the lead composition significantly. Therefore, the lead growth simply by uranium decay from ca. 2170 Ma to the present is unlikely to be the reason for radiogenic galena formation. Instead, it is suggested that the trend is a two-point isochron in which the lead evolution from a source ca. 1963-1913 Ma ($T_1$) in age was completed with subsequent lead separation and the formation of the radiogenic galenas quite late in the geological history, conceivably during the Caledonian orogeny ca. 420-500 Ma ago ($T_2$) (Equation 1; Faure, 1977).

$$R = 1/137.88 \left( \frac{e^{\lambda_2 T_1} - e^{\lambda_2 T_2}}{e^{\lambda_1 T_1} - e^{\lambda_1 T_2}} \right) \quad (1)$$

R = slope of the compositional trend
$\lambda_1$ = decay constant of $^{238}U$ ($1.55125 \times 10^{-10}$ $y^{-1}$; Jaffey et al. 1971)
$\lambda_2$ = decay constant of $^{235}U$ ($9.8485 \times 10^{-10}$ $y^{-1}$; Jaffey et al. 1971)
$T_1$ = age of the source rocks in which the radiogenic lead grew
$T_2$ = age of the lead separation and mineralization

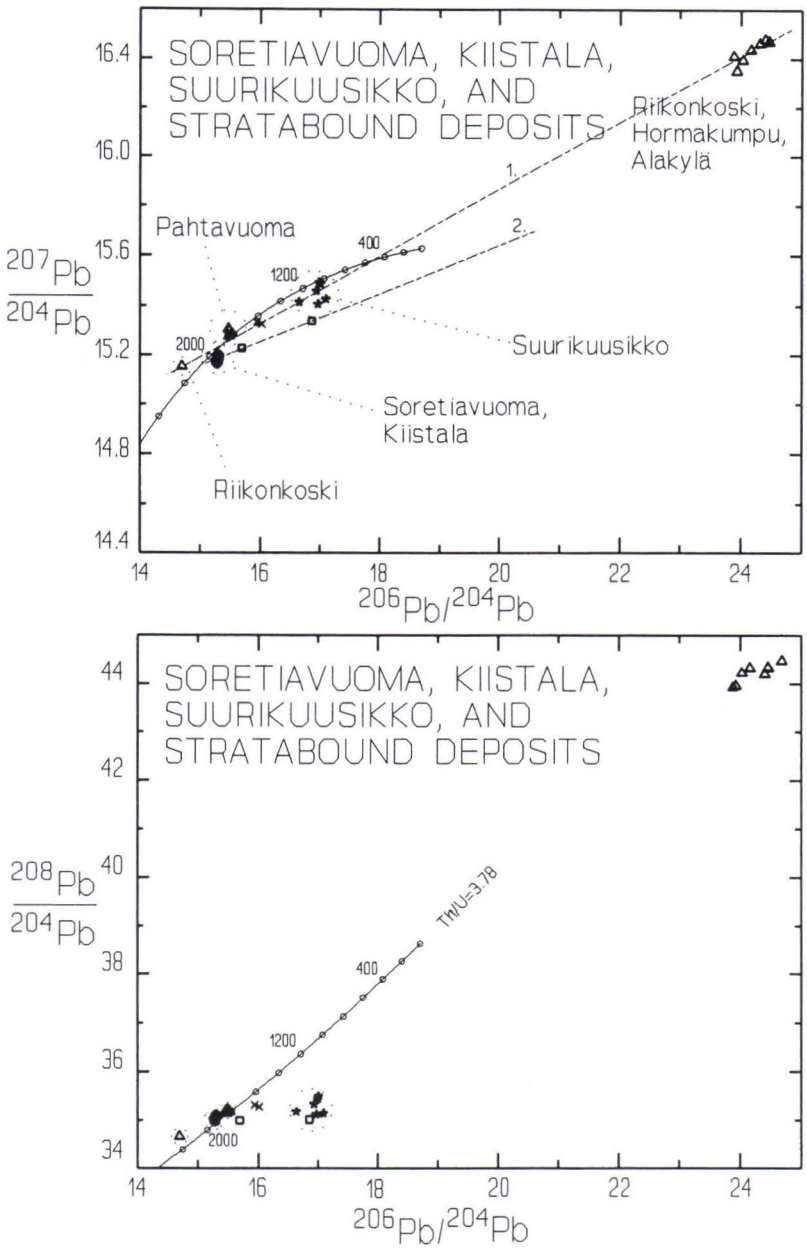


Fig. 12. $^{206}Pb/^{204}Pb$ vs. $^{207}Pb/^{204}Pb$ (upper diagram) and $^{206}Pb/^{204}Pb$ vs. $^{208}Pb/^{204}Pb$ (lower diagram) plots of the lead isotope data from the stratabound base metal deposits and from the Soretiavuoma, Kiistala, and Suurikuusikko gold occurrences. For reference the Stacey and Kramers lead evolution curve (1975) is also presented. *Sulfides:* Δ =Pahtavuoma, Riikonkoski, Hormakumpu, and Alakylä; ○ =Soretiavuoma; ∗=Suurikuusikko and Kiistala. *WR,LE:* x=Pahtavuoma; □ =Soretiavuoma.

Table 6. Calculated model ages and milieu indices (two-stage model of Stacey and Kramers 1975) for the least radiogenic sulfides and carbonates from the Central Lapland greenstone belt.

| DEPOSIT/ SAMPLE | LEAD ISOTOPE RATIOS 206/204 | 207/204 | 208/204 | Ma* | $\mu$ | W |
|---|---|---|---|---|---|---|
| KUOTKO | | | | | | |
| Au | 15.364 | 15.117 | 35.026 | 1693 | 8.9 | 33.4 |
| R305/7.95-PO | 15.255 | 15.111 | 34.927 | 1781 | 9.0 | 34.0 |
| R436/76.40-GA | 15.312 | 15.155 | 34.875 | 1805 | 9.2 | 33.9 |
| R436/76.40-GA | 15.225 | 15.118 | 34.807 | 1818 | 9.1 | 33.5 |
| R436/76.40-PY | 15.285 | 15.191 | 35.045 | 1889 | 9.5 | 37.1 |
| A1168/lamprophyre-PY | 15.269 | 15.131 | 34.928 | 1802 | 9.1 | 34.4 |
| SORETIAVUOMA | | | | | | |
| R307/48.45-CP | 15.277 | 15.177 | 35.033 | 1873 | 9.4 | 36.6 |
| R307/48.45-CP | 15.298 | 15.199 | 35.094 | 1890 | 9.5 | 37.6 |
| R307/48.45-CRB | 15.280 | 15.166 | 34.990 | 1852 | 9.3 | 35.8 |
| R307/48.45-(Pb-rich?) | 15.297 | 15.192 | 35.081 | 1880 | 9.5 | 37.2 |
| R307/48.45-ASPY | 15.279 | 15.178 | 35.043 | 1872 | 9.4 | 36.7 |
| R307/48.70-CRB | 15.294 | 15.178 | 35.035 | 1859 | 9.4 | 36.4 |
| R307/48.70-PY | 15.298 | 15.189 | 35.036 | 1874 | 9.5 | 36.7 |
| KIISTALA | | | | | | |
| G347-GA | 15.313 | 15.186 | 34.965 | 1855 | 9.4 | 35.7 |
| STRATABOUND MINERALIZATIONS | | | | | | |
| Riikonkoski-GA | 14.692 | 15.153 | 34.671 | 2354 | 10.6 | 44.5 |
| Pahtavuoma-GA | 15.468 | 15.304 | 35.207 | 1913 | 10.0 | 39.1 |

* = model age; $\mu = {}^{238}U/{}^{204}Pb$; $W = {}^{232}Th/{}^{204}Pb$; ASPY = arsenopyrite; CP = chalcopyrite; CRB = carbonate; GA = galena; PO = pyrrhotite; PY = pyrite

Palaeozoic galena formation was most probably restricted to pre-existing shear zones, that were reactivated during the Caledonian orogeny. This interpretation is also consistent with the presence of other radiogenic galenas at Hormakumpu and Alakylä, which together with this particular Riikonkoski galena, define a rather well homogenized lead isotope compositional group.

## Gold deposits

### Soretiavuoma

#### Samples

The analysed samples from the Soretiavuoma deposit, namely chalcopyrite, arsenopyrite, an unknown lead rich mineral, carbonate, and wall rock samples, were all taken from the drill core SV-R307 (Appendix 4). The sulfides are quite rich in lead when compared with the other epigenetic gold mineralizations, whereas the U and Th contents of the

Table 7. Pb, U and Th concentrations. For comparison, approximate $^{206}Pb/^{204}Pb$ and $^{208}Pb/^{204}Pb$ are also shown. The Pb/U, Pb/Th, and Th/U are concentration ratios.

| DEPOSIT/ SAMPLE | $\frac{^{206}Pb}{^{204}Pb}$ | $\frac{^{208}Pb}{^{204}Pb}$ | Pb µg/g | Th µg/g | U µg/g | Th/U | U/Pb | Th/Pb |
|---|---|---|---|---|---|---|---|---|
| SORETIAVUOMA | | | | | | | | |
| R307/48.45-CP | 15 | 35 | 41 | ! | ! | | | |
| R307/48.70-PY | 15 | 35 | 45 | ! | ! | | | |
| KUOTKO | | | | | | | | |
| R305/7.95-PO | 15 | 35 | 2 | ! | ! | | | |
| R305/7.95-ASPY | 15 | 35 | 2 | ! | ! | | | |
| R443/18.60-PY | 18 | 38 | 136 | 1.04 | ! | | | <0.01 |
| R436/76.40-GA | 15 | 35 | 710000 | n.a. | n.a. | | | |
| R436/76.40-PY | 15 | 35 | 73 | ! | ! | | | |
| R436/87.85-PY | 16 | 36 | 196 | ! | ! | | | |
| lamprophyre-PY | 16 | 35 | 1240 | 5.05 | 2.41 | 2.1 | <0.01 | <0.01 |
| SUURIKUUSIKKO | | | | | | | | |
| R434/65.80-ASPY | 17 | 35 | 21 | ! | 0.36 | | 0.02 | |
| R434/80.55-ASPY | 17 | 36 | 9 | 0.22 | 0.12 | 1.8 | 0.01 | 0.02 |
| LAMMASVUOMA | | | | | | | | |
| R3/45.00-PY | 29 | 39 | 4 | 0.13 | 0.17 | 0.8 | 0.04 | 0.03 |
| PAHTAVAARA | | | | | | | | |
| R508/111.55-PY | 36 | 35 | 1 | ! | 0.36 | | 0.36 | |
| SAATTOPORA Au-ORE | | | | | | | | |
| A-A1205-PO | 1490 | 40 | 18 | 0.89 | 149 | <0.01 | 8.3 | 0.05 |
| A-A1205-CP | 132 | 37 | 2 | ! | ! | | | |
| B-R208-PY | 97 | 64 | 50 | 0.11 | 0.11 | 1.0 | <0.01 | <0.01 |
| C-ASPY | 97 | 52 | 9 | 3.32 | 88.0 | 0.04 | 9.8 | 0.37 |
| SAATTOPORA Cu-MINERALIZATION | | | | | | | | |
| SP/Cu-CP | 473 | 42 | 6 | ! | 0.24 | | 0.04 | |
| HANGASLAMPI | | | | | | | | |
| R388/22.75-PY | 56 | 82 | 2 | ! | 0.12 | | 0.06 | |
| R388/41.20-PY | 808 | 43 | 3 | 0.15 | 11.5 | 0.01 | 3.8 | 0.05 |
| R388/66.85-PO* | 2893 | 54 | 80 | 7.77 | 315 | 0.02 | 3.9 | 0.10 |
| R388/71.05-PY | 108 | 47 | 2 | ! | 0.11 | 0.06 | | |
| MEURASTUKSENAHO | | | | | | | | |
| R332/179.6-CP | 97 | 48 | 3 | ! | 0.11 | | 0.04 | |
| BIDJOVAGGE | | | | | | | | |
| N20E/197.50-CP | 47 | 43 | 200 | 2.07 | 15.6 | 0.13 | 0.08 | 0.01 |
| N20E/203.55-CP | 29 | 44 | 22 | 0.90 | 0.39 | 2.3 | 0.02 | 0.04 |
| N95F/2.10-PY | 72 | 54 | 2 | 0.39 | 0.32 | 1.2 | 0.16 | 0.20 |
| N95F/14.10-PY | 47 | 45 | 31 | 0.23 | 0.10 | 2.3 | <0.01 | <0.01 |
| N95F/46.70-PY | 36 | 43 | 174 | 0.18 | ! | | | <0.01 |
| N95F/59.45-PY | 781 | 362 | 1 | 0.32 | 0.40 | 0.8 | 0.40 | 0.32 |
| S165B/81.40-PY | 49 | 44 | 3 | 0.13 | 0.47 | 0.28 | 0.16 | 0.04 |
| S154B/96.35-CP | 26 | 42 | 6 | 0.45 | 1.51 | 0.30 | 0.25 | 0.08 |
| N95F/124.65-CP | 40 | 50 | 12 | ! | 0.26 | | 0.02 | |
| S154B/149.8-PY | 37 | 57 | 27 | 0.56 | 0.75 | 0.75 | 0.03 | 0.02 |

*) Brannerite inclusions; ASPY = arsenopyrite; CP = chalcopyrite; GA = galena; PO = pyrrhotite; PY = pyrite; ! = below detection limit; n.a. = not analysed. Pb/AAS; U,Th/ICP-mass spectrometer

sulfides were below the respective detection limits (Table 7 and Appendix 4). Multiple analyses of individual sulfide separates gave coincident results, indicating that lead was well homogenized in the mineralizing fluid.

## Results

The analysed lead isotope compositions from the Soretiavuoma mineralization plot within a narrow compositional field (Figs. 10 and 12). On the $^{206}Pb/^{204}Pb$ vs. $^{207}Pb/^{204}Pb$ diagram (Figs. 10 and 12), the relatively lead rich sulfides (Table 7 and Appendix 4) plot between the average crustal evolution curve of Stacey and Kramers (1975) and the mantle curve of Zartman and Doe (1981). The sulfides have model ages in the range 1850 to 1890 Ma, and a μ-value of ca. 9.4 (Table 6). On the $^{206}Pb/^{204}Pb$ vs. $^{208}Pb/^{204}Pb$ diagram (Fig. 12), the lead isotope compositions of the Soretiavuoma sulfides lie roughly on the Stacey and Kramers (1975) evolution curve.

The uranogenic lead composition of the acid leach fraction of the wall rock sample falls between the sulfide compositional group and the whole rock composition (Fig. 12). These data could be roughly connected with a line (R 0.090-0.105) corresponding to an age approximation with large errors (1424±380 to 1720±300 Ma). This line might indicate that the sulfide lead orginated from the wall rocks.

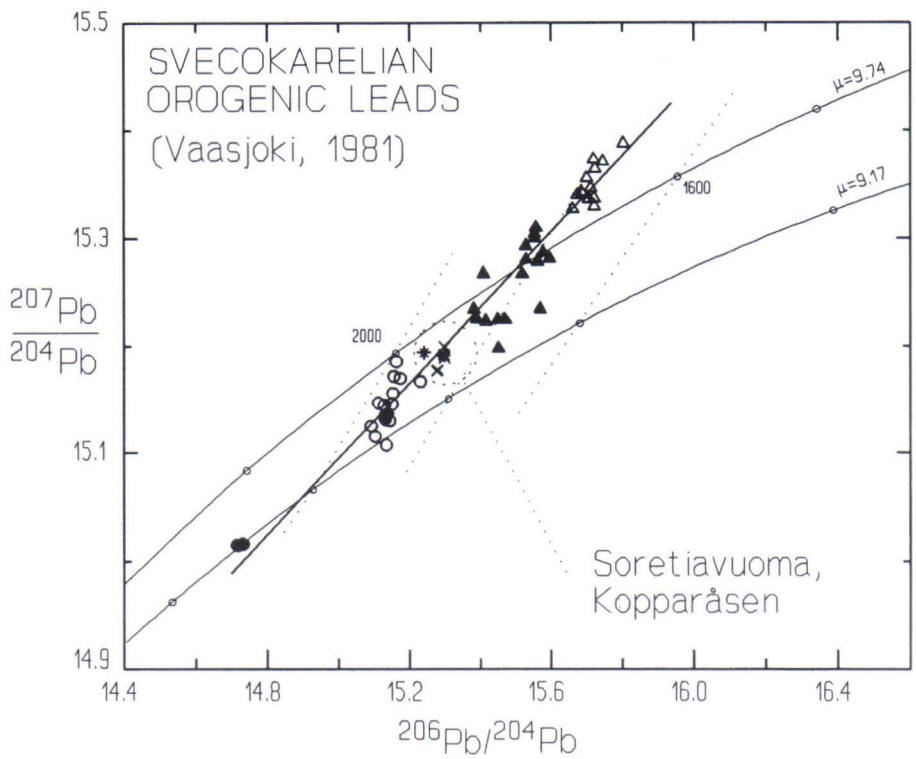


Fig. 13. Svecokarelian orogenic lead trend determined by Vaasjoki (1981). Growth curves according to two-stage model of Stacey and Kramers (1975). *Galena samples (Vaasjoki, 1981)*: • =Outokumpu mine; ○ =Main sulfide ore belt; ▲ =Batholith of Central Finland; Δ =Svecofennian supracrustal formations. Simplified after Figure 2. of Vaasjoki (1981; Fig. 2, p. 13). *Added sulfide lead compositions*: x=Soretiavuoma; ∗ =Kopparåsen (Romer & Boundy, 1988).

### Discussion

The Soretiavuoma lead isotope compositional group plots on the mantle-crustal lead mixing trend of the Svecokarelian orogenic leads defined by Vaasjoki (1981) (Fig. 13). This trend illustrates the mixing of juvenile mantle lead with upper crustal lead during the Svecokarelian orogeny at ca. 1.9 Ga (Vaasjoki, 1981; Huhma, 1986). On this line, the Soretiavuoma samples fall on the high $^{206}Pb/^{204}Pb$ side of the compositional group defined by the main sulfide ore belt galenas, for which an approximate mineralization age interval of 1860 to 1940 Ma has been determined (Vaasjoki, 1981; Kousa et al., 1994).

The lead isotope compositions of the Soretiavuoma sulfides are identical with those of the least radiogenic leads from the Kopparåsen Cu-Zn-U deposit in northern Sweden (Romer & Boundy, 1988; Romer, 1989a) (Fig. 13). It is hosted by the Palaeoproterozoic Kopparåsen greenstone belt, which is exposed as a basement window in the Caledonides. These stratabound deposits hosted by mafic metatuffs and metasediments have been interpreted as volcanic-sedimentary and premetamorphic in origin (Adamek, 1975).

The lead isotopes from the Soretiavuoma sulfides have characteristics, such as homogeneous compositions and relatively lead-rich sulfides, that are typical of volcanic-exhalative mineralization. However, the Soretiavuoma mineralization is regarded as epigenetic and thus younger than the hosting lithologies, which are considered to be older than ca. 2.0 Ga. According to Suoperä (1988) the fracture-related gold bearing veins at Soretiavuoma are deformed and represent the oldest vein phase in the area. Consequently it is suggested that the Soretiavuoma mineralization is temporally connected with the (early- to) synorogenic stage of the Svecokarelian orogeny. As the lead composition coincides with the orogenic mixing line, the lead may originate from the surrounding volcanic rocks.

## Kuotko

### Mineralization

#### *Samples*

The samples from the Kuotko mineralization include the lead-poor sulfides from drill-core R305, the lead-rich and porous pyrite from R443, the lead-rich and lead-poor sulfides from R436, and lead-poor panned metallic gold (Appendix 4 and Table 7). Some carbonates were also analysed. The sulfides typically lack uranium and thorium, although the porous pyrite is an exception, with a Th content of ca. 1 ppm (Table 7).

#### *Results and discussion*

The samples analysed from the Kuotko area can be roughly divided into the following four lead isotope compositional groups (Fig. 14).

Group 1. The lead isotope composition of a lead-rich microfractured idiomorphic pyrite (KU-R436/76.40) (see also Fig. 15, Appendices 4 and 5, Table 7) falls slightly below the Stacey and Kramers (1975) lead evolution curve. This lead composition is similar to that of the Soretiavuoma sulfides, and will subsequently be referred to as "the Soretiavuoma group". This well homogenized lead in the uranium deficient sulfides most probably represents the initial lead composition for that particular phase of mineralization at Soretiavuoma and Kuotko.

Group 2. The second group comprises the relatively nonradiogenic lead-poor samples from drill-core R305 (see also Fig. 16, Appendix 4 and Table 7) and the gold sample (Fig. 17). In addition, the least radiogenic pyrite from the Kuotko lamprophyre has a lead composition similar to that of this group (see Fig. 10).

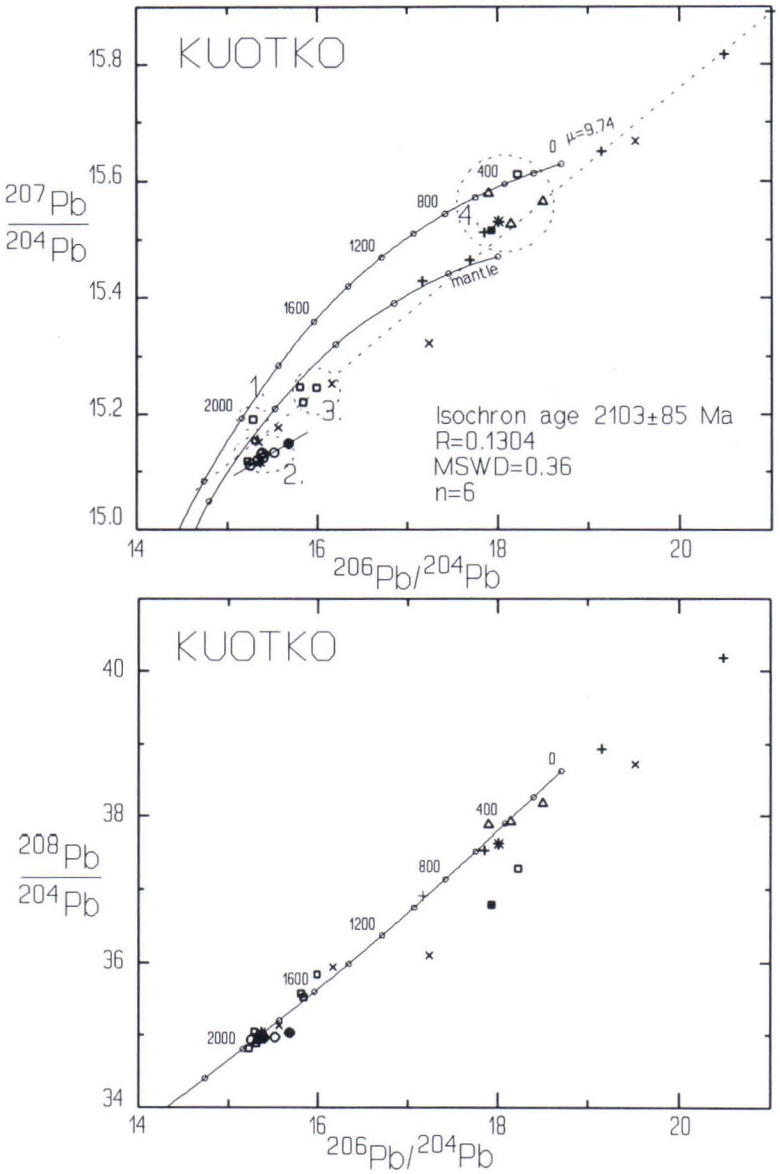


Fig. 14. $^{206}Pb/^{204}Pb$ vs. $^{207}Pb/^{204}Pb$ (upper diagram) and $^{206}Pb/^{204}Pb$ vs. $^{208}Pb/^{204}Pb$ (lower diagram) plots of the lead isotope data from the Kuotko mineralization. The average crustal lead evolution curve of Stacey and Kramers (1975) and the mantle lead evolution curve of the Zartman and Doe (1981) are also shown. The compositional groups 1-4 are distinguished on the diagram. *Sulfides:* ○ =R305/PO/ASPY/PO(hmf); □ =R436/PY/GA/PO(hmf); Δ =R443/PY; + =R443/PY(acid leaches). *Others:* ∗ =Au, • =R305/CRB; ■ = R436/CRB; x =R436/wall rock.

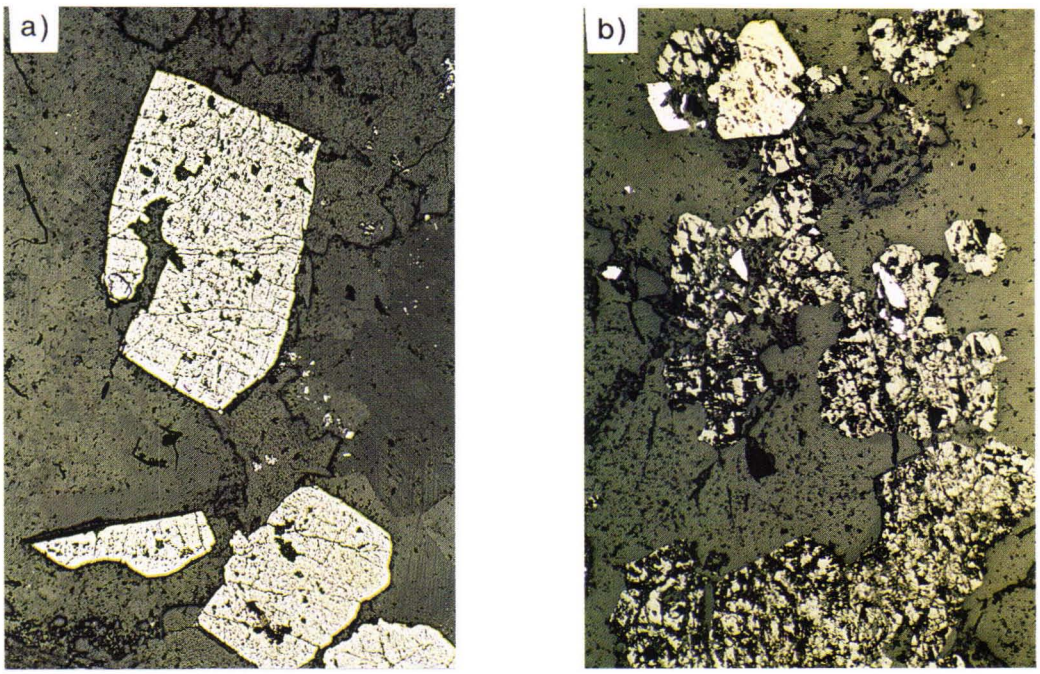


Fig. 15. a) Idiomorphic, microfractured, and lead rich pyrite, b) with relics of magnetite, Kuotko (KU-R436/76.40). Width of view is a) 2.50 mm, b) 1.01 mm, reflected and plane-polarized light.

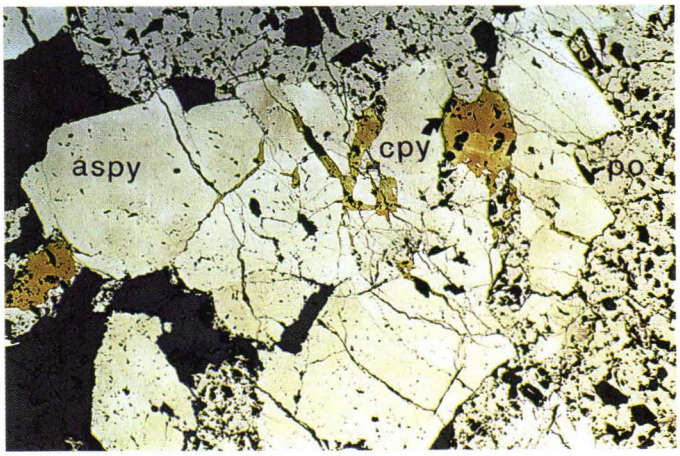


Fig. 16. Arsenopyrite (aspy) and pyrrhotite (po) with minor chalcopyrite (cpy) in a cabonate-quartz vein, Kuotko deposit (KU-R305/7.95). Width of view is 3.70 mm, reflected and plane-polarized light.

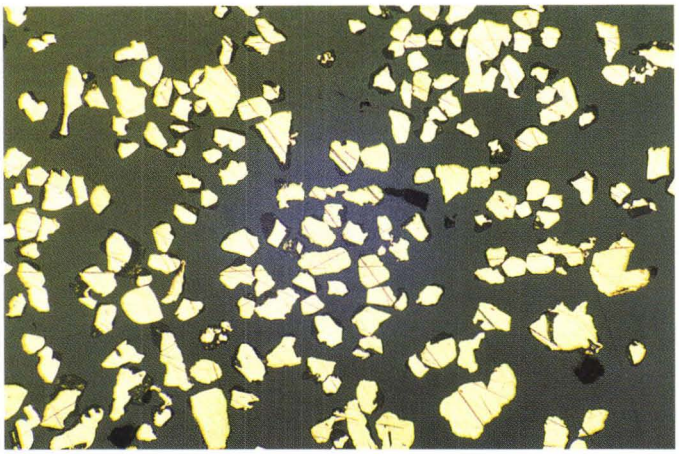

Fig. 17. Panned gold, Kuotko. Width of view is 1.50 mm, reflected and plane-polarized light.

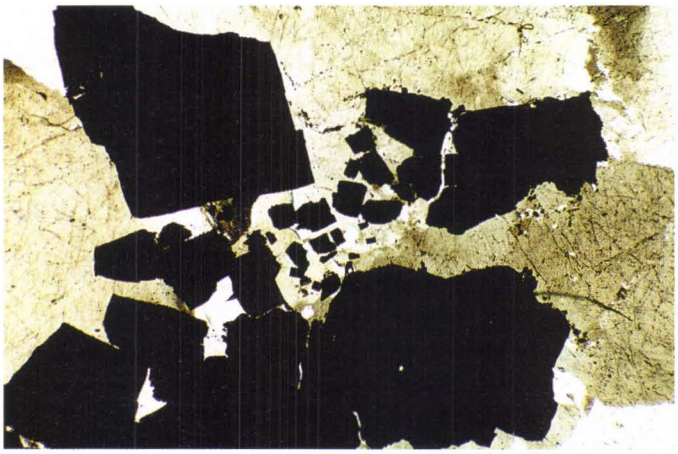

Fig. 18. Sheared quartz vein with overgrown idiomorphic pyrite, Kuotko (KU-R436/87.85). Width of view is 3.70 mm, transmitted and cross-polarized light.

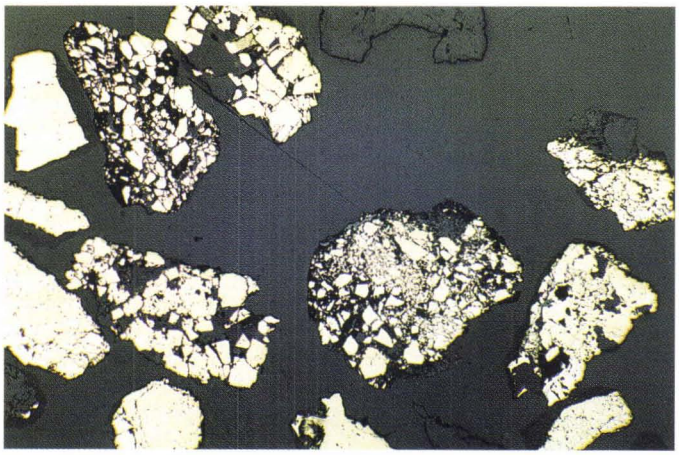

Fig. 19. Pyrite "pellets", Kuotko (KU-R443/18.60). Width of view is 1.50 mm, reflected and plane-polarized light.

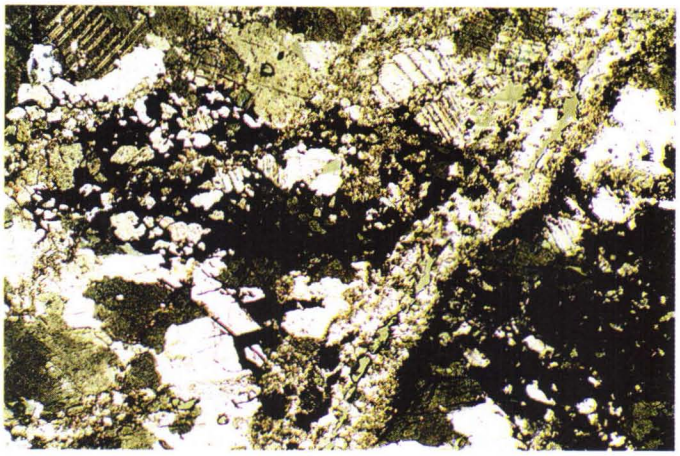

Fig. 20. Pyrrhotite brecciates carbonate in vein, Kuotko (KU-R436/42.20). Width of view is 3.70 mm, transmitted and cross-polarized light.

The lead composition of galena from the drill core section R436/76.40 is slightly heterogeneous and it has $^{207}Pb/^{204}Pb$ ratios intermediate between the Soretiavuoma group (Group 1) and Group 2 from Kuotko (Appendix 4 and Fig. 14). Unfortunately, the relationship between the galena and the other sulfides in the sample is unclear. In thin section only magnetite relicts and pyrite (Group 1), together with minor arsenopyrite were detected (see Fig. 15). On the other hand, in hand specimen galena seems to occur as separate small, compact seams in a restricted area; it may therefore represent a later fracture filling and is not necessarily cogenetic with the Group 1 sulfides.

On the $^{206}Pb/^{204}Pb$ vs. $^{207}Pb/^{204}Pb$ diagram (Fig. 14), the least radiogenic sample plots slightly below the mantle evolution curve of Zartman and Doe (1981), with a μ-value of ca. 9.0 (Table 6). In this group, the samples have a narrow range, defining a gently sloping compositional trend (R=0.0868, n=5, MSWD=0.013, 1356±1400 Ma) which however, is geologically meaningless. On the $^{206}Pb/^{204}Pb$ vs. $^{208}Pb/^{204}Pb$ diagram (Fig. 14), the least radiogenic sample plots on the evolution curve of Stacey and Kramers (1975).

Group 3. The more heterogeneous third group consists of samples which are slightly radiogenic (Fig. 14 and Appendix 4). These include a macroscopically dull, lead-rich pyrite (Fig. 18), two pyrrhotites (magnetic fraction), and a carbonate sample, all separated from drill core R436 (Appendix 4). The slightly radiogenic pyrites from the lamprophyre also have lead compositions resembling those of this group (see Fig. 10). The high lead contents (Table 7 and Appendix 4), marcasite alteration of the pyrrhotite, and the occurrence of the pyrite would suggest a secondary origin for the elevated $^{206}Pb/^{204}Pb$ ratios.

Group 4. In the Kuotko area, the most radiogenic samples, with $^{206}Pb/^{204}Pb$ ratios around 18-20, are the lead-rich pyrite from the drill-core section KU-R443/18.60 (Table 4 and Fig. 19) and the low-lead carbonate with brecciating pyrrhotite from drill-core R436/42.20 (Fig. 20). The R443 pyrite clearly differs petrographically from the other Kuotko pyrites in forming large "pellets", with a carbonate matrix between the small pyrite cubes (see Fig. 19). This might represent some of the latest stages of sulfide formation, as also suggested by Ilkka Härkönen (oral com., 1991).

On the $^{206}Pb/^{204}Pb$ vs. $^{207}Pb/^{204}Pb$ diagram (Fig. 14), the lead isotope compositions of the

total dissolutions and most of the step by step dissolved acid leaches of the porous R443-pyrite form a linear trend with a slope of ca. 0.1304, corresponding to an apparent age of 2103±85 Ma (n=6, MSWD=0.36). The most easily dissolved fractions, possibly representing the carbonate matrix between the small pyrite cubes in a larger pellet, show the highest $^{206}Pb/^{204}Pb$ ratios along this trend.

The relatively high lead content (136 ppm), contrasting with a deficiency in uranium (Table 7), the petrographical appearance, and the assumption that the mineralization was not coeval with the volcanism militate against the possibility of lead growth from ca. 2100 Ma to present being the reason for the radiogenic nature of the pyrite. Therefore it is suggested that lead separation from a ca. 1888-1835 Ma old source took place in early Palaeozoic time at, ca. 420-500 Ma (Equation 1: R=0.1304, $T_1$=1888-1835 Ma, $T_2$=420-500 Ma). In fact, there is evidence that the shear zone in the Kuotko area has been active even during postglacial time (Härkönen oral com., 1991), which enables one to suppose that reactivation of the shear zone could also have taken place previously.

*Summary of discussion*

The lead isotope characteristics of rocks in the Kuotko area, such as their distinctive compositions, the lead contents, and the homogenity of the lead in the two least radiogenic compositional groups (Groups 1 and 2), all indicate the existence of two different phases of sulfide mineralization with separate lead sources. One evidently represents a type of (early- to) synorogenic mineralization resembling that identified at Soretiavuoma. The other indicates a mantle lead source with a lower crustal component, if the least radiogenic sample has preserved an initial lead composition. The gold sample from Kuotko belongs to the latter group and reflects gold concentration, at least during this phase.

Wall rock samples

*Samples*

Three wall rock samples immediately adjacent to the mineralized sections were analysed from drill core R436 (Appendix 4). In addition, whole-rock samples of felsic porphyry and lamprophyre from the Kuotko area and pyrite, apatite, and mixed titanite and apatite fractions from the lamprophyre were analysed. In the Kuotko area, the felsic porphyries are related to early- to synorogenic granitoids, such as the Ruoppapalo granodiorite, which has a U-Pb age of 1915±7 Ma (Hannu Huhma, oral com., 1990).

*Results*

On the $^{206}Pb/^{204}Pb$ vs. $^{207}Pb/^{204}Pb$ diagram (Fig. 21), the lead isotope compositions of the wall rocks adjacent to the mineralization (R436) and the acid leaches from these samples define a sublinear trend with an approximate slope of 0.1130. The corresponding apparent age, 1848±200 Ma, agrees roughly with the reset ages for the Upper Lapponian middle and lower unit volcanics.

On the $^{206}Pb/^{204}Pb$ vs. $^{207}Pb/^{204}Pb$ and $^{206}Pb/^{204}Pb$ vs. $^{208}Pb/^{204}Pb$ diagrams (Figs. 10 and 21), the lead isotope composition of the least radiogenic, lead-rich pyrite (Appendix 4) from the lamprophyre plots in the same compositional group as the Group 2 sulfides of the Kuotko mineralization. The model age for the pyrite is 1802 Ma, and the calculated evolutionary indices are in the same category as the Group 2 sulfides from Kuotko (Table 6).

On the $^{206}Pb/^{204}Pb$ vs. $^{207}Pb/^{204}Pb$ diagram (Fig. 21), the lead isotope compositions of the felsic porphyry (WR), lamprophyre (WR, LE), and apatite, and the mixed titanite and apatite fraction from the lamprophyre form a linear compositional trend with a slope of 0.1052 (n=5, MSWD=2.5). The corresponding apparent age is ca. 1718±40 Ma.

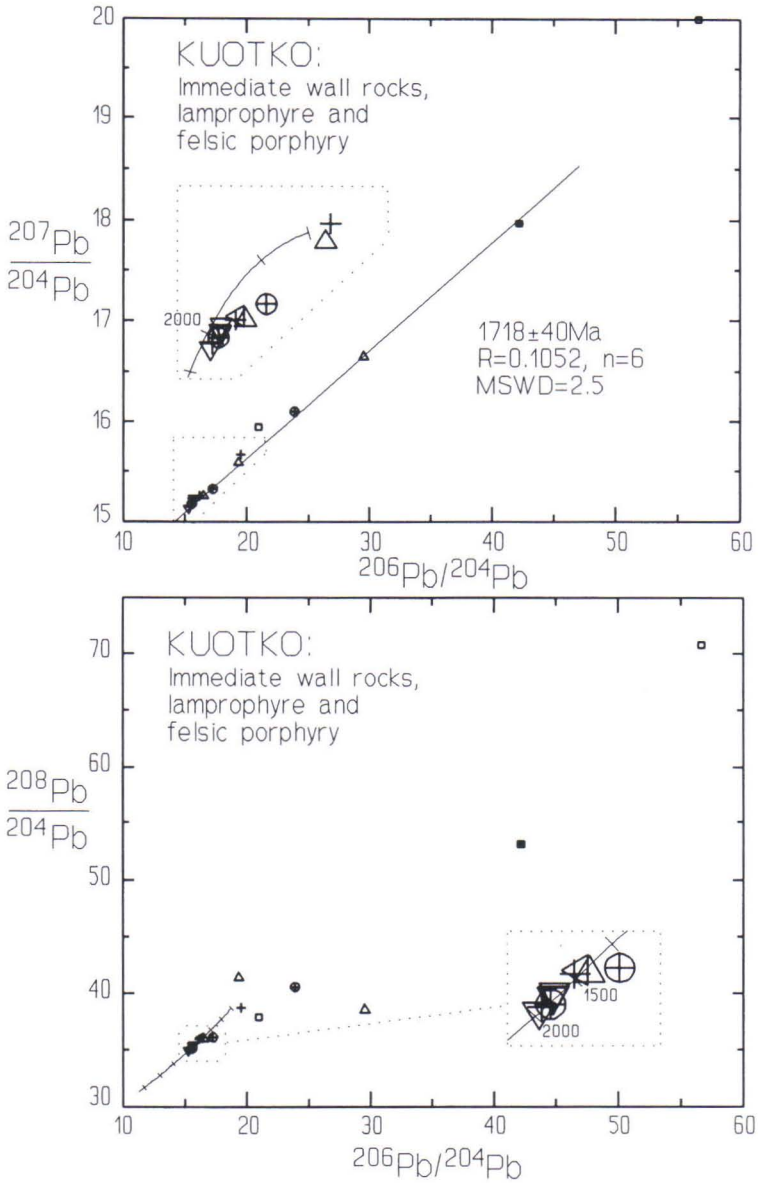


Fig. 21. $^{206}Pb/^{204}Pb$ vs. $^{207}Pb/^{204}Pb$ (upper diagram) and $^{206}Pb/^{204}Pb$ vs. $^{208}Pb/^{204}Pb$ (lower diagram) plots of the lead isotope data for the wall rock samples, lamprophyre, and felsic porphyry from the Kuotko area. *KU-R436/wall rocks:* ⊕ =WR; + =LE. *Lamprophyre:* Δ =APA/TITA/WR; ∇ =PY; ◁ =LE. *Felsic porphyry:* ■ =WR; □ =LE.

Fig. 22. Carbonatized lamprophyre with pyrite cubes in carbonate vein, Kuotko. Width of view is 3.70 mm, transmitted and cross-polarized light.

*Discussion*

In the Kuotko area, the Soretiavuoma group mineralization (Group 1) took place during the (early- to) synorogenic stage of the Svecokarelian orogeny and was followed by the regional resetting of the host rocks. Moreover, the gold bearing sulfide mineralization (Group 2) and the crystallization of the lamprophyre pyrites (±carbonatization?) may be related processes, because the least radiogenic lead compositions of the Group 2 samples and the pyrite from the carbonate filled fractures in the lamprophyre (Fig. 22) are similar. Subsequent to Group 2 mineralization, long lasting continuous or late episodic hydrothermal processes related to deep fracture zones are apparently indicated by the calculated slope age of 1718±40 Ma.

## Suurikuusikko and Kiistala

### Samples

Only two drill core sections from the Suurikuusikko gold deposit were analysed, and a previously analysed galena (M. Vaasjoki) from the gold-rich vein at Kiistala was also included in the study (Appendix 4). The Suurikuusikko samples have moderate lead contents, and the uranium concentrations in the two analysed samples are 0.36 and 0.12 ppm (Table 7).

### Results and discussion

The relationship between the lead isotope compositions of the Suurikuusikko and Kiistala sulfides and the other least radiogenic samples is shown in Figure 10. The Kiistala galena plots in the same compositional group as the Soretiavuoma samples and has a model age of 1855 Ma (Table 6). Thus, the Soretiavuoma group lead composition has been identified from three deposits, namely Soretiavuoma, Kuotko, and Kiistala.

The lead isotope compositions of the Suurikuusikko sulfides are clearly radiogenic, with the $^{206}Pb/^{204}Pb$ ratios at around 16.5-17.0 (Appendix 4 and Figs. 10 and 12). In the uranogenic lead diagram (Fig. 12), the data show significant scatter, indicating either slightly differing initial U/Pb ratios, or modification of the original U/Pb ratios by later processes.

## Pahtavaara and Lammasvuoma

### Samples

Lead isotopic compositions have been analysed from magnetites, pyrites, carbonates,

and wall rocks adjacent the Pahtavaara gold deposit. The sulfides are extremely poor in lead (see chapter "Sample preparation and chemical separation" and Table 7) when compared with the other gold occurrences of this study. The U and Pb concentrations for one analysed sample are 0.36 and 1 ppm, respectively (Table 7). Because the Pahtavaara deposit is hosted by the Sattasvaara komatiites, the lead isotope data from the unmineralized volcanics from the Sattasvaara Formation will also be considered in connexion with these results.

Of the analysed Lammasvuoma pyrites (Appendix 4), one occurs as a dissemination, while the other forms breccia in the host rocks. A wall rock sample from the immediate vicinity of a mineralized section was also analysed.

## Results

On the $^{206}Pb/^{204}Pb$ vs. $^{207}Pb/^{204}Pb$ diagram (Fig. 23), most of the lead isotope compositions of the sulfides, carbonates, wall rocks (WR, LE), and the Sattasvaara volcanics fall on the same sublinear trend. If the whole rock sample EIM-91-1, a few magnetites, and one pyrite are rejected (see Fig. 23) the corresponding apparent slope age becomes 1814±32 Ma (R=0.1109, n=24, MSWD=35.5). Furthermore, if most of the pyrites and magnetites only are included, the corresponding slope age remains virtually unchanged (R=0.1113, n=14, MSWD=44, 1821±43 Ma). Approximately the same slope (R=0.1107, 1811±87 Ma) is obtained for results from four carbonate samples, with a lower MSWD value of 5.

Within the group of least radiogenic samples (Fig. 10), the Pahtavaara carbonate plots on the mantle evolution curve of Zartman and Doe (1981). However, the lead in the carbonate has evolved, with some radiogenic lead addition, and therefore the actual initial lead composition is obscure.

The Pahtavaara sulfides show extremely low Th/U ratios, as can be concluded from the almost constant $^{208}Pb/^{204}Pb$ ratios with increasing $^{206}Pb/^{204}Pb$ ratios (Fig. 23). In contrast, the Th/U trend defined by the lead isotope compositions of the Sattasvaara volcanics indicates relatively high Th contents, albeit this trend is determined by one extreme analysis.

Compared with the Pahtavaara sulfides, the Lammasvuoma sulfides show higher relative thorogenic lead isotope compositions (Fig. 23). Otherwise the sample material from the Lammasvuoma gold occurrence is too small to give any reliable indication of its lead isotope characteristics (Appendix 3).

## Discussion

The uranogenic lead isotope compositions of the Pahtavaara sulfides representing different types of alteration environments (Korkiakoski 1992), namely talc-carbonate veins associated with biotitization and quartz-barite veins related to the later amphibole growth, as well as the surrounding rocks plot roughly along the same uranogenic compositional trend. This indicates an almost contemporaneous resetting of the U-Pb system of the surrounding volcanics and the hydrothermal mineralizing process. In addition, when plotted on the $^{206}Pb/^{204}Pb$ vs. $^{208}Pb/^{204}Pb$ diagram (Fig. 23) the data suggest roughly simultaneous processes for wall rock alteration and sulfide mineralization, coinciding with the cessation of thorogenic lead growth. This may suggest a metamorphically induced resetting of the U-Pb systems in the volcanics and the concomitant formation of a metamorphic mineralizing fluid.

On the other hand, the primary mineralization at Pahtavaara has been linked with a ductile phase of deformation (Korkiakoski 1992; Ward et al. 1989), and another major alteration process affected the area during the retrograde stage of metamorphism (Korkiakoski 1992). In that case the slope age of ca. 1820 Ma for the Pahtavaara samples could be considered as a minimum age approximation for the primary gold mineralization.

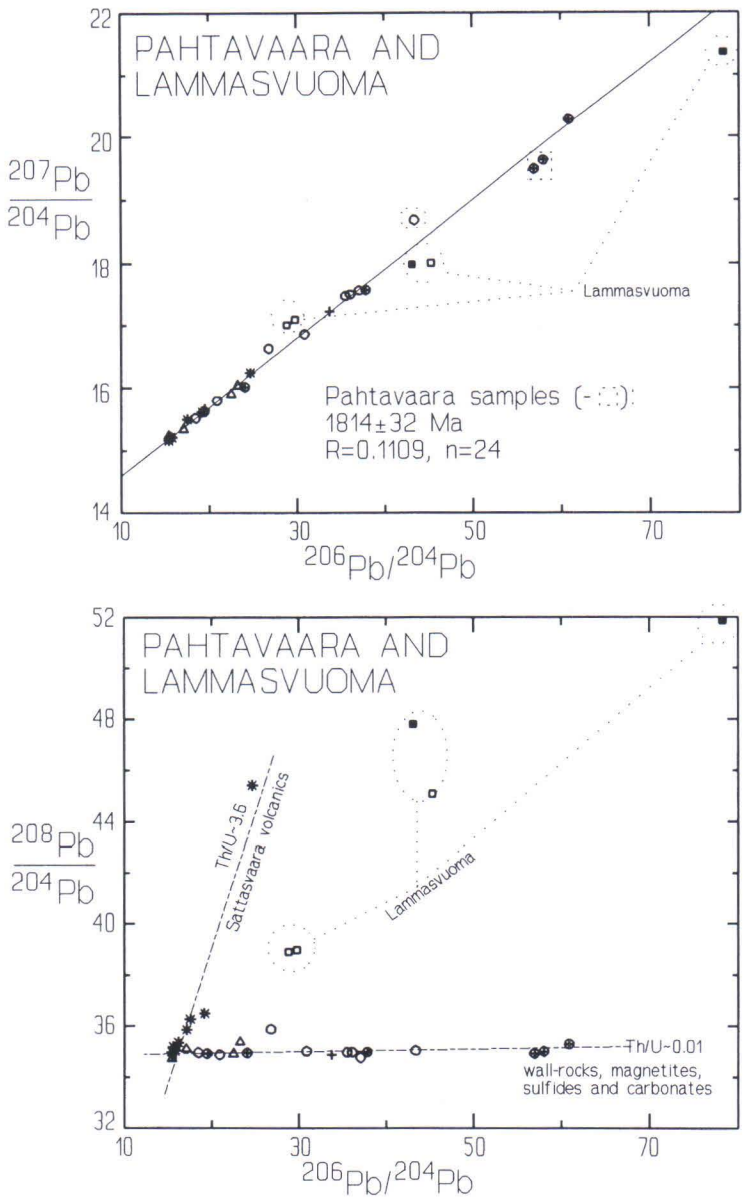


Fig. 23. $^{206}Pb/^{204}Pb$ vs. $^{207}Pb/^{204}Pb$ and $^{206}Pb/^{204}Pb$ vs. $^{208}Pb/^{204}Pb$ plots of the lead isotope data for the Pahtavaara and Lammasvuoma samples. *Pahtavaara deposit:* ○ =PY; ⊕ =MAGN; + =CRB; Δ =WR and LE. *Lammasvuoma deposit:* □ =PY; ■ =WR and LE. *Others:* ∗ =Sattasvaara volcanic rock.

## Saattopora area

### Samples

The Saattopora samples consist of sulfides and wall rocks from the A, B, and C gold ores and from the Saattopora copper mineralization, which was formerly an exploration target of the Outokumpu Finnmines Oy. Gold, vein carbonate, rutile, and thucolite have also been analysed from the A-ore (Appendix 4 and Tables 3 and 4). The ore-related sulfides are extraordinarily radiogenic, showing $^{206}Pb/^{204}Pb$ ratios between 80 and 1500 (Appendix 4), and have variable lead contents, ranging from 2 to 50 ppm (Table 7). The highest measured uranium and thorium contents are 149 and 3.3 ppm (Table 7), respectively.

### Results

#### *Ores*

On the $^{206}Pb/^{204}Pb$ vs. $^{207}Pb/^{204}Pb$ diagram (Fig. 24), the lead isotope compositions of the Saattopora A- and B-ore sulfides with the gold concentrates define a sublinear trend with a slope of 0.1146, or of 0.1159 (line 1) if one or two of the most radiogenic samples are rejected. These slopes correspond to ages of 1873±26 Ma (n=13) or 1894±46 Ma (n=12), respectively. The most radiogenic A-ore pyrrhotite, with a $^{206}Pb/^{204}Pb$ ratio of ca. 1490 reduces the slope (R=0.1082, n=14) so that it corresponds to an age approximation of 1770±66 Ma (not shown).

The lead isotope analyses of the wall rock rutiles, B- and C-ore wall rocks, and C-ore sulfides plot consistently below the compositional trend defined by the A- and B-ore sulfides (Fig. 24). The uranogenic lead isotope compositions of the A- and B-ore wall rocks and carbonates also plot along a trend (Figure 24; line 2, R=0.1044, n=6, 1707±8 Ma). Rejecting the most radiogenic A-ore sample ($^{206}Pb/^{204}Pb$=1668) does not significantly change the result (line 2, R=0.1034, n=5, 1686±75 Ma). This age approximation is similar to the concordant single rutile analysis from the Saattopora wall rock. Moreover, the uranogenic lead compositions of the C-ore sulfides plot on a trend (not shown), which corresponds to an extraordinary low age approximation of 802±570 Ma (n=3, R=0.066).

On the $^{206}Pb/^{204}Pb$ vs. $^{208}Pb/^{204}Pb$ diagram (Fig. 24), the A-ore sulfides differ significantly from the B-ore samples. The A-ore sulfides and their wall rocks, as well as the gold samples record almost no thorogenic lead growth with increasing $^{206}Pb/^{204}Pb$ ratio (Th/U<<0.1). In contrast to the A-ore, the B- and C-ore sulfides are less radiogenic and their Th/U ratios are higher, with values around 0.8 and 0.3, respectively (see also Fig. 24).

#### *Copper mineralization*

As with the Saattopora A-ore, the sulfides from the Saattopora Cu-occurrence show anomalously high $^{206}Pb/^{204}Pb$ ratios (Appendix 4). On the uranogenic lead diagram (Fig. 24), the sulfide lead isotope compositions define a sublinear compositional trend with an apparent slope age of ca. 2000±41 Ma (R=0.1230, n=6). On the $^{206}Pb/^{204}Pb$ vs. $^{208}Pb/^{204}Pb$ diagram (Fig. 24), the sulfides from albite-carbonate schists plot along the same low Th/U trend, together with the A-ore sulfides and the wall rocks.

### Relationship of ca. 1780 Ma age to the gold mineralization

The extremely radiogenic nature of the Saattopora ore leads, together with the high uranium concentrations, and varying $^{206}Pb/^{204}Pb$ ratios detected from multiple analyses of the same mineral fraction, all indicate the existence of $HNO_3$-HCl soluble uranium-rich and thorium-poor inclusions. However, no such inclusions have been identified either

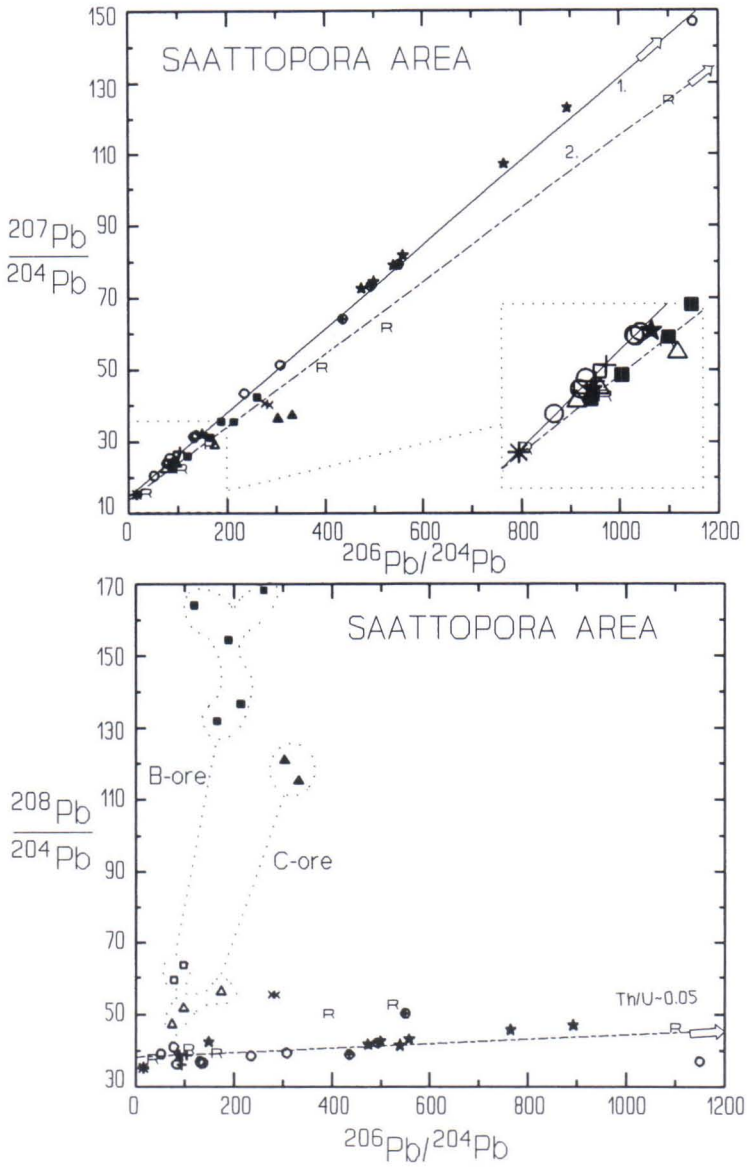


Fig. 24. $^{206}Pb/^{204}Pb$ vs. $^{207}Pb/^{204}Pb$ and $^{206}Pb/^{204}Pb$ vs. $^{208}Pb/^{204}Pb$ plots of the lead isotope data for the Saattopora samples. *Sulfides:* ○ =A-ore (the most radiogenic sample lies off the axis); □ =B-ore; Δ =C-ore; ★ =Cu-mineralization. *Wall rocks:* ■ =B-ore; ▲ =C-ore (A-ore wall rock lies off the axis). *Others:* ⊕ =gold; ∗ =vein carbonate (A-ore); + =WR,LE (A-ore vein); R =rutile. See text for additional information.

from thin sections or from the microprobe analyses. Nevertheless, uranium-rich inclusions were detected in the highly radiogenic Hangaslampi pyrrhotite, and furthermore the occurrence of thucolite also indicates the presence of uranium-rich minerals in the Saattopora ore veins. Consequently, it is suggested that uranium-rich micro-inclusions are the main cause for the high radiogenity and the high uranium contents in the Saattopora ore related sulfides and gold.

In contrast to the slope age of ca. 1870-1900 Ma determined for the sulfides and gold of the Saattopora A- and B-ores, an age of ca. 1780 Ma has been obtained for thucolite from the Saattopora A-ore, and also for monazite from the Saattopora wall rocks (Table 3). Similar ages have been obtained for uraninite from Pahtavuoma and for other uranium-rich minerals from several places from Finnish Lapland (see Table 3). These ages are roughly coeval with the emplacement of the postorogenic granites at ca. 1780 Ma (e.g. Meriläinen, 1976; Lauerma, 1982). However, some uranium concentration had already taken place in the Saattopora ore at the time of sulfide crystallization. Thus, the ca. 1780 Ma age for the Saattopora thucolite may represent a reset age of a mineral related to gold mineralization or the time of uranium mobilization and thucolite crystallization in the ore.

The Pahtavuoma sulfides have lead isotope characteristics that clearly differ from those of the Saattopora sulfides. This may indicate that the hydrothermal processes responsible for the crystallization of the sulfides with high U/Pb and low Th/U ratios in the Saattopora area were not operating at Pahtavuoma.

## Discussion

The uranogenic lead isotopic compositions of the A- and B-ore sulfides and gold samples reflect approximately coeval crystallization with divergent U/Pb ratios. The slope of the trend gives an apparent age of ca. 1870-1900 Ma for the mineralization. The ca. 2000 Ma isochron age from the sulfides of the Cu-occurrence may then indicate the presence of an older mineralization, possibly syngenetically related to the rift-stage volcanism.

Following the mineralization, the intrusion of the postorogenic granites at ca. 1780 Ma caused either some uranium mobilization and thucolite crystallization in the ore or else only reset the thucolite related to the gold mineralization. The concordant U-Pb-age of ca. 1685 Ma for rutile, together with the gently sloping lead isotope compositional trend (ca. 1700 Ma) for the A- and B-ore wall rocks indicates prolonged continuous or episodic hydrothermal processes in the Saattopora area.

In the C-ore, the disseminated arsenopyrites record either late stage episodic radiogenic lead loss, or else the diffusion of radiogenic lead continued long after mineralization and the intrusion of the postorogenic granites. This interpretation is supported by the very gently sloping uranogenic lead isotope compositional trend of the C-ore sulfides, and a contradictory relationship between the most radiogenic A-ore sulfide, with a very high U/Pb concentration ratio, and the C-ore sulfide with an extremely high U/Pb concentration ratio, corresponding to a relatively low $^{206}Pb/^{204}Pb$ ratio (see Table 7).

The $^{208}Pb/^{204}Pb$ ratios remain almost constant while the $^{206}Pb/^{204}Pb$ ratios of the A-ore sulfides and its immediate wall rocks increase, demonstrating the presence of a fluid with high U/Pb and low Th/U ratios. In contrast, the higher Th/U ratios in B- and C-ore sulfides, as well as in their wall rocks reflect higher Th/U ratios in the fluid, or the incorporation of some thorium from the host rocks. The varying structural and lithological controls of the rock sequences around different ores may have had an effect on the physico-chemical conditions which controlled the mineralization processes. This may be, at least in part, the reason for the slightly vary-

ing Th/U ratios in the different ore related sulfides and wall rocks.

The high uranium contents of the crystallizing sulfides indicate a source area with abundant uranium and also the existence of fluids, that were capable of dissolving uranium. In the Saattopora area earlier uraninite concentrations could represent the high U/Pb environments from which the mineralizing fluid might have leached uranium. The Pahtavuoma, Aakenusvaara, and Pahtavuoma-Kolvakero uraninite occurrences (Inkinen 1979; Pääkkönen 1988 and 1989) for instance, located in the vicinity of the Saattopora ore, indicate the presence of exceptionally high U/Pb environments in the area.

## Hangaslampi and Meurastuksenaho

### Samples

The analysed samples from the Hangaslampi deposit in the Kuusamo district consist of several sulfides, one magnetite fraction, some wall rock samples, and a few carbonates. The extremely radiogenic sulfides are lead-poor, while having high uranium contents (Appendix 4 and Table 7). From the Meurastuksenaho deposit, only one sample containing sulfide and magnetite was available.

### Results

On the uranogenic lead diagram (Fig. 25), the lead isotope compositions of the Hangaslampi carbonates and sulfides define a linear trend with a slope of ca. 0.1113. Regardless of the number of analyses included, the corresponding slope age remains at around 1820 Ma (n=5, 1820±15 Ma; n=10, 1820±31 Ma; n=14, 1822±5 Ma). Neither rejection of the one or two most radiogenic samples (HL-R388/66.85) nor inclusion of only the most radiogenic sulfides alter the slope age significantly.

On the $^{206}Pb/^{204}Pb$ vs. $^{208}Pb/^{204}Pb$ diagram (Fig. 25), the extremely low $^{208}Pb/^{204}Pb$ and high $^{206}Pb/^{204}Pb$ ratios, indicate very low thorium and high uranium contents in the sulfides. In comparison with the sulfides, the wall rock samples show clearly higher relative $^{208}Pb$ contents.

### Discussion

The nearly concordant U-Pb age for the uranium-rich and highly radiogenic pyrrhotite is about 1830 Ma (Table 3 and Fig. 3) and the other radiogenic sulfides show $^{207}Pb/^{206}Pb$ ages around 1820-1850 Ma (Table 4). Taking into account the slope age of the lead compositional trend formed by the Hangaslampi and one of the Meurastuksenaho samples (ca. 1820 Ma), the probable age of sulfide formation can be fixed at around 1820-1850 Ma.

In the Hangaslampi sulfides and magnetites, most of the uranium is apparently located in brannerite inclusions. This is regarded as evidence of approximately coeval crystallization of the sulfides and the inclusions. On the other hand, the other detected brannerite grain lies around the boundary between the sulfide and carbonate grains, with the carbonate tending to occupy fractures in the sulfides and magnetites. In this respect, these results do not preclude the possibility that an older mineralization had already existed in the area.

As with the Saattopora and Pahtavaara ores, the brannerite inclusions in the Hangaslampi sulfides indicate specific fluid conditions, that were also capable of leaching uranium. Again, as at Saattopora, several uranium occurrences have been reported from the Kuusamo area (Vuokko 1988; Vanhanen 1989; Pankka et al. 1991). The concentration of uranium may be genetically connected with the same hydrothermal processes responsible for the sulfide mineralization, although uranium enrichment could also have taken place during earlier hydrothermal episodes in the area.

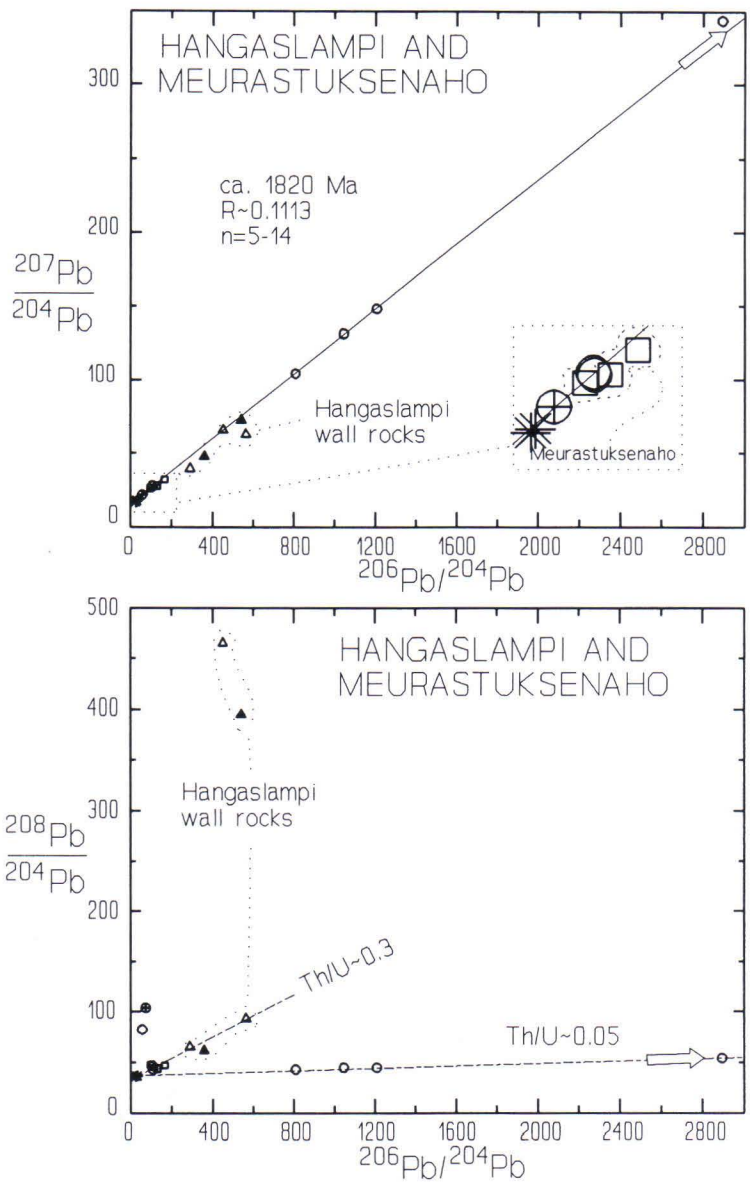


Fig. 25. $^{206}Pb/^{204}Pb$ vs. $^{207}Pb/^{204}Pb$ and $^{206}Pb/^{204}Pb$ vs. $^{208}Pb/^{204}Pb$ plots of the lead isotope data for the Hangaslampi and Meurastuksenaho samples. *Hangaslampi:* ○ =PY, PO; ⊕ =MAGN; ∗ =CRB; ▲ =WR; Δ =LE. *Meurastuksenaho;* □ =MAGN, CP, PO.

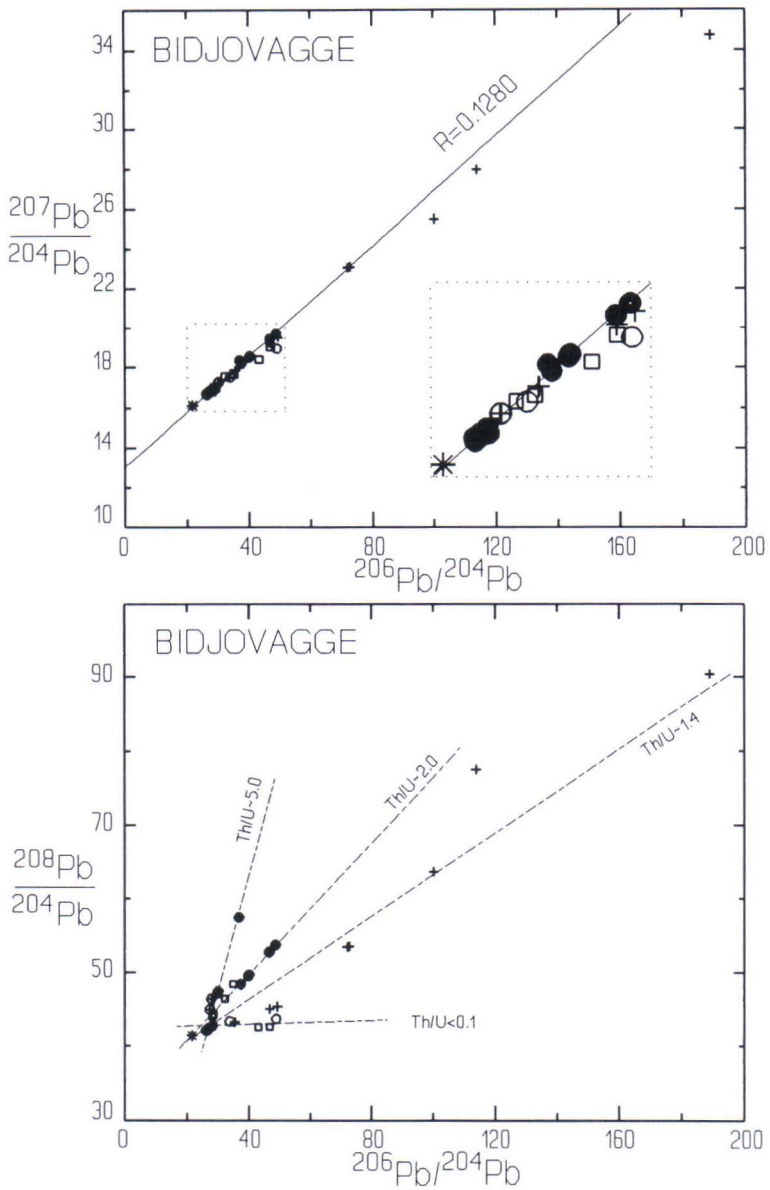


Fig. 26. $^{206}Pb/^{204}Pb$ vs. $^{207}Pb/^{204}Pb$ and $^{206}Pb/^{204}Pb$ vs. $^{208}Pb/^{204}Pb$ plots of the sulphide lead isotope data from the Bidjovagge area. Lead isotope results for the sulfides are grouped according to drill-core and wall rock type. *S154B:* ○ =albite-carbonate rock; ⊕ =metadiabase; • =black schist. *N95F:* + =albite-carbonate rock/coarse grained carbonate rock. *N20E:* □ =albite-carbonate rock. *S186B:* ∗ =GA. The most radiogenic sample lies off the axis.

## Bidjovagge

### Samples

Sulfides hosted by albite felsite, metadiabase, and black schist were sampled from drill cores from the Bidjovagge ore. The lead contents vary between samples, and the $^{206}Pb/^{204}Pb$ ratios in most samples are around 25-50 (Appendix 4 and Table 7).

### Results

On the $^{206}Pb/^{204}Pb$ vs. $^{207}Pb/^{204}Pb$ diagram (Fig. 26), most of the lead isotope compositions of the Bidjovagge sulfides form a sublinear trend with a slope of ca. 0.1280 (n=26) (Fig. 26), corresponding to an apparent age of ca. 2070±67 Ma. However, the most radiogenic chalcopyrite (Appendix 4: N95F/45.30) clearly deviates from the regression line formed by the other sulfides. The wall rock (LE, WR) leads conform to a linear trend with a slope of 0.0727, which corresponds to an age of 1005±19 Ma (not shown). Although the trend depends on the most radiogenic analysis, the slope does not change significantly if this data point is omitted.

On the $^{206}Pb/^{204}Pb$ vs. $^{208}Pb/^{204}Pb$ diagram (Fig. 26), the sulfides define separate trends with different Th/U ratios, depending to some extent on wall rock types. The metadiabase hosted sulfides are moderately radiogenic and possess higher relative $^{208}Pb/^{204}Pb$ ratios than sulfides from the black schist and albitic felsite. The albitic felsite sulfides plot in an area with lower Th/U ratios.

### Discussion

In contrast to the variable $^{206}Pb/^{204}Pb$ ratios of the Saattopora, Hangaslampi, and Pahtavaara sulfides, the Bidjovagge sulfides show a quite restricted range of values at around 30 (Appendix 4 and Fig. 26). The homogenization of the lead may be connected with large scale fluid migration and Pb mobilization in the basement during the Caledonian orogeny (Duane & de Wit, 1988; see also page 19). Accordingly, Bjørlykke et al. (1990) modelled the sulfide lead isotope results from Bidjovagge using a two-stage model and obtained a Svecokarelian source age for radiogenic lead mobilized during the early Palaeozoic times. Similar results (Equation 1: R=0.1280, $T_1$=1850 Ma, $T_2$=425 Ma) could also be obtained using the data of this study. However, the scatter of the data around the regression line indicates incomplete homogenization of the Th-U-Pb systems in all samples.

The significance of the separate trends seen on the $^{206}Pb/^{204}Pb$ vs. $^{208}Pb/^{204}Pb$ plot (Fig. 26) might be spurious. The sulfides on and around the line with the highest Th/U ratios could reflect mobilization and nearly complete homogenization of the lead during the Caledonian orogeny. The others, mainly albite-carbonate rock hosted sulfides occupying the lower relative $^{208}Pb/^{204}Pb$ ratio area, also depart from the uranogenic lead trend (Fig. 26). In these, the lower Th/U ratios might more closely reflect the primary ratios, and thus also indicate the possible existence of low Th/U ratios in sulfides similar to the Saattopora, Hangaslampi, and Pahtavaara sulfides.

In both the uranogenic and thorogenic diagrams, one of the most clearly deviating sulfides is a chalcopyrite sample (BV-N95F/45.30) with a $^{206}Pb/^{204}Pb$ ratio of 189. The $^{207}Pb/^{206}Pb$ age for this sample is ca. 1850 Ma, which is, within error limits, the same as the U-Pb age of 1837 Ma for the Bidjovagge uraninite (Bjørlykke et al., 1990; Cumming et al., 1993). Furthermore, this age represents approximately the same age group as that defined for the Upper Lapponian middle and lower units and the Pahtavaara and Hangaslampi sulfides. The geological significance of the highly discordant $^{207}Pb/^{206}Pb$ ages of ca. 1600 Ma for rutile and titanite (Tables 3 and 4) is equivocal, and these results should only be taken as lower age limits for the minerals. However, as in the case of the Saattopora area, this rough age approximation may reflect prolonged hydrothermal activity in the area.

## SOME ASPECTS RELATING TO FLUID CHARACTERISTICS

The low $^{208}Pb/^{204}Pb$ ratios, which correspond to high $^{206}Pb/^{204}Pb$ ratios in the Saattopora, Hangaslampi, and Pahtavaara sulfides and magnetites, and possibly also in the primary Bidjovagge sulfides, all indicate an extraordinarily low initial Th/U ratio for these minerals. This could reflect a low Th/U ratio for the mineralizing fluid. However, the apparently low $^{208}Pb/^{204}Pb$ ratios of the sulfides related to mineralization do not inevitably indicate thorium poor fluid, since they may alternatively result from fractionation of uranium and thorium between different crystallizing phases. It has also been proposed that an almost total separation of U from Th may occur in hydrothermal fluids under decreasing temperature (Titayeva 1994). Accordingly, uranium titanates (brannerite, davidite) with Th and lanthanides are found in hypothermal deposits, while uranium oxides occur in mesothermal and epithermal deposits. Nonetheless, the existence of uranium-rich inclusions in the sulfides demonstrates that the physico-chemical properties of the fluid were favourable for both leaching and then precipitation of uranium.

The oxidized uranium(VI)-ion (uranyl-ion) readily forms complexes with common water-soluble anions, while thorium may remain unsoluble (e.g. Hostetler & Garrels, 1962; Adamek, 1975; Nash et al., 1981; Ruzicka, 1993). At low temperatures (T<120°C) uranium forms complexes with carbonate, while at higher temperatures it complexes with anions such as chloride, fluoride, sulphate, phosphate, and arsenate. According to Holland (1965, p. 1136-1137), in ore-forming fluid at T=400°C, in the presence of carbonate ($f_{CO_2}$=1 to 100 atm), and with log $f_{O_2}$ between ca. -25 to -31, uraninite can exist in equilibrium with the common sulfides, magnetite, calcite, and quartz. In the presence of such a high oxygen fugacity, gold prefentially complexes with chloride (Jaireth, 1992).

The fluid inclusion and mineral paragenesis studies from many Archaean epigenetic, sulfide-poor, metamorphic gold mineralizations show low NaCl contents (<10 wt-% NaCl-eq.), mineralization temperatures between 300-500°C, reducing fluid conditions (moderate to low $f_{O_2}$), and near neutral to slightly alkaline nature of the $H_2O$-$CO_2$-fluid, in which gold is probably transported as hydrogen sulfide complexes ( $Au(HS)_2$ ) (e.g. Seward, 1973 and 1984; Kerrich, 1983; Phillips & Groves, 1983 and 1984; Colvine et al., 1984; Phillips, 1993; Phillips & Powell, 1993). These fluid characteristics are not favourable for uranium complexing.

However, with the exception of the Pahtavaara ore the Lapland gold deposits are relatively rich in sulfides and differ therefore in this respect from more typical Archaean gold mineralizations. The Archaean atmosphere was poor in oxygen, which is discernible for instance in the lack of evidence (such as sulfate minerals, fractionated sulfide sulfur isotopes) of high marine sulfate contents in massive sulfide mineralizations (Sangster, 1980; Cameron, 1982). The increase in atmospheric oxygen levels during the Palaeoproterozoic time (e.g. Holland, 1962; Karhu, 1993) promoted sedimentation of sulfate-bearing evaporites (Hattori et al., 1983), which could represent a source for oxygenated, metamorphic fluids. Another possible source for oxygenated fluid is sea water, in which gold and base metals are dissolved as chloride complexes: meteoric waters are also oxygenated. Moreover, it has been suggested that felsic magmatism (Cameron & Carrigan, 1987; Cameron & Hattori, 1987) can cause the formation of an oxygenated fluid. Cameron (1988 and 1989) has proposed that even some of the Archaean gold deposits formed in the presence of moderately oxidized fluids, resulting from the introduction of mantle $CO_2$ and partial melting of lower crust, accompanied by release of gold.

If the mineralizing fluid was oxidized, the restricted range of sulfur isotope compositions may be problematic. Normally, when the sulfide minerals crystallize from oxidized fluid they would be expected to show at least some variation due to fractionated sulfur isotope values. However, sulfide deposition under reducing conditions of similar type might be expected to generate quite similar $\delta^{34}S$-values (Ohmoto & Rye, 1979). Also, biased sample material (gold enriched) and the small number of analyses may give a distorted impression of the actual range of sulfur isotope compositions in the area.

In addition to the barite associated with the Pahtavaara gold ore, Lapland records other indications of the presence of a moderately oxidized fluid. Eilu (1994) observed the effects of syn-orogenic, fracture zone related hydrothermal activity with carbonatization and albitization reactions in the Isolaki area. The related fluid had moderate to high fugacities of $O_2$ and $CO_2$ and high $Na^+/K^+$, which are consistent with a magmatic, metamorphic, or sedimentary origin. Furthermore, the fluid inclusion and mineral paragenesis studies from the Bidjovagge (Ettner et al., 1993 and 1994) and Pahtohavare gold ores (Martinsson, 1992; Lindblom & Martinsson, 1990) suggest mineralization in the presence of a saline and oxidized fluid.

## SUMMARY AND DISCUSSION

### An overview

The stratabound base metal deposits and epigenetic gold mineralizations in the Lapland greenstone belt have distinctly different lead isotope characteristics, although a considerable range in compositions has also been recorded from both groups on a deposit scale. In spite of the rather limited sample material, the essential characteristics of the base metal mineralization could be summarized as follows: 1) compared with the Stacey and Kramers (1975) model, the least radiogenic lead isotope compositions show higher μ-values, 2) similarly evolved leads show relatively homogeneous isotope compositions, at least on a deposit scale, and 3) the sulfide minerals are usually rich in lead, and do not show high $^{206}Pb/^{204}Pb$ ratios.

The epigenetic gold deposits and occurrences are divided into two broad groups having different lead isotopic characteristics. The Soretiavuoma, Kiistala, and Kuotko occurrences show relatively nonradiogenic compositions. Furthermore, the least radiogenic compositions of the Soretiavuoma group (Soretiavuoma, Kiistala, Kuotko/Group 1) and Kuotko (Group 2) are isotopically distinctive: the former represent orogenic mixing of mantle and upper crustal lead, and the latter mantle lead with a possible lower crustal component. The highly radiogenic deposits, namely Saattopora, Hangaslampi, and Pahtavaara all show linear to sublinear lead compositional trends on the $^{206}Pb/^{204}Pb$ vs. $^{207}Pb/^{204}Pb$ plots, and the sulfides have extremely low Th/U ratios, mostly due to presence of uranium-rich inclusions. Moreover, and in spite of the Palaeozoic lead homogenization at Bidjovagge, the original lead isotope characteristics might have been similar to the highly radiogenic group. These results are also relevant to mineral exploration, since the economically most interesting deposits typically possess the lead isotope characteristics of the highly radiogenic group.

## Hydrothermal evolution

The lead isotope results from Lapland indicate at least three different phases of orogenic hydrothermal activity that were presumably involved in the epigenetic gold mineralization. These results can be summarized as follows (see also Table 8):

1) Soretiavuoma group: Within the group of deposits containing sulfides with the least radiogenic lead isotope compositions, the Kiistala galena, a lead-rich microfractured pyrite from Kuotko, and the Soretiavuoma samples, all share similar lead isotopic compositions. Each of these deposits is located on the northern side of the Sirkka fracture line, within or near a north-south trending fault zone.

The lead within this group appears to have originated during orogenic mixing of mantle and upper crustal material. All the sulfides show synorogenic model ages (1852-1890 Ma) (Table 4) and the lead analyses form a compositionally homogeneous isotopic group. In addition, the thorogenic lead composition coincides with the average crustal lead growth curve of Stacey and Kramers (1975), and the sulfides are relatively rich in lead. This mineralization event is thought to have coincided with the (early- to) synorogenic phase of the Svecokarelian orogeny and related processes.

A more widespread distribution for this kind of mineralization has not yet been demonstrated, since postmineralization hydrothermal processes could have destroyed the original lead isotopic signatures in other locations. The potential for this type of mineralizating process in producing economically interesting gold deposits may be minor. It may, however, be important for regional scale concentration of gold, prior to further mobilization and upgrading by later hydrothermal processes.

2) Saattopora area: The lead isotopic compositions of the Saattopora A- and B-ore sulfides and gold samples define a sublinear trend, and the corresponding age estimate of ca. 1870-1900 Ma suggests synorogenic mineralization. However, sulfides associated with the copper mineralization give a steeper slope, with an apparent age of ca. 2000 Ma, which is roughly consistent with the age of the surrounding volcanics. In other respects the lead isotope characteristics resemble those of the Hangaslampi and Pahtavaara sulfides. In the C-ore sulfides, a late phase of radiogenic lead depletion is evident.

Thucolite from an ore vein and monazite from the Saattopora area gave ages of ca. 1780 Ma (Table 3), and they are therefore temporally assosiated with the emplacement of the postorogenic granites. The importance of this hydrothermal stage as a gold concentrating process may be relatively minor, because the thucolite age is taken to represent resetting of the U-Pb system or the mobilization of uranium in the area. The U-Pb age for the single rutile extracted from the Saattopora albitic felsite (ca. 1690 Ma), and the apparent Pb-Pb isochron age of ca. 1700 Ma for the Saattopora wall rocks, both plausibly imply prolonged hydrothermal activity in the area. Nevertheless, the effects of these latest events were restricted to disturbance of the U-Pb systems of the more susceptible wall rock minerals.

A late phase of metamorphism, associated with postorogenic granitic intrusions at ca. 1780 Ma is also indicated, for example, by the U-Pb age of titanite from a monzonite (A840; zircon age 1862 Ma) (Hiltunen, 1982), western Lapland. In addition, the ages of uranium-rich minerals from Lapland (Table 3) indicate that uranium was mobile at ca. 1780 Ma. As with the anorogenic disturbances to the U-Pb systems of the Saattopora wall rocks, the whole rock lead isotope data from the Porkonen-Pahtavaara iron formation and from the Toto-Oja felsic volcanics (Appendix 5) give anorogenic slope ages (ca. 1600 Ma). In the

Table 8. Apparent mineralization stages and other hydrothermal processes in the Lapland greenstone belt deduced from lead isotope and age data from gold deposits, base metal deposits, and unmineralized volcanics.

| | SVECOKARELIAN OROGENY | | | | | |
|---|---|---|---|---|---|---|
| DEPOSIT | PRE-OROGENIC | SYNOROGENIC ca.1900-1880 Ma | LATE-OROGENIC ca.1860-1810 Ma | POSTOROGENIC ca. 1800-1770 Ma | ANOROGENIC <1750 Ma | PHANEROZOIC |
| Central Lapland, Upper Lapponian Group: | | | | | | |
| Middle and lower units | volcanism ca. 2200-2050 Ma (Lehtonen et al., 1992) | | METAMORPHISM | | | |
| Kuusamo: | | | | | | |
| Greenstone Formation III | volcanism >2078 ± 8 Ma (Silvennoinen, 1991) | | METAMORPHISM (Silvennoinen, 1991) | | | |
| Jyrävä/quartzite | | | | U-Pb/uraninite (Lauerma & Piispanen, 1967) | | |
| Base metal deposits: | | | | | | |
| Pahtavuoma | mineralization | | | Pb-Pb/uraninite (Vaasjoki, oral com., 1993) | | |
| Riikonkoski, Hormakumpu | mineralization | | | | | radiogenic galena (lead separation) |
| Saattopora | mineralization | | | | | |
| Gold deposits: | | | | | | |
| Saattopora | | MINERALIZATION | | Pb-Pb/thucolite U-Pb/monazite | U-Pb/rutile wall rocks | |
| Pahtavaara | | ? ..... | MINERALIZATION | | | |
| Hangaslampi | | ? ..... | MINERALIZATION U-Pb/pyrrhotite | | | |
| Soretiavuoma | | MINERALIZATION | | | | |
| Kiistala | | MINERALIZATION | | | | |
| Kuotko | | MINERALIZATION (Group 1) ? ..... | MINERALIZATION (Group 2) ..... ? | | U-Pb disturbance in lamprophyre | "porous" pyrite (lead separation) |
| Bidjovagge | | ? ..... | MINERALIZATION U-Pb/uraninite (Cumming et al., 1993) | | resetting of whole-rocks (Bjørlykke et al., 1990) | sulphides (lead separation) |

Bidjovagge area, the whole rock lead isotope data for albitic felsites also reflect anorogenic resetting at 1339±8 Ma (Bjørlykke et al., 1990).

3) Kuotko: In addition to the (early- to) synorogenic Soretiavuoma compositional group, another phase of mineralization having a different lead source is evident at Kuotko. These low-lead sulfides and the related gold sample suggest, on the basis of the Zartman and Doe (1981) model, a mantle lead source with a possible lower crustal component. However, the temporal relations between the two mineralization phases is obscure.

All the other, rather heterogeneous and more radiogenic lead compositions at Kuotko may have diverse origins, such as radiogenic in situ lead addition and later lead mobilization, indicating a multiphase hydrothermal history in the area. The latest local lead separation may have been connected with the Phanerozoic reactivation of a previously existing shear zone.

Phanerozoic (ca. 500-450 Ma) uranium and lead separation in Precambrian host rocks in Finland has previously been recorded from uraninites within some shear zones in southern Finland (Vaasjoki, 1977). These young ages have been linked with the Cambro-Silurian-Ordovician transgression, sedimentation, and diagenesis, whereas the Phanerozoic lead separation in central Lapland may be associated with Caledonian reactivation of the former shear zones.

4) Hangaslampi and Pahtavaara: The sulfides of these deposits, as well as the Saattopora ore, typically have low lead contents and show very high $^{206}Pb/^{204}Pb$ ratios, with low corresponding $^{208}Pb/^{204}Pb$ ratios. After the mineralization, the lead in the sulfides further evolved mainly by addition of uranogenic lead, since the initial lead and uranium contents were in most of the cases low and high, respectively, and the thorogenic lead growth was almost completed at the time of mineralization. The uranium rich inclusions are responsible for the high U/Pb and low Th/U ratios in the sulfides and indicate the involvement of a relatively oxidized fluid. Furthermore, the coexistence of uranium and gold may be a consequence of an anomalously rich uranium and gold source region, in combination with fluid characteristics favouring gold and uranium transportation, and the similar mineralizing conditions, or simultaneous crystallization for uranium rich minerals and gold.

The slope ages for the Hangaslampi and Pahtavaara deposits, the $^{207}Pb/^{206}Pb$ ages of the most radiogenic Hangaslampi sulfides, and the single concordant U-Pb age of the extremely radiogenic Hangaslampi pyrrhotite, all indicate late-orogenic (ca. 1820-1850 Ma), approximately coeval, hydrothermal processes. The U-Pb age from the Bidjovagge uraninite, published by Cumming et al. (1993) falls into the same category. Furthermore, the lead isotope compositions of the unmineralized middle and lower unit volcanics of the Upper Lapponian Group form linear trends with approximately similar slopes corresponding to ages of ca. 1840 and 1870 Ma. This has been attributed to a significant Pb mobilization event, which caused resetting of the U-Pb system in the volcanics. Consequently, these results can be interpreted as indicating the formation of a late-orogenic metamorphic hydrothermal fluid that was also responsible for the gold mineralization.

Implications for the existence of a late-orogenic metamorphic phase (1810-1860 Ma) is indicated by several U-Pb results from the Lapland area. The zircons from the Saaripudas albitite dike (A964; Hiltunen, 1982) cutting across the Kolari greenstone in western Lapland, has a U-Pb age of 2027±33 Ma. However, an age estimate of ca. 1820 Ma from titanite represents the age of metamorphism and recrystallization (Hiltunen, 1982). Moreover, age estimates from the Muonio mapsheet area (Lehtonen 1984), including a value of 1840 Ma for titanite from the Kangosjärvi monzonite (A583) and 1832±7 Ma age for the

Kangosselkä paragneiss (A838) are considered to represent late-orogenic metamorphism. In central Lapland, U-Pb data from a single titanite fraction demonstrates metamorphism of the Kallo quartz-monzonite at about 1832 Ma ago (Olavi Kouvo, 1990, unpublished report of the Laboratory of Isotope Geology, GSF), whereas the intrusive age of this pluton, 1886±4 Ma, has been established by dating of zircons (Lehtonen et al. 1992). In the Kuusamo map-sheet area (Silvennoinen, 1991), a nearly concordant titanite from the greenstone formation III also reflects metamorphism at ca. 1809±18 Ma. The ca. 1800 Ma uraninite age from Jyrävä, Kuusamo (Lauerma & Piispanen, 1967) is also in accordance with this result.

The results of this study indicate similar sulfide lead isotopic characteristics and oxidized fluid conditions for the Saattopora, Hangaslampi, and Pahtavaara mineralizations; a common genesis for these deposits is also therefore implied. However, the differing age estimates for the sulfide mineralizations at Saattopora, and at Pahtavaara and Hangaslampi may demonstrate a time gap between these mineralizations. Alternatively, this may instead be attributed to the existence of a longer lived thermal system at Pahtavaara and Hangaslampi. In contrast to the Saattopora area, no evidence of postorogenic hydrothermal processes was detected in the Hangaslampi and Pahtavaara areas. Therefore the apparent slope ages obtained from the Hangaslampi and Pahtavaara sulfides must be considered as minimum age estimates for the gold mineralization.

5) Bidjovagge: The lead isotope results from sulfides associated with the Bidjovagge ore are in good agreement with previously published interpretations. These include explaining the linear uranogenic lead isotope compositional trend as a two-stage model in which ca. 1850 Ma old lead was separated during the Caledonian orogeny at ca. 420 Ma ago. However, some of the analysed sulfides might have remained unaffected by the Caledonian orogeny. These sulfides may have had low original Th/U ratios, similarly to the Saattopora, Pahtavaara, and Hangaslampi sulfides. Likewise, the age estimates for the late-orogenic hydrothermal phase at Hangaslampi and Pahtavaara, as well as for the metamorphic resetting of the U-Pb systems in the Upper Lapponian volcanics are similar to those obtained for the previously dated Bidjovagge uraninite, ca. 1837 Ma (Cumming et al., 1993). This implies roughly coeval hydrothermal activity throughout central Lapland, and the Kuusamo and Bidjovagge districts.

## COMPARISONS BETWEEN GOLD DEPOSITS IN LAPLAND AND ARCHAEAN LODE GOLD DEPOSITS

### Results from Archaean deposits

#### Lead isotope characteristics

In contrast to the homogeneous lead isotope compositions characteristics of volcanogenic massive sulfide mineralizations (e.g. Stanton & Russell, 1959; Ostic et al., 1967; Cumming & Robertson, 1969; Sato et al., 1981; Godwin et al., 1982; Fehn et al., 1983; Gulson, 1985), lead isotopic studies of epigenetic vein gold mineralization from different terrains and with different ages tend to record heterogeneous compositions, even within a single metallogenic province.

Sulfide lead isotope data from Archaean gold mineralizations often define deposit scale linear uranogenic compositional trends

(Browning et al., 1987; Dahl et al., 1987; Perring & McNaughton, 1990; McNaughton et al., 1990a and 1990b) with quite restricted $^{206}Pb/^{204}Pb$ ranges (e.g. Yilgarn Block, western Australia: ca. 13.0-18.3). Lead isotopes commonly show a provincial character, suggesting a dependence on regional lithology, with different source areas or conduits for the mineralizing fluids (e.g. Zimbabwe: Robertson, 1973; Kramers and Foster, 1984, Australia: Dahl et al., 1987; Perring & McNaughton, 1992, Canada: Hattori, 1993). The lead isotope data from the Ross and Kirkland deposits of the Abitibi belt in Canada have been interpreted as resulting from mixing of the original fluid lead with lead from the channelway host rocks (Hattori, 1993).

The uranogenic lead isotope trends in the Yilgarn craton originated either in Pb mobilization processes postdating the mineralization or in the mixing of leads from different sources at the time of mineralization (McNaughton, 1987). Lead mobilization is supported by observations (McNaughton et al., 1992) that the uranogenic lead compositions of the individual deposits form linear, commonly similary sloping trends, and within such trends, some of the galenas are too radiogenic for any known rock type in the Archaean but could instead have been formed during Proterozoic lead mobilization (Perring and McNaughton, 1990). For each trend, the similarities in least radiogenic lead compositions inside a radius of 100 km and regardless of the degree of metamorphism and the type of host rock (McNaughton et al., 1990a) are all considered to indicate the primary lead composition of the mineralizing fluid.

## Relationships between gold mineralization and orogeny

The relative age of the individual greenstone hosted gold deposits with respect to magmatism, metamorphism, and deformation is in many cases well constrained by the structural relationships between them. Multiphase hydrothermal activity has been documented for instance from the Archaean Norseman-Wiluna mining camp, where petrographical studies of the gold mineralizations indicate pre-, syn-, and post-peak metamorphic fluid activity (McCuaig, 1990). In addition, textural and structural features recorded from the southern Abitibi greenstone hosted gold mineralizations indicate two phases of hydrothermal activity, namely pre- and late-, and postpeak metamorphism (Marquis et al., 1990).

Direct datings of mineralization is usually difficult and a variety of ages can result from the application of different dating methods on different minerals. For example, some of the age determinations on hydrothermal vein minerals and minerals from the alteration halos from the Abitibi greenstone belt, Canada, show "early gold" ages of ca. 2690-2670 Ma (e.g. ca. 2690 Ma/ microprobe U-Pb on hydrothermal zircon: Claoue-Long et al., 1990) coinciding broadly with the regional metamorphism and plutonism at ca. 2.68-2.70 Ga (e.g. Wong et al., 1991; Feng et al., 1992; Hanes et al., 1992). This is in contrast to the "late gold ages" varying between ca. 2625 and 2570 Ma (e.g. 2602±20 Ma/Sm-Nd on scheelite: Anglin, 1990; ca. 2600 Ma/Ar-Ar on muscovite: Hanes et al., 1987, 1989 and 1992; 2577-2625 Ma/U-Pb on rutile and titanite: Jemielita et al., 1989 and 1990; 2570 Ma/Ar-Ar on muscovite: Kerrich et al., 1984; 2624±62 Ma/U-Pb on rutile: Schandl et al., 1990; 2599±9 Ma/U-Pb on rutile: Wong et al., 1989 and 1991), that suggest a distinct time gap between the gold mineralization event, and regional metamorphism and plutonism. Some of the interpretations in favour of "late mineralization" (Colvine et al., 1988; Fyon et al., 1988) advocate continued magmatic and metamorphic fluid activity in the deep crust following the peak of metamorphism.

Kerrich and Cassidy (1994) deal with the

relationships of lode gold mineralization to accretion, magmatism, metamorphism, and deformation. They criticize the relatively young published age data supporting mineralization, mostly in Archaean terranes, ca. 100 to 240 Ma after the terrane accretion. They argue that such young ages are not in accordance with the tectonic, structural, and metamorphic relationships of the mineralized areas but reflect instead reactivation of earlier shear zones and the resetting of the primary isotopic signatures. Kerrich and Cassidy (1994) also presented a generalized appraisal of the relationship between Proterozoic collisional orogenic belts and gold mineralization, according to which, Proterozoic gold mineralization is typically related to post-peak metamorphic brittle-ductile reactivation of the syn-collisional ductile structures during subsequent uplift and cooling.

## Proterozoic vs. Archaean deposits

The lead isotope data from the Palaeoproterozoic greenstone hosted gold deposits in Lapland apparently resemble those from Archaean lode gold deposits in general, but in detail interpretation of the results is rather complicated. Similarities include the regionally observed least radiogenic lead isotope composition (Soretiavuoma group) and the linear trends for the uranogenic sulfide lead isotope compositions (Pahtavaara, Hangaslampi, and Saattopora) having approximately uniform slopes (Pahtavaara and Hangaslampi). In addition, as is the case with the Abitibi Belt and Norseman-Wiluna gold camps, for instance, several phases of hydrothermal action have been revealed in connection with the lead isotopic studies in the Lapland area.

In Lapland, the observed least radiogenic lead composition of the Soretiavuoma group does not necessarily represent the initial lead composition of the gold mineralizing fluid in every deposit. Instead, it is likely to relate to a different type of mineralization process preceding the major hydrothermal activity that accompanied the introduction of gold. Lead isotope compositional trends from Archaean lode gold deposits show limited ranges of $^{206}Pb/^{204}Pb$ ratios, whereas in Lapland, the extraordinarily wide range of ratios in sulfides from some gold prospects indicates the existence of uranium rich inclusions in the sulfides. Therefore the uranogenic compositional trends for the Saattopora, Pahtavaara, and Hangaslampi sulfides are considered to record the decay of uranium from the time of mineralization to the present. Consequently, in contrast to Archaean gold deposits, neither lead mixing nor later mobilization need inevitably be invoked to interpret the majority of the results.

The temporal relationship between gold mineralization in Lapland and orogenic processes agrees well with the views of Kerrich and Cassidy (1994). In the northern Fennoscandian Shield, it has been proposed that metamorphism and shear deformation were roughly coeval (Berthelsen and Marker, 1986; Pharaoh and Brewer, 1990; Bjørlykke et al. 1993). The Soretiavuoma group mineralization, characterized by deformed gold bearing veins most probably took place during the (early-) to synorogenic phase. Moreover, if the so-called synorogenic granitoid magmatism at ca. 1880-1900 Ma was coeval with the metamorphism and shear deformation, the Saattopora mineralization can be correlated with the synorogenic phase. On the other hand, the U-Pb age data from Lapland zircons and titanites indicate the presence of a late-orogenic metamorphic phase ca. 1810-1850 Ma, which is approximately the same age as estimates for the sulfides associated with the Pahtavaara and Hangaslampi deposits. The metamorphism of the Upper Lapponian vol-

canics is also evidently conneceted with this late-orogenic phase, occurring temporally between the intrusions of syn- and postorogenic granitoids. By analogy with the evidence for the timing of gold mineralizations in other areas, the lead isotopes and U-Pb age determinations from the Saattopora area reflect several phases of postorogenic and anorogenic hydrothermal activity, none of which, however, seem to have been significant with respect to primary gold mineralization.

## CONCLUSIONS

The primary purpose of this study was to characterize the lead isotopic signatures of greenstone-hosted epigenetic gold mineralization in Lapland. In addition, the results of some sulfur isotope studies were considered, suggesting a magmatic source for the sulfide sulfur. The main conclusions of the study can be summarized as follows.

1) Based on their sulfide lead isotope characteristics, the epigenetic gold mineralizations can be classified into two groups, a) deposits with relatively nonradiogenic lead compositions and b) deposits with highly radiogenic sulfides. The economically most interesting deposits belong into the latter group. Accordingly, lead isotope characteristics may be used as an adjunct in mineral exploration.

a) Within the nonradiogenic group, the Soretiavuoma compositional group represents a distinctively different type of gold mineralization identified for three deposits, namely Soretiavuoma, Kiistala, and Kuotko. These are all characterized by relatively lead-rich sulfides, homogeneous lead compositions, initial Th/U ratios close to average crustal lead growth values, and lead isotopic compositions coinciding with the Svecokarelian orogenic lead trend determined by Vaasjoki (1981), suggesting orogenic mixing of mantle and upper crustal leads. At Kuotko, a distinctly different lead composition is also present, possibly recording a combination of mantle and lower crustal leads in the lead-poor sulfides and gold concentrate. This indicates that gold mineralization took place in two stages and represent two different sources.

b) The highly radiogenic deposits including Saattopora, Hangaslampi, and Pahtavaara exhibit lead poor and highly radiogenic sulfides with low Th/U and high U/Pb ratios. On the uranogenic lead diagrams analyses define linear to sublinear compositional trends. Because the extremely high $^{206}Pb/^{204}Pb$ ratios in the sulfides are mostly caused by uranium rich inclusions, the physico-chemical characteristics of the fluid were favourable for the uranyl-ion transportation, and thus a relatively oxidized fluid is proposed. The similarities in lead isotope characteristics suggest a common genesis for the mineralization in these deposits.

2) In Lapland, the Svecokarelian orogeny initiated several phases of hydrothermal activity, which continued after the emplacement of the postorogenic granites. Some of the earliest activity was also responsible for the concentration of gold. The lead isotope results for the greenstone-hosted gold mineralization in Lapland allow the following hydrothermal phases to be distinguished and classified in relation to the intrusion of synorogenic and postorogenic granites: i) (Early- to) synorogenic Soretiavuoma group mineralization took place at Soretiavuoma, Kiistala, and Kuotko. ii) Formation of the Saattopora gold ore is connected with the synorogenic processes (ca. 1870-1900 Ma). iii) At Kuotko, a further hydrothermal phase associated with gold mineralization is also evident. iv) The results from the Pahtavaara, Hangaslampi, and Bidjovagge (previously published data) deposits indicate major hydrothermal activity

during the late-orogenic phase, occurring temporally between the intrusion of the synorogenic and postorogenic granites (ca. 1850-1810 Ma). This age approximation is considered as a minimum age estimate for the gold mineralization at Pahtavaara and Hangaslampi. The slightly earlier to approximately coeval (ca. 1840-1870 Ma) regional metamorphism caused resetting of the U-Pb system in the unmineralized lower and middle unit volcanics of the Upper Lapponian Group and may thus reflect related and roughly contemporaneous processes. v) At Saattopora, the intrusion of the postorogenic granites at ca. 1780 Ma reset the U-Pb system in thucolite or alternatively caused mobilization of uranium and thucolite crystallization in the ore veins, as well as the monazite crystallization in the wall rocks adjacent to the ore. vi) At Saattopora, a slow cooling history or a late phase of hydrothermal activity (ca. 1.7 Ga) was responsible for the disturbance of the U-Pb systems in the more susceptible wall rocks. vii) Finally, Phanerozoic lead separation took place in the Bidjovagge area, and apparently was also responsible for the formation of radiogenic galenas in some stratabound base metal deposit in the Kittilä region. In addition, some of the Kuotko sulfides may have been modified in Phanerozoic times.

## ACKNOWLEDGEMENTS

This study was financially supported by the Finnish Academy during the years 1991-1993. I express my thanks to Professor Veikko Lappalainen, Director of the Geological Survey, and to Professor Atso Vorma for making it possible to carry out this work, and for approving publication of this paper as a Bulletin of the Geological Survey of Finland. The official reviewers, Pekka Nurmi and Matti Vaasjoki, as well as Ilmari Haapala and Hannu Huhma are gratefully acknowledged for their valuable comments and suggestions for improving the manuscript. My respectful gratitude also goes to Olavi Kouvo for his continuous enthusiasm in isotope geology and for making unpublished analyses available. In addition, the interest that Juha Karhu has shown in the project is greatly appreciated, as are his suggestions for making the early version of the manuscript more concise.

I am grateful to the personnel of the Mineralogical Laboratory at Geological Survey, namely Säde Harle, Leena Järvinen, Matti Karhunen, Anneli Lindh, and Mirja Saarinen, for the essential work in crushing and milling the samples, and in separating and identifying the minerals, as well as to my co-workers at the isotope laboratory, Lasse Heikkinen and Arto Pulkkinen, for technical assistance and basic training on the old mass spectrometer. My friendly thanks go also to Marita Niemelä and Tuula Hokkanen for the warm atmosphere they generated in the laboratory.

Sample material together with background information on their geological context, and help in choosing the samples were given by several persons from the Outokumpu Finnmines Oy and Geological Survey of Finland, Rovaniemi. They, including Rauno Hugg, Osmo Inkinen, Ilkka Härkönen, and Esko Korkiakoski are all thanked for their co-operation.

In addition, I want to acknowledge the staff of the microprobe laboratory, Bo Johansson, Kari Kojonen, and Lassi Pakkanen, for tracking and analysing the inclusions and mineral grains. Peter Sorjonen-Ward is thanked for the demanding work in revising the English of the manuscript, Eeva Kallio for the ICP-analyses, Juraj Michalko in contributing the sulfur isotope analyses, Stiina Seppänen and Jukka Seutu in editing the text, Jouko Pääkkönen and Andrej Wennström for preparing the thin sections, the ever helpful library staff, and Liisa Sirén and Kirsti Keskisaari for drawing the maps.

## REFERENCES

**Adamek, P.M. 1975.** Geology and mineralogy of the Kopparåsen uraninite-sulphide mineralization, Norrbotten county, Sweden. Sveriges Geol. Unders., Ser. C 712. 69 p.

**Anglin, C.D. 1990.** Preliminary Sm-Nd isotopic analyses on scheelites from Val d'Or, Quebec. Canadian Geol. Surv., Pap. 90-1C, 255-259.

**Ansdell, K.M. & Kyser, T.K. 1992.** Mesothermal gold mineralization in a Proterozoic greenstone belt: Western Flin Flon Domain, Saskatchewan, Canada. Econ. Geol. 87, 1496-1524.

**Anttonen, R., Korkalo, T. & Oravainen, H. 1989.** Lapin kultaa Saattoporan kaivoksesta (in Finnish). English summary: Gold from Lapland - Outokumpu OY's Saattopora mine. Vuoriteollisuus-Bergshanteringen 47, 104-108.

**Baalen, M.R., Van, 1993.** Titanium mobility in metamorphic systems: a review. Chem. Geol. 110, 233-249.

**Bachinski, D.J. 1969.** Bond strength and sulfur isotopic fractionation in coexisting sulfides. Econ. Geol. 64, 56-65.

**Bernard-Griffiths, J., Peucat, J.J., Postaire, B., Vidal, Ph., Convert, J. & Moreau, B. 1984.** Isotopic data (U-Pb, Rb-Sr, Pb-Pb and Sm-Nd) on mafic granulites from Finnish Lapland. Precambrian Res. 23, 325-348.

**Berthelsen, A. & Marker, M. 1986.** 1.9-1.8 Ga old strike-slip megashears in the Baltic Shield, and their plate tectonic implications. Tectonophysics 128, 163-181.

**Bjørlykke, A., Hagen, R. & Söderholm, K. 1987.** Bidjovagge copper-gold deposit in Finnmark, northern Norway. Econ. Geol. 82, 2059-2075.

**Bjørlykke, A., Cumming, G.L. & Krstic, D. 1990.** New isotopic data from davidites and sulfides in the Bidjovagge gold-copper deposit, Finnmark, northern Norway. Mineral. Petrol. 43, 1-21.

**Bjørlykke, A., Nilsen, K.S., Anttonen, R. & Ekberg, M. 1993.** Geological setting of the Bidjovagge deposit and related gold-copper deposits in the northern part of the Baltic Shield. *In:* Maurice, Y.T. (ed.), Proceedings of the Eight Quadrennial IAGOD Symposium. Ottawa, Canada, August 12-18, 1990, 667-680.

**Browning, P., Groves, D.I., Blockley, J.G. & Rosman, K.J.R. 1987.** Lead isotope constraints on the age and source of gold mineralization in the Archean Yilgarn block, western Australia. Econ. Geol. 82, 971-986.

**Cameron, E.M. 1982.** Sulphate and sulphate reduction in early Precambrian oceans. Nature 296, 145-148.

**Cameron, E.M. 1988.** Archean gold: Relation to granulite formation and redox zoning in the crust. Geology 16, 109-112.

**Cameron, E.M. 1989.** Derivation of gold by oxidative metamorphism of a deep ductile shear zone: Part 1. Conceptual model. J. Geochem. Explor. 31, 135-147.

**Cameron, E.M. & Carrigan, W.J. 1987.** Oxygen fugacity of Archean felsic magmas: relationship to gold mineralization. Geol. Surv. Canada, Current Res., Part A., Paper 87-1A, 281-298.

**Cameron, E. M. & Hattori, K. 1987.** Archean gold mineralization and oxidized hydrothermal fluids. Econ. Geol. 82, 1177-1191.

**Cannon, R.S. & Pierce, A.P. 1967.** Isotopic varieties of lead in stratiform deposits. Econ. Geol., Monogr. 3, 427-433.

**Cannon, R.S. & Pierce, A.P. 1969.** Lead isotope guides for Mississippi Valley lead-zinc exploration. U.S. Geol. Surv., Bull. 1312-G, G1-G20.

**Cannon, R.S., Stieff, L.R. & Stern, T.W. 1958.** Radiogenic lead in non radioactive minerals: a clue in the search for uranium and thorium. U.N. Int. Conf. Peaceful Uses of At. Energy Proc. 2, 215-223.

**Cannon, R.S., Pierce, A.P., Antweiler, J.C. & Buck, K.L. 1961.** The data of lead isotope geology related to problems of ore genesis. Econ. Geol. 56, 1-38.

**Carlson, L. 1991.** The Pahtohavare copper-gold prospect. Geol. Fören. Stockholm Förh. 113, 45-46.

**Carlson, L., Hålenius, U. & Johansson, L. 1988.** Pahtohavare, a new copper gold deposit in the Kiruna greenstone belt, northern Sweden. Bicentennial Gold 88, Extended abstracts, Poster programme, Geol. Soc. Australia, Abstracts Series 23, p. 175.

**Claoue-Long, J.C., King, R.W., & Kerrich, R. 1990.** Archean hydrothermal zircon in the Abitibi greenstone belt: Constraints on the timing of gold mineralization. Earth Plan. Sci. Lett. 98, 109-128.

**Colvine, A.C., Andrews, A.J., Cherry, M.E., Durocher, M.E., Fyon, A.J., Lavigne, M.J., Macdonald, A.J., Marmount, S., Poulsen, K.H., Springer, J.S. & Troop, D.G. 1984.** An integrated model for the origin of Archean lode gold deposits. Ontario Geol. Surv., Open File Rep. 5524. 98 p.

**Colvine, A.C., Fyon, J.A., Heather, K.B., Marmont, S., Smith, P.M. & Troop, D.G. 1988.** Archean lode gold deposits in Ontario. Ontario Geol. Surv., Misc. Pap. 139. 136 p.

**Cumming, G.L. & Robertson, D.K. 1969.** Isotopic

composition of lead from the Pine Point deposit. Econ. Geol. 64, 731-732.

**Cumming, G.L., Krstic, D., Bjørlykke, A. & Aasen, H. 1993.** Further analyses of radiogenic minerals from the Bidjovagge gold-copper deposit, Finnmark, Northern Norway. Mineral. Petrol. 49, 63-70.

**Dahl, N., McNaughton, N.J. & Groves, D.I. 1987.** A lead isotope study of sulfides associated with gold mineralization in selected gold deposits from the eastern goldfields of western Australia. Geol. Dept. Univ. Extens., Univ. Western Australia, Publ. No. 11, 189-201.

**Dodson, M.H. 1973.** Closure temperature in cooling geochronological and petrological systems. Contrib. Mineral. Petrol. 40, 259-274.

**Dodson, M.H. 1976.** Kinetic processes and thermal history of slowly cooling solids. Nature 259, 551-553.

**Dodson, M.H. 1981.** Thermochronometry. Nature 293, 606-607.

**Doe, B.R. & Stacey, J.S. 1974.** The application of lead isotopes to the problems of ore genesis and ore prospect evaluation: A review. Econ. Geol. 69, 757-776.

**Duane, M.J. & de Wit, M.J. 1988.** Pb-Zn ore deposits of the northern Caledonides: Products of continental-scale fluid mixing and tectonic expulsion during continental collision. Geology 16, 999-1002.

**Eilu, P. 1994.** Hydrothermal alteration in volcanosedimentary rocks in the Central Lapland greenstone belt, Finland. Geol. Surv. Finland, Bull. 374. 145 p.

**Ettner, D.C., Bjørlykke, A. & Andersen, T. 1993.** Fluid evolution and Au-Cu genesis along a shear zone: a regional fluid inclusion study of shear zone-hosted alteration and gold and copper mineralization in the Kautokeino greenstone belt, Finnmark, Norway. J. Geochem. Explor. 49, 233-267.

**Ettner, D.C., Bjørlykke, A & Andersen, T. 1994.** A fluid inclusion and stable isotope study of the Proterozoic Bidjovagge Au-Cu deposit, Finnmark, northern Norway. Mineral. Deposita 29, 16-29.

**Faure, G. 1977.** Principles of isotope geology. New York: John Wiley & Sons. 464 p.

**Fehn, U., Doe, B.R. & Delevaux, M.H. 1983.** The distribution of lead isotopes and origin of Kuroko ore deposits in the Hokuroku district, Japan. Econ. Geol., Mon. 5, 488-506.

**Feng, R., Kerrich, R., McBride, S. & Farrar, E. 1992.** $^{40}Ar/^{39}Ar$ age constraints on the thermal history of the Archaean Abitibi greenstone belt and the Pontiac subprovince: implications for terrane collision, differential uplift, and overprinting of gold deposits. Can. J. Earth Sci. 29, 1389-1411.

**Force, E.R. 1991.** Geology of titanium-mineral deposits. Geol. Soc. Am., Spec. Pap. 259, 112 p.

**Frietsch, R. 1991.** New ore types in the northern part of the Fennoscandian Shield. Geol. Fören. Stockholm Förh. 113, 46-48.

**Fyon, J.A., Troop, D.G., Marmont, S. & Mcdonald, A.J. 1988.** Introduction of gold into Archean crust, Superior Province, Ontario - coupling between mantle-initiated magmatism and lower crustal thermal maturation. Econ. Geol., Mon. 6, 479-490.

**Gaál, G. 1990.** Tectonic styles of Early Proterozoic ore deposition in the Fennoscandian Shield. Precambrian Res. 46, 83-114.

**Gaál, G. & Gorbatschev, R. 1987.** An outline of the Precambrian evolution of the Baltic Shield. Precambrian Res. 35, 15-52.

**Gaál, G. & Ward, P. 1990.** Comparisons between Late Archaean and Early Proterozoic tectonics and mineralization in the Fennoscandian Shield. *In:* Glover, J.E. and Ho, S.E. (eds.), Third International Archaean Symposium, Perth, 1990. Extended abstracts volume. Geoconferences Inc. Perth, 55-57.

**Geological Map, Northern Fennoscandia, 1:1 000 000.** Geological Surveys of Finland, Norway and Sweden. Helsinki 1987.

**Gjelsvik, T. 1958.** Epigenetiske koppermineraliseringer på Finnmarksvidda (in Swedish). Nor. Geol. Unders. 203, 49-59.

**Godwin, C.I., Sinclair, A.J. & Ryan, B.D. 1982.** Lead isotope models for the genesis of carbonate-hosted Zn-Pb, shale-hosted Ba-Zn-Pb and silver-rich deposits in the northern Canadian Cordillera. Econ. Geol. 77, 82-94.

**Groves, D.I. & Phillips, G.N. 1987.** The genesis and tectonic control on Archaean gold deposits of western Australian shield - a metamorphic replacement model. Ore Geol. Rev. 2, 287-322.

**Gulson, B.L. 1985.** Shale-hosted lead-zinc deposits in northern Australia: lead isotope variations. Econ. Geol. 80, 2001-2012.

**Gulson, B.L. 1986.** Lead isotopes in mineral exploration. Developments in Economic Geology, 23. Elsevier. 245 p.

**Gulson, B.L. & Mizon, K.J. 1979.** Lead isotopes as a tool for gossan assessment in base metal exploration. J. Geochem. Explor. 11, 299-320.

**Gulson, B.L., Korsch, M.J., Cameron, M., Vaasjoki, M., Mizon, K.J., Porritt, P.M., Carr, G.R., Kamper, C., Dean, J.A. & Calvez, J-Y. 1984.** Lead isotope ratio measurements using the isomass 54E in fully automatic mode. Int. J. Mass

Spectrom. Ion Proc. 59, 125-142.

**Hanes, J.A., Archibald, D.A., Hodgson, C.J. & Robert, F. 1987.** Timing of Archean Au-mineralization in Sigma mine by $^{40}Ar/^{39}Ar$ dating. Geol. Assoc. Canada, Program with Abstracts v. 12, p. A52.

**Hanes, J.A., Archibald, D.A., Hodgson, C.J. & Robert, F. 1989.** Preliminary $^{40}Ar/^{39}Ar$ geochronology and timing of Archean gold mineralization at the Sigma mine, val d'Or, Quebec. Canada Geol. Surv., Pap. 89-1C, 135-142.

**Hanes, J.A., Archibald, D.A., Hodgson, C.J. & Robert, F. 1992.** Dating of auriferous quartz vein deposits in the Abitibi greenstone belt, Canada: $^{40}Ar/^{39}Ar$ evidence for a 70- to 100-M.y.-time gap between plutonism-metamorphism and mineralization. Econ. Geol. 87, 1849-1861.

**Härkönen, I. 1992.** Tutkimustyöselostus Kittilän kunnassa valtausalueella Suurikuusikko 1, Kaiv. rek. n:o 4283/1 suoritetuista malmitutkimuksista (in Finnish). Unpubl. Report M 06/2743/-92/1/10, Geol. Surv. Finland. 5 p.

**Härkönen, I. & Karvinen, A. 1987.** Kertomus Keski-Lapin vihreäkivivyöhykkeen kultaprojektin toiminnasta vuonna 1986 (in Finnish). Unpubl. Report 28.1.1987, Ore prospecting group of northern Finland, Geol. Surv. Finland, 28-36.

**Härkönen, I. & Keinänen, V. 1989.** Exploration of structurally controlled gold deposits in the Central Lapland greenstone belt. Current Research 1988, Geol. Surv. Finland, Spec. Paper 10, 79-82.

**Hattori, K. 1993.** Diverse metal sources of Archaean gold deposits: evidence from in situ lead-isotope analysis of individual grains of galena and altaite in the Ross and Kirkland Lake deposits, Abitibi greenstone belt, Canada. Contrib. Mineral. Petrol. 113, 185-195.

**Hattori, K., Krouse, H.R. & Campbell, F.A. 1983.** The start of sulfur oxidation in continental environments. About 2.2 x $10^9$ years ago. Science 221, 549-551.

**Hiltunen, A. 1982.** The Precambrian geology and skarn iron ores of the Rautuvaara area, northern Finland. Geol. Surv. Finland, Bull. 318, 133 p.

**Holland, H.D. 1962.** Model for the evolution of the earth's atmosphere. *In:* Engel, A.E.J., James, H.L. & Leonard, B.F. (eds.), Petrologic studies - A volume in honour of A.F. Buddington, Geol. Soc. America, 447-477.

**Holland, H.D. 1965.** Some applications of thermochemical data to problems of ore deposits II. Mineral assemblages and the composition of ore-forming fluids. Econ. Geol. 60, 1101-1166.

**Hostetler, P.B. & Garrels, R.M. 1962.** Transportation and precipitation of uranium and vanadium at low temperatures, with special reference to sandstone-type uranium deposits. Econ. Geol. 57, 137-167.

**Huhma, H. 1986.** Sm-Nd, U-Pb and Pb-Pb isotopic evidence for the origin of the early Proterozoic Svecokarelian crust in Finland. Geol. Surv. Finland, Bull. 337, 48 p.

**Hulkki, H. 1990.** Sodankylän Sattasvaaran komatiittikompleksin Au-kriittinen muuttumisvyöhyke (in Finnish). Unpubl. M.Sc thesis. Univ. Helsinki, Dept. Geol. Mineral. 190 p.

**Inkinen, O. 1979.** Copper, zink, and uranium occurrences at Pahtavuoma in the Kittilä greenstone complex, northern Finland. Econ. Geol. 74, 1153-1165.

**Inkinen, O. 1985.** Kittilän Sirkan kulta-kupariesiintymästä (in Finnish). English summary: Gold-copper occurrence at Sirkka, Kittilä. Geologi 37, 8-11.

**Jaffey, A.H., Flynn, K.F., Glendenin, L.E., Bentley, W.C. & Essling, A.M. 1971.** Precision measurement of half-lives and specific activities of $^{235}U$ and $^{238}U$. Phys. Rev. C 4, 1889.

**Jaireth, S. 1992.** The calculated solubility of platinum and gold in oxygen-saturated fluids and the genesis of platinum-palladium and gold mineralization in the unconformity-related uranium deposits. Mineral. Deposita 27, 42-54.

**Jemielita, R.A., Davis, D.W., Krogh, T.E. & Spooner, E.T.C. 1989.** Chronological constraints on the origin of Archean lode gold deposits in the southern Superior province from U-Pb isotopic analysis of hydrothermal rutile and sphene. Geol. Soc. America, Abstracts with Programs 21, p. A351.

**Jemielita, R.A., Davis, D.W. & Krogh, T.E. 1990.** U-Pb evidence for Abitibi gold mineralization postdating greenstone magmatism and metamorphism. Nature 346, 831-834.

**Johansson, Å. 1983.** Lead isotope composition of Caledonian sulfide-bearing veins in Sweden. Econ. Geol. 78, 1674-1688.

**Johansson, Å. & Rickard, D. 1984.** Isotopic composition of Phanerozoic ore leads from the Swedish segment of the Fennoscandian Shield. Mineral. Deposita 19, 249-255.

**Kajiwara, Y. & Krouse, H.R. 1971.** Sulfur isotope partitioning in metallic sulfide systems. Can. J. Earth Sci. 8, 1397-1408.

**Karhu, J.A. 1993.** Paleoproterozoic evolution of the carbon isotope ratios of sedimentary carbonates in the Fennoscandian Shield. Geol. Surv. Finland, Bull. 371. 87 p.

**Keinänen, V. 1987.** Vein-type gold occurrence in Soretiavuoma carbonate rocks, Finnish Lapland. Program and abstracts: Gold '87. Turku, Finland 12.-13.5.1987. Univ. Turku, Instit. Geol. Miner-

al., Publication No 19, p. 8.

**Keinänen, V., Johansson, P. & Lehmuspelto, P. 1988.** Soretiavuoman volframi- ja kultatutkimuksista (in Finnish). *In:* Lappalainen, V. & Papunen, H. (eds.), Tutkimuksia geologian alalta. Ann. Univ. Turkuensis. Sarja C, osa 68, 69-77.

**Kerrich, R. 1983.** Geochemistry of gold deposits in the Abitibi greenstone belt. The Canadian Inst. Mining Met., Spec. Vol. 27. 75p.

**Kerrich, R. & Fyfe, W.S. 1981.** The gold-carbonate association: source of $CO_2$, and $CO_2$ fixation reactions in Archean lode deposits. Chem. Geol. 33, 265-294.

**Kerrich, R. & Cassidy, K.F. 1994.** Temporal relationships of lode gold mineralization to accretion, magmatism, metamorphism and deformation — Archean to present: A review. Ore Geol. Rev. 9, 263-310.

**Kerrich, R., Kishida, A., Wilmore, L.M. & Fryer, B.J. 1984.** Timing of Abitibi belt lode gold deposits: Evidence from $^{49}Ar/^{40}Ar$ and $^{87}Rb/^{87}Sr$ (abs.). Geol. Assoc. Canada, Program with Abstracts v. 9, p. A78.

**Kojonen, K. & Johansson, B. 1989.** Pahtavaaran Au-malmiaiheen malmimineraaleista (in Finnish). Unpublished Report M 40/3714/-99/1/41.2, Sodankylä, Pahtavaara, Geol. Surv. Finland, 2 p.

**Korkiakoski, E.A. 1987.** Mineralogical and geochemical alteration of the komatiite-associated Pahtavaara gold prospect, Northern Finland. Program and Abstracts; Gold '87, Turku, Finland 12.-13.5.1987. Univ. Turku, Inst. Geol. Mineral., Publication No 19, p. 4.

**Korkiakoski, E.A. 1992.** Geology and geochemistry of the metakomatiite-hosted Pahtavaara gold deposit in Sodankylä, northern Finland, with emphasis on hydrothermal alteration. Geol. Surv. Finland, Bull. 360. 96 p.

**Korkiakoski, E.A., Karvinen, A. & Pulkkinen, E. 1989.** Geochemistry and hydrothermal alteration of the komatiite-hosted Pahtavaara gold mineralization, Finnish Lapland. Current Res. Geol. Surv. Finland, Spec. Paper 10, 83-89.

**Kousa, J., Marttila, E. & Vaasjoki, M. 1994.** Petrology, geochemistry and dating of Paleoproterozoic metavolcanic rocks in the Pyhäjärvi area, Central Finland. Geol. Surv. Finland, Spec. Pap. 19, 7-27.

**Kouvo, O. 1958.** Radioactive age of some Finnish Pre-Cambrian minerals. Bull. Comm. Geol. Finlande 182. 70 p.

**Kouvo, O. & Kulp, J.L. 1961.** Isotopic composition of Finnish galenas. Ann. N.Y. Acad. Sci. 91, 476-491.

**Kramers, J.D. & Foster, R.P. 1984.** A reappraisal of lead isotope investigations of gold deposits in Zimbabwe. *In:* Foster, R.P. (ed.), Gold '82. The geology, geochemistry and genesis of gold deposits. A.A. Balkema, Rotterdam 1984. Geol. Soc. Zimbabwe, Spec. Publ. No. 1, 569-582.

**Krill, A.G., Bergh, S., Lindahl, I., Mearns, E.W., Often, M., Olerud, S., Olesen, O., Sandstad, J.S., Siedlecka, A. & Solli, A. 1985.** Rb-Sr, U-Pb and Sm-Nd isotopic dates from Precambrian rocks in Finnmark. Nor. Geol. Unders., Bull. 403, 37-54.

**Krogh, T.E. 1973.** A low-contamination method for hydrothermal decomposition of zircon and extraction of U and Pb for isotopic age determinations. Geochim. Cosmochim. Acta 37, 485-494.

**Kröner, A. & Compston, W. 1990.** Archaean tonalitic gneiss of Finnish Lapland revisited: zircon ion-microprobe ages. Contrib. Mineral. Petrol. 104, 348-352.

**Kröner, A., Puustinen, K. & Hickman, M. 1981.** Geochronology of an Archaean tonalitic gneiss dome in northern Finland and its relation with an unusual overlying volcanic conglomerate and komatiitic greenstone. Contrib. Mineral. Petrol. 76, 33-41.

**Kulikov, V.S., Galdobina, L.P., Voinov, A.S., Golubev, A.I., Kashpirov, S.I., Polehovsky, Yu.S. & Svetov, A.P. 1980.** Jatulian geology of the Paanajärvi-Kuolajärvi synclinorium. *In:* Silvennoinen, A. (ed.), Jatulian geology in the eastern part of the Baltic Shield. Proceedings of a Finnish-Soviet Symposium held in Finland 21st-26th August 1979. The committee for Scientific and Technical Co-operation between Finland and Soviet Union. Rovaniemi, 73-96.

**Laajoki, K. 1990.** Early Proterozoic tectofacies in eastern and northern Finland. *In:* Naqvi, S.M. (ed.), Precambrian continental crust and its economic resources. Amsterdam: Elsevier. 437-452.

**Lamberg, P. & Toikkanen, P. 1991.** Chemical, petrographical and mineralogical study of five mineralized drill holes containing Au-Cu-(Te) ore (C2-, C3, C4-, E- and K-ore) and its immediate surroundings in Bidjovagge Au-Cu-ore, Finnmark, Norway - with interpretations of adjacent alterations. Outokumpu/Mining Services, Geoanalytical Laboratory. Unpublished report 074/Bidjo, ore types/PPL, PT/1991, 126 p.

**Lambert, I.B., Phillips, G.N. & Groves, D.I. 1984.** Sulphur isotope compositions and genesis of Archaean gold mineralization, Australia and Zimbabwe. *In:* Foster, R.P. (ed.), Gold '82: The geology, geochemistry and genesis of gold deposits. A.A. Balkema, Rotterdam 1984. Geol. Soc. Zimbabwe, Spec. Publ. No. 1, 373-387.

**Lauerma, R. 1982.** On the ages of some granitoid and schist complexes in northern Finland. Bull.

Geol. Soc. Finland 54, 85-100.

**Lauerma, R. & Piispanen, R. 1967.** Worm-shaped casts in Precambrian quartzite from Kuusamo, northeastern Finland. Comptes Rendus Soc. Geol. Finlande 39, 189-197.

**Lehtonen, M. 1984.** Muonion kartta-alueen kallioperä. Summary: Pre-Quartenary rocks of the Muonio map-sheet area. Explanation to the maps of the Pre-Quartenary rocks, sheet 2723 Muonio. Geological map of Finland, 1:100 000, 71 p.

**Lehtonen, M., Manninen, T., Rastas, P., Väänänen, J., Roos, S.I. & Pelkonen, R. 1984.** Geological map of Central Lapland, northern Finland, 1:200 000.

**Lehtonen, M., Manninen, T., Rastas, P., Väänänen, J., Roos, S.I. & Pelkonen, R. 1985.** Keski-Lapin geologisen kartan selitys (in Finnish). Summary and discussion: Explanation to the geological map of Central Lapland. Geol. Surv. Finland, Rep. Invest. 71. 56 p.

**Lehtonen, M., Manninen, T., Rastas, P. & Räsänen, J. 1992.** On the Early Proterozoic metavolcanic rocks in Finnish Central Lapland. *In:* Balagansky, V.V. & Mitrofanov, F.P. (eds.), Correlation of Precambrian formations of the Kola-Karelian region and Finland. Russian Academy of Sciences, Kola Science Centre and Geological Institute, Apatity 1992, 65-85.

**Lindblom, S. & Martinsson, O. 1990.** Fluids associated with Cu-Au mineralization in the Kiruna greenstone belt at Viscaria and Pahtohavare, northern Sweden. *In:* Robert, F., Sheahan, P.A. & Green, S.B. (eds.), Greenstone gold and crustal evolution, Nuna Conference Volume, Abstracts, Geol. Ass. Canada, Mineral Deposits Division, p. 185.

**Ludwig, K.R. 1980.** Calculation of uncertainties of U-Pb isotope data. Earth Plan. Sci. Lett. 46, 212-220.

**Ludwig, K.R. 1990.** Isoplot. A plotting and regression program for radiogenic-isotope data, for IBM-PC compatible computers. U. S. Geol. Surv., Open-file Report 88-557. 31 p.

**Mäkelä, K. 1968.** Sirkka-muodostumasta ja sen stratigrafian yleispiirteistä Keski-Lapin liuskealueella (in Finnish). Unpubl. Phil. Lic. thesis, Oulu University, Geol. Dept. 88 p.

**Mäkelä, M. & Tammenmaa, J. 1978.** Lapin rikkiisotooppitutkimus vuosina 1974-1976 (in Finnish). English summary: Sulfur isotope studies in Finnish Lapland 1974-1976. Geol. Surv. Finland, Rep. Invest. 24. 64 p.

**Manninen, T. 1991.** Sallan alueen vulkaniitit (in Finnish). English summary: Volcanic rocks in the Salla area, northeastern Finland. A report of the Lapland Volcanite Project. Geol. Surv. Finland, Rep. Invest. 104. 97 p.

**Manninen, T., Hanski, E. & Kesola, Reino, 1987.** Lapland volcanite project, Annual Report 1986 (in Finnish). Unpublished Report K/1987/1, Geol. Surv. Finland. 47 p.

**Marquis, P., Hubert, C. & Brown, A.C. 1990.** Timing and control of hydrothermal activity in relation to the tectonic evolution of the Dumagami structural zone of the Bousquet gold district, southern Abitibi greenstone belt. *In:* Glover, J.E. & Ho, S.E. (eds.), Third International Archaean Symposium, Perth, 1990. Extended abstracts Vol., p. 389.

**Martinsson, O. 1991.** Geological and geochemical evidence for the genesis of the Viscaria Cu-deposit, northern Sweden. Geol. Fören. Stockholm Förh. 113, 58-59.

**Martinsson, O. 1992.** The Viscaria and Pahtohavare sulfide deposits and the stratigraphy of the Kiruna greenstones. Research Programme Ore Geology Related to Prospecting (Ramprogrammet Prospekteringsinriktad Malmgeologi), Dept. Econ. Geol., Luleå University of Technology, Project nr 88-05116 P. 79 p.

**McCuaig, T.C. 1990.** Characterizing Archean Au-mineralization at Norseman, W.A.: pre- or post-peak metamorphic timing? *In:* Glover, J.E. & Ho, S.E. (eds.), Third International Archaean Symposium, Perth, 1990. Extended abstracts Vol., 421-422.

**McNaughton, N.J. 1987.** Lead isotope systematics for Archaean sulphide studies. *In:* Ho, S.E. & Groves, D.I. (eds.), Recent advances in understanding Precambrian gold deposits. Geol. Dept. (Key Centre) & Univ. Extension, Univ. West. Australia, Publ. 11, 181-188.

**McNaughton, N.J., Cassidy, K.F., Dahl, N., Groves, D.I., Perring, C.S. & Sang, J.H. 1990a.** 2.3. Sources of ore fluid and ore components. 2.3.1. Lead isotope studies. *In:* Ho, S.E., Groves, D.I. & Bennett, J.M. (eds.), Gold deposits of the Archaean Yilgarn craton, western Australia: Nature, genesis and exploration guides. Geol. Dept. (Key Centre) & Univ. Extension, Univ. West. Australia, Publ. 20, 226-236.

**McNaughton, N.J., Cassidy, K.F., Groves, D.I., & Perring, C.S. 1990b.** Constraints on genesis of primary gold deposits. Timing of mineralization. *In:* Ho, S.E., Groves, D.I. & Bennett, J.M. (eds.), Gold deposits of the Archaean Yilgarn Craton, western Australia: Nature, genesis and exploration guides. Geol. Dept. (Key Centre) & Univ. Extension, Univ. West. Australia, Publ. 20, 221-225.

**McNaughton, N.J., Cassidy, K.F., Dahl, N., de Laeter, J.R., Golding, S.D., Groves, D.I., Ho, S.E., Mueller, A.G., Perring, C.S., Sang, J.H.**

**& Turner, J.V. 1992.** The source of ore components in lode-gold deposits of the Yilgarn Block, western Australia. *In:* Glover, J.E. & Ho, S.E. (eds.), The Archaean: Terrains, processes and metallogeny. Geol. Dept. (Key Centre) & Univ. Extension, Univ. West. Australia, Publ. 22, 351-363.

**Meriläinen, K. 1976.** The granulite complex and adjacent rocks in Lapland, northern Finland. Geol. Surv. Finland, Bull. 281. 129 p.

**Mezger, K., Hanson, G.N. & Bohlen, S.R. 1989.** High-precision U-Pb ages of metamorphic rutile: application to the cooling history of high-grade terranes. Earth Plan. Sci. Lett. 96, 106-118.

**Mikkola, E. 1941.** The general geological map of Finland. Sheets Muonio-Sodankylä-Tuntsajoki. Explanation to the map of the rocks. B7-C7-D7, 1:400 000. 286 p.

**Mutanen, T. 1989.** Koitelainen intrusion and Keivitsa-Satovaara complex. Excursion guide, 5th International Platinum symposium. Geol. Surv. Finland, Guide 28. 49p.

**Nash, J.T., Granger, H.C. & Adams, S.S. 1981.** Geology and concepts of genesis of important types of uranium deposits. Econ. Geol., 75th Anniv. Vol., 63-116.

**Nilsen, K.S. & Bjørjykke, A. 1991.** Geological setting of the Bidjovagge gold-copper deposit, Finnmark, northern Norway. Geol. Fören. Stockholm Förh. 113, 60-61.

**Nurmi, P.A. 1991.** Geological setting, history of discovery and exploration economics of Precambrian gold occurrences in Finland. J. Geochem. Explor. 39, 273-287.

**Nurmi, P.A. & Sorjonen-Ward, P. (eds.), 1993.** Geological development, gold mineralization and exploration methods in the Late Archean Hattu schist belt, Ilomantsi, Eastern Finland. Geol. Surv. Finland, Spec. Paper 17. 386 p.

**Nurmi, P.A., Lestinen, P. & Niskavaara, H. 1991.** Geochemical characteristics of mesothermal gold deposits in the Fennoscandian Shield, and a comparison with selected Canadian and Australian deposits. Geol. Surv. Finland, Bull. 351. 101 p.

**Ohmoto, H. & Rye, R.O. 1979.** Isotopes of sulphur and carbon. *In:* Barnes, H.L. (ed.), Geochemistry of hydrothermal ore deposits. New York: John Wiley, 509-567.

**Olsen, K.I. & Nilsen, K.S. 1985.** Geology of the southern part of the Kautokeino greenstone belt, West-Finnmark; Rb-Sr geochronology and geochemistry of associated gneisses and late intrusions. Nor. Geol. Unders., Bull. 403, 131-160.

**Ostic, R.G., Russell, R.D. & Stanton, R.L. 1967.** Additional measurements of the isotopic composition of lead from stratiform deposits. Can. J. Earth Sci. 4, 245-269.

**Paakkola, J. 1971.** The volcanic complex and associated magnaniferous iron formation of the Porkonen-Pahtavaara area in Finnish Lapland. Bull. Comm. Geol. Finlande 247. 83 p.

**Pääkkönen, K. 1988.** Uraanimalmitutkimukset Pahtavuoman-Kolvakeron alueella Kittilässä ja Muoniossa vuosina 1982-1985 (in Finnish). Unpubl. Report M19/2741/-88/1/60, Geol. Surv. Finland. 34 p.

**Pääkkönen, K. 1989.** Uraanimalmitutkimukset Aakenusvaran länsiosassa Kittilässä 19811-1982 (in Finnish). Unpubl. Report M19/2741/-89/1/60, Geol. Surv. Finland. 22 p.

**Padget, P. 1959.** Leucodiabase and associated rocks in the Karelidic zone of Fennoscandia. Geol. Fören. Stockh. Förh. 81, 316-332.

**Pankka, H. 1989.** Epigeneettiset Au-Co-U-malmiesiintymät Kuusamon liuskealueella (in Finnish). Unpubl. Phil. Lic. thesis, Univ. Turku, Dept. Geol. Mineral. 126 p.

**Pankka, H.S. & Vanhanen, E.J. 1992.** Early Proterozoic Au-Co-U mineralization in the Kuusamo district, northeastern Finland. Precambrian Res. 58, 387-400.

**Pankka, H., Puustinen, K. & Vanhanen, E. 1991.** Kuusamon liuskealueen kulta-koboltti-uraaniesiintymät (in Finnish). English summary: Au-Co-U-deposits in the Kuusamo volcano-sedimentary belt, Finland. Geol. Surv. Finland, Rep. Invest. 101. 53 p.

**Patchett, P.J., Kouvo, O., Hedge, C.E. and Tatsumoto, M. 1981.** Evolution of continental crust and mantle heterogeneity: evidence from Hf isotopes. Contrib. Mineral. Petrol. 78, 279-297.

**Perring, C.S. & McNaughton, N.J. 1990.** Proterozoic remobilization of ore metals within Archaean gold deposits: lead isotope evidence from Norseman, western Australia. Aust. J. Earth Sci. 37, 369-372.

**Perring, C.S. & McNaughton, N.J. 1992.** The relationship between Archaean gold mineralization and spatially associated minor intrusions at the Kambalda and Norseman gold camps, western Australia: Lead isotope evidence. Mineral. Deposita 27, 10-22.

**Pharaoh, T.C. & Brewer, T.S. 1990.** Spatial and temporal diversity of early Proterozoic volcanic sequences - comparisions between the Baltic and Laurentian shields. Precambrian Res. 47, 169-189.

**Phillips, G.N. 1993.** Metamorphic fluids and gold. Mineral. Magazine 5, 365-374.

**Phillips, G.N. & Groves, D.I. 1983.** The nature of Archean gold-bearing fluids as deduced from gold deposits of Western Australia. J. Geol. Soc. Aust. 30, 25-39.

**Phillips, G.N. & Groves, D.I. 1984.** Fluid access and fluid-wall rock reactions in the genesis of the Archean gold-quartz vein deposit at the Hunt mine, Kambalda, Western Australia. *In:* Foster, R.P. (ed.), Gold '82, Geol. Soc. Zimbabwe, Spec. Publ. No. 1., Rotterdam: Balkema, 389-416.

**Phillips, G.N. & Powell, R. 1993.** Link between gold provinces. Econ. Geol. 88, 1084-1098.

**Pihlaja, P. & Manninen, T. 1988.** The metavolcanic rocks of the Peurasuvanto area, northern Finland. *In:* Marttila, E. (ed.), Archaean geology of the Fennoscandian Shield. Proceedings of a Finnish - Soviet Symposium in Finland, 28.7.-7.8.1986. The Committee for Scientific and Technical co-operation between Finland and the Soviet Union. Geol. Surv. Finland, Spec. Paper 4, 201-213.

**Puustinen, K. 1977.** Exploration in the northeast region of the Koitelainen gabbro complex, Sodankylä, Finnish Lapland. *In:* Davis, G.R. (ed.), Prospecting in the areas of glaciated terrain, Inst. Min. Met., London, 6-13.

**Puustinen, K. 1985.** Kittilän Riikonkosken alueen vulkanismi (in Finnish). Summary: Volcanism and ore deposits in the Riikonkoski area, Kittilä, Finnish Lapland. Geologi 37, 38-44.

**Rastas, P. 1980.** Stratigraphy of the Kittilä area. *In:* Silvennoinen A. (ed.), Jatulian geology in the eastern part of the Baltic Shield. Proceedings of a Symposium held in Finland 21st-26th August, 1979. The committee for Scientific and Technical Co-operation between Finland and the Soviet Union, 143-153.

**Rickard, D.T. 1978.** The Svecokarelian anomalous ore lead line. Geol. Fören. Stockholm Förh. 100, 19-29.

**Robertson, D.K. 1973.** A model discussing the early history of the earth based on the study of lead isotopes from veins in some Archaean cratons of Africa. Geochim. Cosmochim. Acta 37, 2099-2124.

**Roddick, J.C. & Compston, W. 1977.** Strontium isotopic equilibration: a solution to a paradox. Earth Plan. Sci. Lett. 34, 238-246.

**Romer, R.L. 1989a.** Interpretation of the lead isotopic composition from sulfide mineralizations in the Proterozoic Sjangeli area, northern Sweden. Nor. Geol. Unders., Bull. 415, 57-69.

**Romer, R.L. 1989b.** Implications of isotope data on the metamorphism of the basic volcanites from the Sjangeli window, northern Sweden. Nor. Geol. Unders., Bull. 415, 39-56.

**Romer, R.L. 1989c.** Trace lead composition of sulfides from mineralizations in the Proterozoic Råppe supracrustal belt, northern Sweden. Geol. Fören. Stockholm Förh. 111, 155-160.

**Romer, R.L. 1990.** Lead mobilization during foreland metamorphism in orogenic belts: Examples from northern Sweden. Geol. Rundschau 79, 693-707.

**Romer, R.L. 1991.** Contrasting lead isotopic signature and style of formation of Phanerozoic metamorphogenic metal deposits on the Proterozoic Baltic Shield of northern Europe. *In:* Pagel & Leroy (eds.), Source, transport and deposition of metals. Rotterdam: Balkema, 337-339.

**Romer, R.L. 1993.** Metallogeny and lead isotopic composition of base metal sulfide deposits in the Rappen area, northern Sweden. Mineral. Deposita 28, 37-46.

**Romer, R.L. & Boundy, T.M. 1988.** Interpretation of lead isotope data from the uraniferous Cu-Fe-sulfide mineralizations in the Proterozoic greenstone belt at Kopparåsen, northern Sweden. Mineral. Deposita 23, 256-261.

**Romer, R.L. & Wright, J.E. 1993.** Lead mobilization during tectonic reactivation of the western Baltic shield. Geochim. Cosmochim. Acta 57, 2555-2570.

**Ronde, de, C.E.J., Spooner, E.T.C., De Wit, M.J. & Bray, C.J. 1992.** Shear zone-related, Au-quartz vein deposits in the Barberton greenstone belt, South Africa: Field and petrograpic characteristics, fluid properties, and light stable isotope geochemistry. Econ. Geol. 87, 366-402.

**Ruzicka, V. 1993.** Vein uranium deposits. Ore Geol. Rev. 8, 247-276.

**Saarnisto, M., Tamminen, E. & Vaasjoki, M. 1991.** Gold in bedrock and glacial deposits in the Ivalojoki area, Finnish Lapland. J. Geochem. Explor. 39, 303-322.

**Sakai, H. 1957.** Fractionation of sulfur isotopes in nature. Geochim. Cosmochim. Acta 12, 150-169.

**Sakai, H. 1968.** Isotopic properties of sulfur compounds in hydrothermal processes. Geochem. J. 2, 29-49.

**Sangster, D.F. 1980.** Quantitative characteristics of volcanogenic massive sulphide deposits. Can. Mining Metall. Bull. 73, 74-81.

**Sato, K., Delevaux, M.H. & Doe, B.R. 1981.** Lead isotope measurements on ores, igneous and sedimentary rocks from the Kuroko mineralization area. Geochem. J. 15, 135-140.

**Schandl, E.S., Davis, D.W. & Krogh, T.E. 1990.** Are the alteration halos of massive sulfide deposits syngenetic? Evidence from U-Pb dating of hydrothermal rutile at the Kidd volcanic center, Abitibi subprovince, Canada. Geology 18, 505-508.

**Seward, T.M. 1973.** Thio complexes of gold in hydrothermal ore solutions. Geochim. Cosmochim. Acta 37, 379-399.

**Seward, T.M. 1984.** The transport and deposition of

gold in hydrothermal systems. *In:* Foster, R.P. (ed.), Gold '82. Rotterdam, Balkema, 165-181.

**Silvennoinen, A. 1985.** On the Proterozoic stratigraphy of Northern Finland. Geol. Surv. Finland, Bull. 331, 107-116.

**Silvennoinen, A. 1991.** Kuusamon ja Rukatunturin kartta-alueiden kallioperä (in Finnish). Summary: Pre-Quaternary rocks of the Kuusamo and Rukatunturi map-sheet areas. Explanation to the maps of Pre-Quartenary rocks, Sheets 4524, 45542, 4613. Geological map of Finland 1:100 000, 62 p.

**Silvennoinen, A., Honkamo, M., Juopperi, H., Lehtonen, M., Mielikäinen, P., Perttunen, V., Rastas, P., Räsänen, J. & Väänänen, J. 1980.** Main features of the stratigraphy of the North Finland. *In:* Silvennoinen, A. (ed.), Jatulian geology in the eastern part of the Baltic Shield. Proceedings of a Finnish-Soviet Symposium held in Finland 21st-26st August, 1979. The committee for scientific and technical co-operation between Finland and Soviet Union, 153-162.

**Skiöld, T. 1986.** On the age of the Kiruna greenstones, northern Sweden. Precambrian Res. 32, 35-44.

**Skiöld, T. 1987.** Aspects of the Proterozoic geochronology of northern Sweden. Precambrian Res. 35, 161-167.

**Skiöld, T. & Cliff, R.A. 1984.** Sm-Nd and U-Pb dating of early Proterozoic mafic-felsic volcanism in northernmost Sweden. Precambrian Res. 26, 1-13.

**Söderholm, K. & Nixon, F. 1988.** Geology, exploration and exploitation of high grade gold zones, Bidjovagge mine, northern Norway. Bicentennial Gold 88, Extended Abstracts Vol 1, Geol. Soc. Australia, Abstracts 23, 210-211.

**Sorjonen-Ward, P. Claoué-Long, J. & Huhma, H. 1994.** SHRIMP isotope studies of granulite zircons and their relevance to Early Proterozoic tectonics in northern Fennoscandia. 8th Int. Conf. Geochronology, Cosmochronology and Isotope Geology (ICOG 8). Berkeley, California, USA. June 5-11, 1994. Abstracts Vol., p. 229.

**Stacey, J.S. & Kramers, J.D. 1975.** Approximation of terrestial lead isotope evolution by a two-stage model. Earth Planet. Sci. Let. 26, 207-221.

**Stacey, J.S., Zartman, R.E. & Nkomo, I.T. 1968.** A lead isotope study of galenas and selected feldspars from mining districts in Utah. Econ. Geol. 63, 796-814.

**Stanton, R.L. & Russell, R.D. 1959.** Anomalous leads and the emplacement of lead sulfide ores. Econ. Geol. 54, 588-607.

**Steiger, R. & Jäger, E. 1977.** Subcommission on Geochronology: Convention on the use of decay constants in geo- and cosmochronology. Earth Plan. Sci. Lett. 36, 359-362.

**Sundblad, K. 1991.** Evidence for pre-Svecofennian influence in the Proterozoic Cu-Zn-Pb sulphide deposits at Tjåmotis, northern Sweden. Geol. Fören. Stockholm Förh. 113, 64-65.

**Sundblad, K. & Røsholt, B. 1986.** A lead isotopic study of galena and amazonite in the Kiuri-Rassåive sulphide deposits - consequences for the timing of ore forming procesesses in the Proterozoic of northernmost Sweden. 17 Nordiska Geologmötet, Abstracts. Helsingfors 12.-15.5.1986, p. 196.

**Suoperä, S. 1988.** Kittilän Soretiavuoman kultapitoisten karbonaattikivien mineralogia ja muuttumisilmiöt (in Finnish). Unpubl. Phil. Lic. thesis, Univ. Oulu, Geol. Dept., 74 p.

**Tamminen, E. (in prep.).** Saattoporan kultamalmi (in Finnish). Unpubl. Phil. Lic. thesis, Univ. Oulu, Geol. Dept.

**Tatsumi, T. 1965.** Sulfur isotopic fractionation between coexisting sulfide minerals from some Japanese ore deposits. Econ. Geol. 60, 1645-1659.

**Titayeva, N.A. 1994.** Nuclear geochemistry. Advances in science and technology. Moscow: Mir Publishers. 296 p.

**Ustinov, V.I. & Grinenko, V.A. 1965.** Precizionnyj mass-spektrometri eskij metod opredelenija izotopnogo sostava sery (in Russian). Moscow: Nauka. 96 p.

**Vaasjoki, M. 1977.** Phanerozoic resetting of U-Pb ages in some south-Finnish uraninites. Fifth European Colloquium of Geochronology, Cosmochronology and Isotope Geology, Abstract Vol. Pisa, September 5-10, 1977.

**Vaasjoki, M. 1981.** The lead isotopic composition of some Finnish galenas. Geol. Surv. Finland, Bull. 316. 30 p.

**Vaasjoki, M. 1989.** Isotopic studies on the Rauhala base metal deposit and its environment in western Finland. Current Research. Geol. Surv. Finland, Spec. Paper 10, 37-38.

**Vaasjoki, M., in press.** Sulphide leads from Late Archaean and Early Proterozoic mineralization in the Fennoscandian Shield: Constraints on early crust-forming processes. Contrib. Mineral. Petrol.

**Vaasjoki, M. & Kontoniemi, O. 1991.** Isotopic studies from the Proterozoic Osikonmäki gold prospect at Rantasalmi, southeastern Finland. Geol. Surv. Finland, Spec. Paper 12, 53-57.

**Vaasjoki, M., Sorjonen-Ward, P. & Lavikainen, S. 1993.** U-Pb age determinations and sulfide Pb-Pb characteristics from the Late Archean Hattu Schist Belst, Ilomantsi, Eastern Finland. *In:* Nur-

mi, P.A. & Sorjonen-Ward, P. (eds.), Geological development, gold mineralization and exploration methods in the Late Archean Hattu schist belt, Ilomantsi, Eastern Finland. Geol. Surv. Finland, Spec. Paper 17, 103-131.

**Vanhanen, E. 1989.** Uraniferous mineralizations in the Kuusamo schist belt, northeastern Finland. Proceedings of a technical committee meeting on metallogenesis of uranium deposits, 9-12 March 1987, Vienna. International Atomic Energy Agency, Vienna, 169-186.

**Vinogradov, A.P., Tarasov, L.S. & Zykov, S.I. 1959.** Isotopic composition of leads from the ores of the Baltic Shield. Geochemistry 7, 689-749.

**Vuokko, J. 1988.** Kuusamon Kouervaaran kalliopera ja siihen liittyvä uraaniesiintymä (in Finnish). Unpubl. M.Sc. thesis, Univ. Turku, Geol. Dept., 105 p.

**Wahl, W. 1940.** Några iakttagelser angående förekomsten av en ny radioaktiv omvandlingsserie. Finska Kemistsamfundets Medd. 49. p. 88.

**Wahl, W. 1941.** Die Bedeutung der Isotopenforschung für die Geologie. Geol. Rundschau 32, 550-562.

**Ward, P., Härkönen, I., Nurmi, P.A. & Pankka, H. 1989.** Structural studies in the Lapland greenstone belt, northern Finland and their application to gold mineralization. Current Research 1988, Geol. Surv. Finland, Spec. Paper 10, 71-77.

**Ward, P., Nurmi, P., Härkönen, I. & Pankka, H. 1992.** Epigenetic gold mineralization and tectonic evolution of a Lower Proterozoic greenstone terrain in the northern Fennoscandian (Baltic) Shield. *In:* Sarkar, S.C. (ed), Metallogeny related to the tectonics of Proterozoic mobile belts. New Delhi: Oxford & IBH Publishing Co., 37-52.

**Wong, L., Davis, D.W., Hanes, J.A., Archibald, D.A., Hodgson, C.J. & Robert, F. 1989.** An integrated U-Pb and Ar-Ar geochronological study of the Archean Sigma gold deposit, Val d'Or, Quebec (abs.). Geol. Assoc. Canada, Program with Abstracts v. 14, p. A45.

**Wong, L., Davis, D.W., Krogh, T.E. & Robert, F. 1991.** U-Pb zircon and rutile chronology of Archean greenstone formation and gold mineralization in the Val d'Or region, Quebec. Earth Planet Sci. Lett. 104, 325-336.

**York, D. 1969.** Least squares fitting of a straight line with correlated errors. Earth Planet. Sci. Lett. 5, 320-324.

**Zartman, R.E. & Doe, B.R. 1981.** Plumbotectonics - the model. Tectonophysics 75, 135-162.

**Appendix 1.** U-Pb analytical results from the Hetta granite; A891 Kappera, Kittilä and A355 Peltovuoma, Enontekiö.

| Analysed mineral fraction | Concentrations | | Measured | Atomic abundances*: $^{206}Pb = 100$ | | | Atomic ratios** | | | Age(Ma) | | |
|---|---|---|---|---|---|---|---|---|---|---|---|---|
| | $^{238}U/ppm/^{206}Pb$ | | $^{206}Pb/^{204}Pb$ | $^{204}Pb$ | $^{207}Pb$ | $^{208}Pb$ | $^{206}Pb/^{238}U$ | $^{207}Pb/^{235}U$ | $^{207}Pb/^{206}Pb$ | $^{206}Pb/^{238}U$ | $^{207}Pb/^{235}U$ | $^{207}Pb/^{206}Pb$ |
| A891A Kappera zircon/elongated crystals +4.3/-100 | 494.3 | 137.9 | 2440 | 0.03705 | 13.365 | 17.222 | 0.32242 | 5.7227 | 0.12874 | 1801 ± 11 | 1934 ± 6 | 2080 ± 5 |
| A891B Kappera zircon +4.3/-100 | 444.2 | 126.7 | 2796 | 0.03374 | 13.798 | 19.862 | 0.32969 | 6.0704 | 0.13355 | 1836 ± 11 | 1986 ± 7 | 2145 ± 4 |
| A891C Kappera zircon/elongated crystals +4.2/+100 | 610.5 | 169.0 | 3210 | 0.02941 | 13.955 | 12.319 | 0.31991 | 5.9847 | 0.13569 | 1789 ± 10 | 1973 ± 6 | 2173 ± 4 |
| A891D Kappera zircon +4.2/+100 | 529.9 | 151.4 | 3579 | 0.02695 | 14.124 | 11.572 | 0.33026 | 6.2706 | 0.13771 | 1839 ± 9 | 2014 ± 5 | 2198 ± 3 |
| A891E Kappera zircon/elongated crystals 4.2-4.3/+300 | 765.7 | 187.7 | 1858 | 0.05127 | 12.332 | 22.197 | 0.28330 | 4.5467 | 0.11642 | 1607 ± 9 | 1739 ± 14 | 1902 ± 27 |
| A891F Kappera zircon 4.2-4.3/+300 | 719.5 | 179.5 | 2715 | 0.03588 | 12.378 | 21.137 | 0.28828 | 4.7282 | 0.11896 | 1632 ± 9 | 1772 ± 7 | 1940 ± 10 |
| A891G Kappera titanite 3.4-3.5 | 92.26 | 25.43 | 841.3 | 0.1179 | 12.439 | 21.992 | 0.31863 | 4.7572 | 0.10829 | 1783 ± 15 | 1777 ± 13 | 1770 ± 22 |
| A891H Kappera zircon/HF 4.2-4.3/-300 | 522.6 | 136.7 | 6514 | 0.01247 | 11.576 | 22.467 | 0.30232 | 4.7545 | 0.11407 | 1702 ± 10 | 1776 ± 5 | 1865 ± 3 |
| A891I Kappera zircon 4.2-4.3/-300 | 581.2 | 144.0 | 2505 | 0.03734 | 11.803 | 23.609 | 0.28629 | 4.4589 | 0.11297 | 1622 ± 11 | 1723 ± 7 | 1847 ± 5 |
| A355A Peltovuoma zircon +4.6/-100 | 347.2 | 98.81 | 3187 | 0.03019 | 13.917 | 13.989 | 0.32889 | 6.1322 | 0.13524 | 1832 ± 8 | 1994 ± 4 | 2167 ± 4 |
| A355B Peltovuoma zircon/HF, crushed 4.2-4.6/-100/ | 749.3 | 199.8 | 5453 | 0.01751 | 12.519 | 11.822 | 0.30815 | 5.2199 | 0.12286 | 1731 ± 8 | 1855 ± 4 | 1998 ± 3 |
| A355C Peltovuoma zircon/HF +4.2/+100 | 649.4 | 169.3 | 3269 | 0.02981 | 13.270 | 10.314 | 0.30126 | 5.3478 | 0.12875 | 1697 ± 8 | 1876 ± 5 | 2081 ± 5 |
| A355D Peltovuoma zircon/HF, crushed 4.0-4.2/100-200 | 1148 | 256.9 | 4099 | 0.02388 | 11.353 | 11.612 | 0.25871 | 3.9344 | 0.11030 | 1483 ± 7 | 1620 ± 4 | 1804 ± 3 |
| A355E Peltovuoma zircon/HF 4.0-4.3/+100 | 1363 | 264.6 | 1349 | 0.07324 | 13.322 | 12.898 | 0.22441 | 3.8202 | 0.12347 | 1305 ± 7 | 1597 ± 5 | 2007 ± 6 |

* = Blank corrected values; ** = Corrected for blank and age related common lead (Stacey and Kramers 1975). All analyses by Olavi Kouvo, GSF.

**Appendix 1.** Continued.

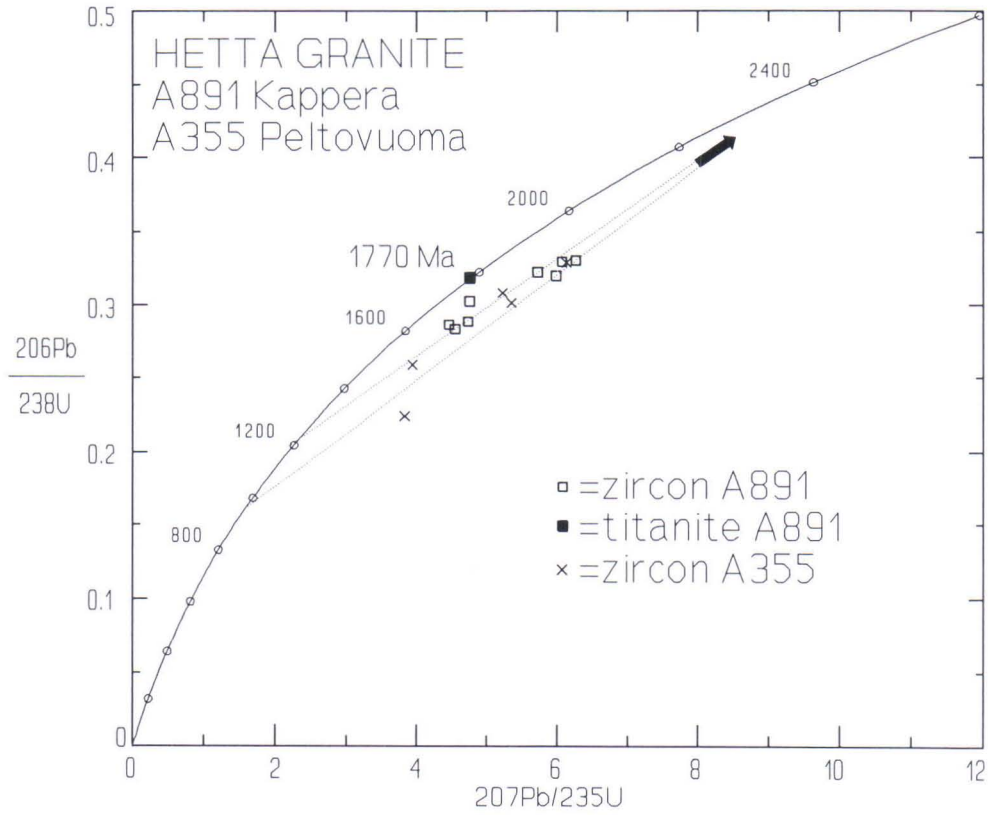


**Appendix 2.** Explanation of abbreviations used in text.

| | |
|---|---|
| WR | total dissolution of whole-rock sample |
| LE | acid leach of whole-rock sample |
| SULF | sulfide mineral |
| PY | pyrite |
| CP | chalcopyrite |
| ASPY | arsenopyrite |
| PO | pyrrhotite |
| MAGN | magnetite |
| GA | galena |
| APA | apatite |
| CRB | carbonate |
| TITA | titanite |
| HMF | hand magnet fraction (PO, MAGN) |

**Appendix 3.** Lead isotope compositions of selected Upper Lapponian volcanics from the Central Lapland greenstone belt.

| SAMPLE NO/ FORMATION | | LOCATION | ROCK TYPE (UNIT)* | LEAD ISOTOPE RATIOS 206/204 | 207/204 | 208/204 | 207/206 | 208/206 |
|---|---|---|---|---|---|---|---|---|
| 7412 | Veikasenmaa | Kiimarova | pillow lava (3) | 38.168 | 17.786 | 37.341 | 0.4660 | 0.9786 |
| 7472 | Veikasenmaa | Kiimarova | pillow lava (3) | 73.607 | 21.916 | 42.886 | 0.2977 | 0.5826 |
| 9771 | Veikasenmaa | Veikasenmaa | pillow lava (3) | 20.368 | 15.743 | 37.385 | 0.7730 | 1.8355 |
| 9782 | Veikasenmaa | Veikasenmaa | basic porphyrite (3) | 20.082 | 15.613 | 38.539 | 0.7775 | 1.9191 |
| 9701 | Veikasenmaa | Veikasenmaa | basic lava (3) | 20.996 | 15.718 | 36.527 | 0.7486 | 1.7397 |
| 5165 | Vesmajärvi | Rajala | Mg-tholeiite (3) | 17.726 | 15.384 | 35.287 | 0.8679 | 1.9907 |
| 5155 | Vesmajärvi | Järvikäinen | basic lava (3) | 17.916 | 15.426 | 37.332 | 0.8610 | 2.0837 |
| 5489 | Vesmajärvi | Järvikäinen | pillow lava (3) | 20.295 | 15.756 | 36.161 | 0.7763 | 1.7818 |
| 5333 | Vesmajärvi | Penikkajärvi | pillow lava (3) | 15.385 | 15.185 | 34.857 | 0.9870 | 2.2657 |
| 5170 | Vesmajärvi | Rajala | Mg-tholeiite (3) | 30.056 | 16.892 | 38.564 | 0.5620 | 1.2831 |
| 10090 | Linkupalo | Linkupalo | pillow lava (2) | 49.324 | 18.975 | 76.698 | 0.3847 | 1.5550 |
| 10093 | Linkupalo | Linkupalo | pillow lava (2) | 50.224 | 18.974 | 74.902 | 0.3778 | 1.4914 |
| 10098 | Linkupalo | Linkupalo | pillow lava (2) | 36.352 | 17.346 | 59.092 | 0.4772 | 1.6256 |
| 10220 | Köngäs | Köngäs | pillow lava (2) | 46.613 | 18.488 | 62.028 | 0.3966 | 1.3307 |
| 10225 | Köngäs | Köngäs | pillow lava (2) | 30.625 | 17.019 | 50.847 | 0.5557 | 1.6603 |
| 10474 | Sinermä | Palovaara | basic lava (2) | 96.405 | 24.210 | 104.37 | 0.2511 | 1.0826 |
| 10490 | Sinermä | Palovaara | basic lava (2) | 40.078 | 17.851 | 54.058 | 0.4454 | 1.3488 |
| 6579 | Tarvasenvaara | Tarvasenvaara | amygdale lava (2) | 28.986 | 16.662 | 44.756 | 0.5748 | 1.5440 |
| 5963 | Kautoselkä | Kivipurnuvaara | Fe-tholeiite (2) | 18.913 | 15.542 | 38.984 | 0.8218 | 2.0612 |
| 9299 | Peuramaa | Peuramaa | picritic lava (1) | 15.751 | 15.226 | 35.360 | 0.9667 | 2.2450 |
| 9336 | Peuramaa | Peuramaa | picritic lava (1) | 23.723 | 16.124 | 41.519 | 0.6797 | 1.7502 |
| 8924 | Jeesiörova | Jeesiörova | komatiitic lava (1) | 15.504 | 15.199 | 35.039 | 0.9803 | 2.2600 |
| 8938 | Jeesiörova | Jeesiörova | komatiitic lava (1) | 15.787 | 15.216 | 35.059 | 0.9638 | 2.2207 |
| 8805 | Sattasvaara | Visakuppura | basalttic komatiite (1) | 15.410 | 15.167 | 34.967 | 0.9842 | 2.2691 |
| 5482 | Sattasvaara | Visakuppura | peridotitic komatiite (1) | 15.767 | 15.212 | 35.028 | 0.9648 | 2.2216 |
| 5655 | Sattasvaara | Visakuppura | peridotitic komatiite (1) | 15.617 | 15.222 | 35.173 | 0.9747 | 2.2522 |
| 7711 | Sattasvaara | Mikkuurova | Mg-basalt (1) | 24.651 | 16.241 | 45.439 | 0.6589 | 1.8433 |
| 6621 | Sattasvaara | Sattasvaara | peridotitic komatiite (1) | 17.539 | 15.505 | 36.283 | 0.8840 | 2.0687 |
| 6629 | Sattasvaara | Vanttion Rolli | peridotitic komatiite (1) | 19.177 | 15.623 | 36.499 | 0.8147 | 1.9033 |

(UNITS)*: Lower (1), middle (2), and upper (3) volcanic units of the Upper Lapponi Group (Lehtonen et al. 1992).
Source of samples: Pentti Rastas and Jorma Räsänen, GSF (Lapland Volcanite Project).

**Appendix 4.** Lead isotope compositions of selected sulfides, carbonates, and adjacent wall rocks from stratabound base metal and epigenetic gold deposits in the Lapland greenstone belt.

| ANAL. NO. | DEPOSIT/ SAMPLE | MINERALIZATION TYPE/ ORE MINERALS | HOST ROCK | ANALYSED FRACTION | ANALYSED MINERAL | *Pb* | LEAD ISOTOPE RATIOS 206/204 | 207/204 | 208/204 | 207/206 | 208/206 |
|---|---|---|---|---|---|---|---|---|---|---|---|
| 59AB-le | PVU/EIM-91-6 | | black schist | acid leach | LE | b-db | 15.943 | 15.333 | 35.319 | 0.9617 | 2.2153 |
| 59-wr | PVU/EIM-91-6 | | black schist | total dissolution | WR | b-db | 16.020 | 15.325 | 35.281 | 0.9566 | 2.2024 |
| 118## | PVU/EIM-91-6 | breccia/cp,aspy | black schist | fr.nm.0.6A | ASPY,CP | bl | 15.489 | 15.295 | 35.221 | 0.9875 | 2.2740 |
| 119## | PVU/EIM-91-6 | breccia/cp,aspy | black schist | fr.nm.0.6A; -200 | ASPY,CP | bl | 15.478 | 15.276 | 35.156 | 0.9869 | 2.2713 |
| 126 | PVU/EIM-91-6 | breccia/cp,aspy | black schist | fr.nm.0.6A; +200 | CP | db-bl | 15.527 | 15.286 | 35.187 | 0.9845 | 2.2662 |
| 129## | PVU/EIM-91-6 | breccia/cp,aspy | black schist | fr.nm.0.6A | GA | | 15.468 | 15.304 | 35.207 | 0.9894 | 2.2762 |
| 41 | G202/Hormakumpu | breccia/py,cp,po | black schist | several fractions | GA | | 24.316 | 16.498 | 44.712 | 0.6785 | 1.8388 |
| 44 | G202/Hormakumpu | breccia/py,cp,po | black schist | fr.m.1.4A; +100 | PY(dull) | db | 23.881 | 16.411 | 43.930 | 0.6872 | 1.8396 |
| 45 | G202/Hormakumpu | breccia/py,cp,po | black schist | fr.nm.1.4A; +100 | PY | db-bl | 24.162 | 16.436 | 44.330 | 0.6802 | 1.8347 |
| 46 | G202/Hormakumpu | breccia/py,cp,po | black schist | fr.m.1.4A; +100 | CP | db | 24.676 | 16.639 | 44.482 | 0.6743 | 1.8026 |
| 208A | G202/Hormakumpu | breccia/py,cp,po | black schist | | GA | | 23.931 | 16.351 | 43.964 | 0.6833 | 1.8371 |
| 208B | G202/Hormakumpu | breccia/py,cp,po | black schist | | GA | | 24.029 | 16.395 | 44.230 | 0.6823 | 1.8407 |
| 188A | G127/Alakylä | shear plane/ga,cp,py | black schist | | GA | | 24.316 | 16.463 | 45.054 | 0.6770 | 1.8528 |
| 188B | G127/Alakylä | shear plane/ga,cp,py | black schist | | GA | | 24.455 | 16.469 | 44.327 | 0.6734 | 1.8126 |
| 189A | G178/Riikonkoski | breccia/po | ab-se schist | | GA | | 24.458 | 16.471 | 44.339 | 0.6734 | 1.8128 |
| 189B | G178/Riikonkoski | breccia/po | ab-se schist | | GA | | 24.403 | 16.478 | 44.203 | 0.6753 | 1.8113 |
| 209AB | G228/Riikonkoski | sulf-crb vein/po,cp,ga | ab-se schist | | GA | | 14.692 | 15.153 | 34.671 | 1.0314 | 2.3599 |
| 96 | SV-R307/48.4-48.5 | (crb-)sulf-qtz vein/cp | umr/crb-ab-ch rock | fr.m.0.6A | CP | db | 15.270 | 15.177 | 35.033 | 0.9935 | 2.2932 |
| 100## | SV-R307/48.4-48.5 | (crb-)sulf-qtz vein/cp | umr/crb-ab-ch rock | fr.nm. 0.6A; +200 | CP | db-bl | 15.298 | 15.199 | 35.094 | 0.9935 | 2.2941 |
| 97 | SV-R307/48.4-48.5 | (crb-)sulf-qtz vein/cp | umr/crb-ab-ch rock | d<3.3 | CRB(inclusions) | - | 15.280 | 15.166 | 34.990 | 0.9926 | 2.2900 |
| 144## | SV-R307/48.4-48.5 | (crb-)sulf-qtz vein/cp | umr/crb-ab-ch rock | fr.nm.0.6A/n.2mg | Pb-rich | | 15.297 | 15.192 | 35.081 | 0.9931 | 2.2933 |
| 144b | SV-R307/48.4-48.5 | (crb-)sulf-qtz vein/cp | umr/crb-ab-ch rock | fr.nm.0.6A | ASPY | lb | 15.279 | 15.178 | 35.043 | 0.9934 | 2.2936 |
| 135 | SV-R307/48.7-48.8 | crb-sulf breccia/py | umr/crb-ab-ch rock | d<3.3; acid leach | CRB | lb | 15.294 | 15.178 | 35.035 | 0.9924 | 2.2907 |
| 60AB | SV-R307/48.7-48.8 | crb-sulf breccia/py | umr/crb-ab-ch rock | fr.m.1.4A | PY | db | 15.298 | 15.189 | 35.036 | 0.9929 | 2.2903 |
| 72-le | SV-R307/55.3-55.4 | | umr/crb-ab-ch rock | acid leach | LE | - | 15.695 | 15.229 | 34.992 | 0.9704 | 2.2296 |
| 72-wr | SV-R307/55.3-55.4 | | umr/crb-ab-ch rock | total dissolution | WR | - | 16.861 | 15.338 | 35.016 | 0.9096 | 2.0767 |
| 201-w | KU/panned | sulf-crb breccia/aspy,po | mtuf/crb-ab rock | acid leach | GOLD | - | 18.009 | 15.531 | 37.629 | 0.8624 | 2.0894 |
| 201 | KU/panned | sulf-crb breccia/aspy,po | mtuf/crb-ab rock | total dissolution | GOLD | - | 15.364 | 15.117 | 35.026 | 0.9839 | 2.2797 |
| 23 | KU-R305/7.95 | sulf-crb breccia/aspy,po | mtuf/crb-ab rock | d<3.3 | CRB(bulk) | - | 15.679 | 15.149 | 35.027 | 0.9662 | 2.2339 |
| 16 | KU-R305/7.95 | sulf-crb breccia/aspy,po | mtuf/crb-ab rock | hand magnet | PO(bulk) | - | 15.516 | 15.133 | 34.963 | 0.9753 | 2.2534 |
| 11 | KU-R305/7.95 | sulf-crb breccia/aspy,po | mtuf/crb-ab rock | fr.m.<0.2A; +200 | PO | - | 15.255 | 15.111 | 34.927 | 0.9906 | 2.2896 |

BV = Bidjovagge; HL = Hangaslampi; KU = Kuotko; LAM = Lammasvuoma; MA = Meurastuksenaho; PV = Pahtavaara; PVU = Pahtavuoma; SK = Suurikuusikko; SP(A,B,C) = Saattopora gold ore/ A-, B-, C-ores; SP-Cu = Saattopora Cu-mineralization; SV = Soretiavuoma; diss = dissemination; ab = albite; amph = amphibole; bar = barite; bt = biotite; ch = chlorite; crb = carbonate; qtz = quartz; se = sericite; sulf = sulfide; tlc = talc; tour = tourmaline; tre = tremolite; ASPY = arsenopyrite; CP = chalcopyrite; GA = galena; LE = acid leach of whole rock powder; MAGN = magnetite; PO = pyrrhotite; PY = pyrite; WR = total dissolution of whole rock powder; graph-schist = graphite-rich schist; mtuf = mafic tuffite; metased = metasedimentary; umr = ultramafic rock; d = density; fr.nm/fr.m. = non magnetic/magnetic fraction with a specific current; +200,-100 = size fractions; Pb* = the colour of the anode precipitation (- = colourless, llb = brownish, lb = light brown, b = brown, db = dark brown, bl = black).

**Appendix 4.** Continued 2/7.

| ANAL. NO. | DEPOSIT/ SAMPLE | MINERALIZATION TYPE/ ORE MINERALS | HOST ROCK | ANALYSED FRACTION | ANALYSED MINERAL | *Pb* | LEAD ISOTOPE RATIOS 206/204 | 207/204 | 208/204 | 207/206 | 208/206 |
|---|---|---|---|---|---|---|---|---|---|---|---|
| 35 | KU-R305/7.95 | sulf-crb breccia/aspy,po | mtuf/crb-ab rock | fr.m.<0.2A;-200 | PO(aspy) | lb | 15.378 | 15.130 | 34.985 | 0.9839 | 2.2750 |
| 10 | KU-R305/7.95 | sulf-crb breccia/aspy,po | mtuf/crb-ab rock | fr.nm.0.6A; +200 | ASPY | - | 15.335 | 15.120 | 34.938 | 0.9860 | 2.2783 |
| 36 | KU-R305/7.95 | sulf-crb breccia/aspy,po | mtuf/crb-ab rock | fr.nm.0.6A; -200 | ASPY | - | 15.397 | 15.124 | 34.950 | 0.9823 | 2.2699 |
| 12 | KU-R305/7.95 | sulf-crb breccia/aspy,po | mtuf/crb-ab rock | fr.m.0.6A | ASPY | - | 15.386 | 15.133 | 34.972 | 0.9836 | 2.2729 |
| 52 | KU-R443/18.6-18.9 | sulf-crb vein/py | mtuf/? | fr.nm.0.6A; +100 | PY(porous) | db | 18.499 | 15.565 | 38.176 | 0.8414 | 2.0637 |
| 37 | KU-R443/18.6-18.9 | sulf-crb vein/py | mtuf/? | fr.nm.0.6A; -100 | PY(porous) | db | 17.898 | 15.579 | 37.872 | 0.8705 | 2.1160 |
| 53 | KU-R443/18.6-18.9 | sulf-crb vein/py | mtuf/? | fr.nm.0.6A; -200 | PY(porous) | b | 18.144 | 15.527 | 37.919 | 0.8558 | 2.0899 |
| 52-1L | KU-R443/18.6-18.9 | sulf-crb vein/py | mtuf/? | fr.nm.0.6A; +100 | PY-2N HCl | b-db | 20.993 | 15.891 | 40.738 | 0.7570 | 1.9406 |
| 52-2L | KU-R443/18.6-18.9 | sulf-crb vein/py | mtuf/? | fr.nm.0.6A; +100 | PY-6N HCl | lb-b | 21.003 | 15.901 | 40.778 | 0.7571 | 1.9415 |
| 52-3L | KU-R443/18.6-18.9 | sulf-crb vein/py | mtuf/? | fr.nm.0.6A; +100 | PY-7N HNO3 | db | 17.851 | 15.512 | 37.536 | 0.8690 | 2.1027 |
| 53-1L | KU-R443/18.6-18.9 | sulf-crb vein/py | mtuf/? | fr.nm.0.6A; -200 | PY-2N HCl | b | 20.485 | 15.817 | 40.181 | 0.7721 | 1.9614 |
| 53-2L | KU-R443/18.6-18.9 | sulf-crb vein/py | mtuf/? | fr.nm.0.6A; -200 | PY-6N HCl | llb | 19.146 | 15.650 | 38.935 | 0.8174 | 2.0335 |
| 53-3L | KU-R443/18.6-18.9 | sulf-crb vein/py | mtuf/? | fr.nm.0.6A; -200 | PY-7N HNO3 | db | 17.168 | 15.428 | 36.913 | 0.8986 | 2.1502 |
| 53-R | KU-R443/18.6-18.9 | sulf-crb vein/py | mtuf/? | fr.nm.0.6A; -200 | PY-residual | lb | 17.693 | 15.464 | 41.376 | 0.8740 | 2.3385 |
| 73-le | KU-R436/21.3-21.4 | | mtuf/crb-se-ch schist | leach | LE | - | 19.516 | 15.668 | 38.716 | 0.8029 | 1.9839 |
| 73-wr | KU-R436/21.3-21.4 | | mtuf/crb-se-ch schist | total dissolution | WR | - | 23.884 | 16.103 | 40.549 | 0.6742 | 1.6978 |
| 61a | KU-R436/42.2-42.3 | sulf-crb breccia/po | mtuf/crb-ab-qtz | d<3.3 | CRB(inclusions) | - | 17.932 | 15.516 | 36.796 | 0.8653 | 2.0520 |
| 61b | KU-R436/42.2-42.3 | sulf-crb breccia/po | mtuf/crb-ab-qtz | hand magnet | PO(bulk) | llb | 18.222 | 15.612 | 37.290 | 0.8567 | 2.0464 |
| 65-le | KU-R436/73.4-73.5 | | mtuf/crb-ch-ab rock | acid leach | LE | - | 16.159 | 15.253 | 35.939 | 0.9439 | 2.2240 |
| 65-wr | KU-R436/73.4-73.5 | | mtuf/crb-ch-ab rock | total dissolution | WR | - | 17.240 | 15.321 | 36.105 | 0.8887 | 2.0943 |
| 86-le | KU-R436/76.3-76.4 | | mtuf/crb-ch-ab rock | acid leach | LE | b-db | 15.346 | 15.151 | 35.034 | 0.9873 | 2.2830 |
| 86-wr## | KU-R436/76.3-76.4 | | mtuf/crb-ch-ab rock | total dissolution | WR | b | 15.563 | 15.177 | 35.123 | 0.9752 | 2.2568 |
| 88A | KU-R436/76.4-76.5 | qtz-sulf-crb vein/py,aspy | mtuf/crb-ch-ab rock | fr.nm.1.4A | GA | | 15.312 | 15.155 | 34.875 | 0.9897 | 2.2776 |
| 88B | KU-R436/76.4-76.5 | qtz-sulf-crb vein/py,aspy | mtuf/crb-ch-ab rock | fr.nm.1.4A | GA | | 15.225 | 15.118 | 34.807 | 0.9930 | 2.2862 |
| 91/130 | KU-R436/76.4-76.5 | qtz-sulf-crb vein/py,aspy | mtuf/crb-ch-ab rock | fr.nm 1.4A; +100 | PY(idiomorphic) | bl | 15.285 | 15.191 | 35.045 | 0.9939 | 2.2928 |
| 92 | KU-R436/86.3-86.4 | sulf vein/po | mtuf/se-ab-qtz schist | hand magnet | PO(bulk) | lb | 15.987 | 15.246 | 35.834 | 0.9536 | 2.2415 |
| 93 | KU-R436/87.8-87.9 | qtz-sulf vein/py,cp | mtuf/crb-ab-qtz rock | fr.nm.1.4A; +100 | PY(dull) | db | 15.838 | 15.221 | 35.517 | 0.9610 | 2.2425 |
| 123 | KU-R436/87.8-87.9 | qtz-sulf vein/py,cp | mtuf/crb-ab-qtz rock | fr.nm.1.4A; -100 | PY(dull) | db | 15.804 | 15.247 | 35.570 | 0.9647 | 2.2507 |
| 6B | KU-A1168 | diss in crb-vein/py | lamprophyre | fr.nm.(60mg) | PY(idiomorphic) | db | 15.269 | 15.131 | 34.928 | 0.9909 | 2.2875 |
| 90-le | KU/R308+R311 | | lamprophyre | acid leach | LE | b | 16.240 | 15.270 | 36.058 | 0.9403 | 2.2204 |
| 90-wr | KU/R308+R311 | | lamprophyre | total dissolution | WR | lb | 16.501 | 15.254 | 35.960 | 0.9244 | 2.1793 |
| 48a-ic | KU/R308+R311 | | lamprophyre | d:3.16-3.22 | APATITE | | 19.336 | 15.589 | 41.377 | 0.8062 | 2.1398 |
| 48b-ic | KU/R308+R311 | | lamprophyre | d:3.16-3.22 | TITANITE(apatite) | | 29.545 | 16.644 | 38.526 | 0.5633 | 1.3040 |
| 49=55 | KU/R308+R311 | diss in crb-vein/py | lamprophyre | fr.em.1.4A; +200 | PY(idiomorphic) | db | 15.650 | 15.233 | 35.424 | 0.9734 | 2.2636 |
| 55=49 | KU/R308+R311 | diss in crb-vein/py | lamprophyre | fr.em.1.4A ;+200 | PY(idiomorphic) | bl | 15.633 | 15.201 | 35.347 | 0.9724 | 2.2610 |
| 127## | KU/R308+R311 | diss in crb-vein/Pb-? | lamprophyre | fr.em.1.4A; +200 | rich in Pb? | | 15.616 | 15.204 | 35.328 | 0.9736 | 2.2622 |

BV = Bidjovagge; HL = Hangaslampi; KU = Kuotko; LAM = Lammasvuoma; MA = Meurastuksenaho; PV = Pahtavaara; PVU = Pahtavuoma; SK = Suurikuusikko; SP(A,B,C) = Saattopora gold ore/ A-, B-, C-ores; SP-Cu = Saattopora Cu-mineralization; SV = Soretiavuoma; diss = dissemination; ab = albite; amph = amphibole; bar = barite; bt = biotite; ch = chlorite; crb = carbonate; qtz = quartz; se = sericite; sulf = sulfide; tlc = talc; tour = tourmaline; tre = tremolite; ASPY = arsenopyrite; CP = chalcopyrite; GA = galena; LE = acid leach of whole rock powder; MAGN = magnetite; PO = pyrrhotite; PY = pyrite; WR = total dissolution of whole rock powder; graph-schist = graphite-rich schist; mtuf = mafic tuffite; metased = metasedimentary; umr = ultramafic rock; d = density; fr.nm/fr.m. = non magnetic/magnetic fraction with a specific current; +200,-100 = size fractions; Pb* = the colour of the anode precipitation (- = colourless, llb = brownish, lb = light brown, b = brown, db = dark brown, bl = black).

**Appendix 4.** Continued 3/7.

| ANAL. NO. | DEPOSIT/ SAMPLE | MINERALIZATION TYPE/ ORE MINERALS | HOST ROCK | ANALYSED FRACTION | ANALYSED MINERAL | *Pb* | LEAD ISOTOPE RATIOS 206/204 | 207/204 | 208/204 | 207/206 | 208/206 |
|---|---|---|---|---|---|---|---|---|---|---|---|
| 74-le | KU-A1262 | | felsic porphyry | acid leach | LE | IIb | 56.669 | 20.000 | 70.744 | 0.3529 | 1.2484 |
| 74-wr | KU-A1262 | | felsic porphyry | total dissolution | WR | - | 42.202 | 17.968 | 53.035 | 0.4258 | 1.2567 |
| 99 | KU-A1262 | diss/aspy,py | felsic porphyry | acid leach | ASPY(py) | db | 20.965 | 16.947 | 37.892 | 0.7606 | 1.8074 |
| 121 | SK-R434/65.8 | qtz-sulf-crb vein/aspy,py | mtuf/graph-schist/ch-ab | fr.nm.2.3A; +200 | ASPY(py) | Ib-b | 16.493 | 16.327 | 34.955 | 0.9293 | 2.1194 |
| 18 | SK-R434/65.8 | qtz-sulf-crb vein/aspy,py | mtuf/graph-schist/ch-ab | fr.nm.2.3A; +200 | ASPY(py) | Ib-b | 16.642 | 16.413 | 35.166 | 0.9261 | 2.1131 |
| 24 | SK-R434/65.8 | qtz-sulf-crb vein/aspy,py | mtuf/graph-schist/ch-ab | fr.nm.2.3A; -200 | ASPY(py) | Ib-b | 17.090 | 16.427 | 35.127 | 0.9027 | 2.0554 |
| 132 | SK-R434/65.8 | qtz-sulf-crb vein/aspy,py | mtuf/graph-schist/ch-ab | fr.nm.2.3A; -200 | ASPY(py) | Ib | 16.969 | 16.406 | 35.096 | 0.9079 | 2.0683 |
| 19 | SK-R434/80.5-80.8 | breccia/aspy,py | mtuf/graph-schist/ch-ab | fr.nm.2.3A; +200 | ASPY,PY | Ib | 16.992 | 16.491 | 35.428 | 0.9117 | 2.0850 |
| 122 | SK-R434/80.5-80.8 | breccia/aspy,py | mtuf/graph-schist/ch-ab | fr.nm.2.3A; -100 | ASPY(py) | - | 16.936 | 16.460 | 35.327 | 0.9129 | 2.0859 |
| 40 | SK-R434/80.5-80.8 | breccia/aspy,py | mtuf/graph-schist/ch-ab | fr.nm.2.3A; -200 | ASPY,PY | Ib | 17.009 | 16.494 | 35.458 | 0.9109 | 2.0847 |
| MV## | G347/Kiistala | sulf-crb vein/aspy,ga | mtuf/graph-schist/ch-ab | | GA | | 16.313 | 16.186 | 34.965 | 0.9917 | 2.2834 |
| 221a | PV-R508/87.3 | ab-crb-qtz vein/magn,py | umr/amph-ch-crb schist | hand magnet | MAGN | - | 60.913 | 20.278 | 35.285 | 0.3329 | 0.5793 |
| 221b | PV-R508/87.3 | ab-crb-qtz vein/magn,py | umr/amph-ch-crb schist | fr.nm.1.4A | PY | - | 43.396 | 18.687 | 35.025 | 0.4306 | 0.8071 |
| 71-le | PV-R508/96.4-96.5 | | umr/bt-tlc-crb schist | acid leach | LE | - | 22.469 | 16.901 | 34.889 | 0.7077 | 1.5528 |
| 71-wr | PV-R508/96.4-96.5 | | umr/bt-tlc-crb schist | total dissolution | WR | - | 23.207 | 16.033 | 35.356 | 0.6909 | 1.5235 |
| 101 | PV-R508/111.5-111.7 | sulf patches/py,magn | umr/tre-crb rock | fr.em.1.4A; coarse | PY | - | 36.091 | 17.500 | 34.970 | 0.4849 | 0.9690 |
| 102 | PV-R508/111.5-111.7 | sulf patches/py,magn | umr/tre-crb rock | fr.m.1.4A; fine | PY | IIb | 35.529 | 17.472 | 34.962 | 0.4918 | 0.9840 |
| 220a | PV-R508/111.9 | diss/magn,py | umr/amph-crb-ch rock | hand magnet | MAGN | - | 24.027 | 16.013 | 34.932 | 0.6664 | 1.4538 |
| 220B1 | PV-R508/111.9 | diss/magn,py | umr/amph-crb-ch rock | fr.nm.1.4A | PY | - | 19.445 | 15.636 | 34.911 | 0.8041 | 1.7954 |
| 220B2 | PV-R508/111.9 | diss/magn,py | umr/amph-crb-ch rock | fr.nm.1.4A | PY | - | 18.454 | 15.528 | 34.945 | 0.8415 | 1.8936 |
| 220c | PV-R508/111.9 | diss/magn,py | umr/amph-crb-ch rock | fr.m.1.4A | PY | - | 30.860 | 16.863 | 35.002 | 0.5464 | 1.1342 |
| 220D1 | PV-R508/111.9 | diss/magn,py | umr/amph-crb-ch rock | d<3.3; acid leach | CRB | - | 15.468 | 15.217 | 34.913 | 0.9837 | 2.2570 |
| 220D2 | PV-R508/111.9 | diss/magn,py | umr/amph-crb-ch rock | d<3.3; acid leach | CRB | - | 15.430 | 15.188 | 34.828 | 0.9843 | 2.2571 |
| 222a | PV-R508/117.3 | tlc-crb-sulf lens/magn,py | umr/bt-ch schist | hand magnet | MAGN | - | 37.844 | 17.571 | 34.976 | 0.4643 | 0.9242 |
| 222b | PV-R508/117.3 | tlc-crb-sulf lens/magn,py | umr/bt-ch schist | fr.nm.1.4A | PY | - | 20.886 | 15.807 | 34.864 | 0.7568 | 1.6692 |
| 57-le | PV-R508/124.0-124.1 | | umr/ch-amph rock | acid leach | LE | - | 15.429 | 15.239 | 34.706 | 0.9877 | 2.2494 |
| 57-wr | PV-R508/124.0-124.1 | | umr/ch-amph rock | total dissolution | WR | - | 17.073 | 15.346 | 35.086 | 0.8989 | 2.0551 |
| 219A1 | PV-R509/110.9 | diss/tlc-bar lens/magn,(py) | umr | hand magnet | MAGN | - | 58.049 | 19.626 | 34.999 | 0.3381 | 0.6029 |
| 219A2 | PV-R509/110.9 | diss/tlc-bar lens/magn,(py) | umr | hand magnet | MAGN | - | 56.980 | 19.485 | 34.925 | 0.3420 | 0.6129 |
| 219b1 | PV-R509/110.9 | diss/tlc-bar lens/magn,(py) | umr | d>3.3; acid leach | CRB(sulf) | - | 33.746 | 17.230 | 34.861 | 0.5106 | 1.0330 |
| 219c | PV-R509/110.9 | diss/tlc-bar lens/magn,(py) | umr | d<3.3; acid leach | CRB | - | 19.511 | 15.675 | 34.915 | 0.8034 | 1.7894 |
| 223b | PV-4A | diss/magn,(py) | umr/amph rock | d>3.3; acid leach | PY | - | 26.757 | 16.631 | 35.873 | 0.6216 | 1.3407 |

BV = Bidjovagge; HL = Hangaslampi; KU = Kuotko; LAM = Lammasvuoma; MA = Meurastuksenaho; PV = Pahtavaara; PVU = Pahtavuoma; SK = Suurikuusikko; SP(A,B,C) = Saattopora gold ore/ A-, B-, C-ores; SP-Cu = Saattopora Cu-mineralization; SV = Soretiavuoma; diss = dissemination; ab = albite; amph = amphibole; bar = barite; bt = biotite; ch = chlorite; crb = carbonate; qtz = quartz; se = sericite; sulf = sulfide; tlc = talc; tour = tourmaline; tre = tremolite; ASPY = arsenopyrite; CP = chalcopyrite; GA = galena; LE = acid leach of whole rock powder; MAGN = magnetite; PO = pyrrhotite; PY = pyrite; WR = total dissolution of whole rock powder; graph-schist = graphite-rich schist; mtuf = mafic tuffite; metased = metasedimentary; umr = ultramafic rock; d = density; fr.nm/fr.m. = non magnetic/magnetic fraction with a specific current; +200,-100 = size fractions; Pb* = the colour of the anode precipitation (- = colourless, IIb = brownish, Ib = light brown, b = brown, db = dark brown, bl = black).

**Appendix 4.** Continued 4/7.

| ANAL. NO. | DEPOSIT/ SAMPLE | MINERALIZATION TYPE/ ORE MINERALS | HOST ROCK | ANALYSED FRACTION | ANALYSED MINERAL | *Pb* | LEAD ISOTOPE RATIOS 206/204 | 207/204 | 208/204 | 207/206 | 208/206 |
|---|---|---|---|---|---|---|---|---|---|---|---|
| 87-le | PV/EIM-91-1 | | umr/ch-tlc-amph rock | acid leach | LE | IIb | 16.197 | 15.325 | 35.343 | 0.9461 | 2.1820 |
| 87-wr | PV/EIM-91-1 | | umr/ch-tlc-amph rock | total dissolution | WR | - | 17.121 | 15.503 | 35.851 | 0.9055 | 2.0940 |
| 139 | LAM-3/45.0-45.1 | breccia/diss/py | ?/bt-ch-ab-qtz schist | fr.nm.1.4A; +100 | PY | Ib | 28.807 | 17.008 | 38.901 | 0.5904 | 1.3504 |
| 138 | LAM-3/45.0-45.1 | breccia/diss/py | ?/bt-ch-ab-qtz schist | fr.nm.1.4A ;-100 | PY | Ib | 29.777 | 17.100 | 38.958 | 0.5743 | 1.3083 |
| 209 | LAM-3/45.8-45.9 | breccia/diss/py | ?/bt-ch-ab-qtz schist | fr.nm.1.4A; -100 | PY | - | 45.306 | 18.009 | 45.116 | 0.3975 | 0.9958 |
| 69-le | LAM-3/45.8-45.9 | | mtuf/crb-ab rock | acid leach | LE | - | 43.153 | 17.982 | 47.809 | 0.4167 | 1.1079 |
| 69-wr | LAM-3/45.8-45.9 | | mtuf/crb-ab rock | total dissolution | WR | - | 78.236 | 21.371 | 51.884 | 0.2732 | 0.6632 |
| 7 | SP-A1205 | sulf-crb vein/po,cp | mtuf/ab-crb schist | fr.nm.1.4A; +100 | CP(py) | - | 137.05 | 31.754 | 36.751 | 0.2317 | 0.2682 |
| 8=34 | SP-A1205 | sulf-crb vein/po,cp | mtuf/ab-crb schist | fr.m.1.4A; +100 | CP | - | 132.19 | 31.166 | 36.609 | 0.2358 | 0.2769 |
| 34=8 | SP-A1205 | sulf-crb vein/po,cp | mtuf/ab-crb schist | fr.m.1.4A; +200 | CP | Ib | 131.00 | 31.340 | 37.143 | 0.2392 | 0.2835 |
| 9=22 | SP-A1205 | sulf-crb vein/po,cp | mtuf/ab-crb schist | fr.m.0.4A; +100 | PO | - | 1148.9 | 146.87 | 37.146 | 0.1278 | 0.0323 |
| 22=9 | SP-A1205 | sulf-crb vein/po,cp | mtuf/ab-crb schist | fr.m.0.4A; +100 | PO | - | 1489.7 | 172.11 | 40.333 | 0.1155 | 0.0271 |
| 34-2L | SP-A1205 | sulf-crb vein/po,cp | mtuf/ab-crb schist | fr.m.1.4A; +200 | CP-6N HCL | - | 227.08 | 41.873 | 38.011 | 0.1844 | 0.1674 |
| 34-3L | SP-A1205 | sulf-crb vein/po,cp | mtuf/ab-crb schist | fr.m.1.4A; +200 | CP-7N HNO3 | IIb | 196.71 | 38.662 | 37.805 | 0.1965 | 0.1922 |
| 34-R | SP-A1205 | sulf-crb vein/po,cp | mtuf/ab-crb schist | fr.m.1.4A; +200 | CP-residual | Ib-b | 120.55 | 30.164 | 37.000 | 0.2502 | 0.3069 |
| 29-le | SP-A1205 | sulf-crb vein/po,cp | mtuf/ab-crb schist | acid leach | LE/vein | - | 90.113 | 24.990 | 37.018 | 0.2773 | 0.4108 |
| 31-wr | SP-A1205 | sulf-crb vein/po,cp | mtuf/ab-crb schist | total dissolution | WR/vein | - | 92.042 | 24.881 | 36.280 | 0.2703 | 0.3942 |
| 51a-ic | SP-A1205 | sulf-crb vein/po,cp | mtuf/ab-crb schist | d:4.0-4.3 | RUTILE | | 99.851 | 23.124 | 41.145 | 0.2316 | 0.4121 |
| 51b-ic | SP-A1205 | sulf-crb vein/po,cp | mtuf/ab-crb schist | d:4.0-4.3 | RUTILE(abr 1h) | | 516.62 | 62.544 | 53.395 | 0.1211 | 0.1034 |
| 218=51 | SP-A1205 | sulf-crb vein/po,cp | mtuf/ab-crb schist | d:4.0-4.3 | RUTILE(abr 2h) | | 385.78 | 51.324 | 50.766 | 0.1330 | 0.1316 |
| 89-le | SP-A1205 | | mtuf/ab-crb schist | acid leach | LE | IIb | 103.67 | 27.194 | 38.781 | 0.2623 | 0.3741 |
| 89-wr | SP-A1205 | | mtuf/ab-crb schist | total dissolution | WR | - | 92.748 | 25.012 | 36.165 | 0.2697 | 0.3899 |
| 76A-ic | SP(A)-R257/61.4-61.5 | sulf-crb vein/po,cp | mtuf/ab-crb rock | | THUCOLITE | | 33560 | 3642.1 | 49.468 | 0.1085 | 0.0015 |
| 76B-ic | SP(A)-R257/61.4-61.5 | sulf-crb vein/po,cp | mtuf/ab-crb rock | | THUCOLITE | | 36013 | 3903.9 | 48.902 | 0.1084 | 0.0014 |
| 77A-ic | SP(A)-R257/61.4-61.5 | sulf-crb vein/po,cp | mtuf/ab-crb rock | | THUCOLITE | | 41110 | 4436.7 | 50.709 | 0.1079 | 0.0012 |
| 77B-ic | SP(A)-R257/61.4-61.5 | sulf-crb vein/po,cp | mtuf/ab-crb rock | | THUCOLITE | | 44427 | 4805.1 | 50.180 | 0.1082 | 0.0011 |
| 63-le | SP(A)-R257/70.6-70.7 | | mtuf/ab-crb rock | acid leach | LE | IIb | 2101.6 | 237.77 | 42.793 | 0.1131 | 0.0204 |
| 63-wr | SP(A)-R257/70.6-70.7 | | mtuf/ab-crb rock | total dissolution | WR | - | 1667.8 | 187.66 | 49.858 | 0.1125 | 0.0299 |
| 110 | SP(A)-R257/74.6-74.7 | tour-sulf vein/po,py,cp | mtuf/ab-crb rock | hand magnet | PO(bulk) | IIb | 77.001 | 23.921 | 41.031 | 0.3107 | 0.5329 |
| 114 | SP(A)-R257/74.6-74.7 | tour-sulf vein/po,py,cp | mtuf/ab-crb rock | fr.nm.0.6A; +200 | PY(cp) | IIb | 51.444 | 20.543 | 39.169 | 0.3993 | 0.7614 |
| 190 | SP(A)-R257/74.6-74.7 | tour-sulf vein/po,py,cp | mtuf/ab-crb rock | d>4.0/fr.nm.0.6A | RUTILE | | 156.15 | 29.927 | 40.065 | 0.1917 | 0.2566 |
| 111 | SP(A)-R257/82.2-82.3 | qtz-sulf vein/po,cp | mtuf/ab-tour schist | d>3.3/magn. | PO(bulk) | Ib | 307.62 | 51.345 | 39.393 | 0.1669 | 0.1281 |
| 115 | SP(A)-R257/82.2-82.3 | qtz-sulf vein/po,cp | mtuf/ab-tour schist | fr.nm.0.6A; +200 | CP | IIb | 234.27 | 43.391 | 38.590 | 0.1852 | 0.1647 |
| 116 | SP(A)-R257/82.2-82.3 | qtz-sulf vein/po,cp | mtuf/ab-tour schist | fr.m.0.6A | PO | - | 82.943 | 25.415 | 36.316 | 0.3064 | 0.4378 |

BV = Bidjovagge; HL = Hangaslampi; KU = Kuotko; LAM = Lammasvuoma; MA = Meurastuksenaho; PV = Pahtavaara; PVU = Pahtavuoma; SK = Suurikuusikko; SP(A,B,C) = Saattopora gold ore/ A-, B-, C-ores; SP-Cu = Saattopora Cu-mineralization; SV = Soretiavuoma; diss = dissemination; ab = albite; amph = amphibole; bar = barite; bt = biotite; ch = chlorite; crb = carbonate; qtz = quartz; se = sericite; sulf = sulfide; tlc = talc; tour = tourmaline; tre = tremolite; ASPY = arsenopyrite; CP = chalcopyrite; GA = galena; LE = acid leach of whole rock powder; MAGN = magnetite; PO = pyrrhotite; PY = pyrite; WR = total dissolution of whole rock powder; graph-schist = graphite-rich schist; mtuf = mafic tuffite; metased = metasedimentary; umr = ultramafic rock; d = density; fr.nm/fr.m. = non magnetic/magnetic fraction with a specific current; +200,-100 = size fractions; Pb* = the colour of the anode precipitation (- = colourless, IIb = brownish, Ib = light brown, b = brown, db = dark brown, bl = black).

**Appendix 4.** Continued 5/7.

| ANAL. NO. | DEPOSIT/ SAMPLE | MINERALIZATION TYPE/ ORE MINERALS | HOST ROCK | ANALYSED FRACTION | ANALYSED MINERAL | *Pb* | LEAD ISOTOPE RATIOS 206/204 | 207/204 | 208/204 | 207/206 | 208/206 |
|---|---|---|---|---|---|---|---|---|---|---|---|
| 62 | SP(A)/EIM-91-2b | sulf-crb vein | mtuf/ab-crb rock | d:2.8-2.95 | CRB | - | 16.455 | 15.300 | 35.470 | 0.9298 | 2.1556 |
| 134 | SP(A)/EIM-91-2b | sulf-crb vein | mtuf/ab-crb rock | d:2.8-2.95 | CRB | - | 15.806 | 15.285 | 35.186 | 0.9670 | 2.2261 |
| 83-le | SP(B)-R208/109.1-109.2 | | mtuf/ab-crb schist | acid leach | LE | IIb | 88.144 | 22.463 | 170.47 | 0.2548 | 1.9341 |
| 83-wr | SP(B)-R208/109.1-109.2 | | mtuf/ab-crb schist | total dissolution | WR | - | 118.83 | 25.871 | 164.29 | 0.2177 | 1.3826 |
| 84-le | SP(B)-R208/112.6-112.7 | | mtuf/ab-crb-tour schist | acid leach | LE | - | 187.74 | 35.578 | 154.29 | 0.1895 | 0.8218 |
| 84-wr | SP(B)-R208/112.6-112.7 | | mtuf/ab-crb-tour schist | total dissolution | WR | - | 165.15 | 31.051 | 131.80 | 0.1880 | 0.7981 |
| 85-le | SP(B)-R208/120.8-120.9 | | mtuf/ab-crb-tour schist | acid leach | LE | IIb | 260.30 | 42.272 | 168.27 | 0.1624 | 0.6464 |
| 85-wr | SP(B)-R208/120.8-120.9 | | mtuf/ab-crb-tour schist | total dissolution | WR | - | 213.17 | 35.463 | 136.35 | 0.1664 | 0.6396 |
| 109-a | SP(B)-R208/124.4-124.5 | sulf-qtz-crb vein/py,po | mtuf/ab-tour-crb schist | fr.nm.0.6A | PY(dull) | Ib-b | 77.532 | 24.179 | 59.333 | 0.3119 | 0.7653 |
| 109-b | SP(B)-R208/124.4-124.5 | sulf-qtz-crb vein/py,po | mtuf/ab-tour-crb schist | fr.nm.0.6A | PY | Ib | 96.672 | 26.405 | 63.589 | 0.2731 | 0.6578 |
| 94A | SP(C)/EIM-91-3 | diss/aspy | mtuf/ab-crb rock | fr.nm.0.6A; +100 | ASPY | IIb | 97.445 | 23.936 | 51.634 | 0.2456 | 0.5299 |
| 94Ba## | SP(C)/EIM-91-3 | diss/aspy | mtuf/ab-crb rock | fr.nm.0.6A; +100 | ASPY | Ib | 174.20 | 28.889 | 56.162 | 0.1658 | 0.3224 |
| 94Bb | SP(C)/EIM-91-3 | diss/aspy | mtuf/ab-crb rock | fr.nm.0.6A; +100 | PY(50mg) | - | 73.861 | 22.240 | 47.132 | 0.3011 | 0.6381 |
| 210-le | SP(C)/EIM-91-3 | | mtuf/ab-crb rock | acid leach | LE | - | 302.84 | 36.266 | 120.89 | 0.1198 | 0.3992 |
| 210-wr | SP(C)/EIM-91-3 | | mtuf/ab-crb rock | total dissolution | WR | - | 331.76 | 37.234 | 115.27 | 0.1122 | 0.3476 |
| 80-ic | SP-G443/concentrate | sulf-crb-qtz vein/po,cp,py | mtuf/ab-crb rock | fr.nm.1.4A | MONAZITE | | 7121.9 | 789.11 | 2617.2 | 0.1108 | 0.3675 |
| 203 | SP/concentrate | sulf-crb-qtz vein/po,cp,py | mtuf/ab-crb rock | fine grained | GOLD | - | 550.45 | 79.326 | 50.224 | 0.1441 | 0.0912 |
| 204 | SP/concentrate | sulf-crb-qtz vein/po,cp,py | mtuf/ab-crb rock | coarse grained | GOLD | - | 492.35 | 73.417 | 42.469 | 0.1491 | 0.0863 |
| 205 | SP/concentrate | sulf-crb-qtz vein/po,cp,py | mtuf/ab-crb rock | hand magnet | GOLD | - | 435.21 | 64.257 | 39.014 | 0.1476 | 0.0896 |
| 75A | SP-Cu/EIM-91-4 | sulf-crb vein/cp,po,py | mtuf/ab schist | fr.m.1.4A; +100 | CP | - | 472.98 | 72.728 | 41.659 | 0.1538 | 0.0881 |
| 75B | SP-Cu/EIM-91-4 | sulf-crb vein/cp,po,py | mtuf/ab schist | fr.em.1.4A; +100 | PY(cp) | - | 497.96 | 74.640 | 42.528 | 0.1499 | 0.0854 |
| 136## | SP-Cu/EIM-91-4 | sulf-crb vein/cp,po,py | mtuf/ab schist | fr.m.0.2A; -100 | PO(markasite) | Ib-b | 65.09 | 107.16 | 45.662 | 0.1401 | 0.0597 |
| 137## | SP-Cu/EIM-91-4 | sulf-crb vein/cp,po,py | mtuf/ab schist | fr.m.0.4A; -100 | PO(markasite) | b-db | 893.54 | 123.03 | 46.973 | 0.1377 | 0.0526 |
| 98A | SP-Cu/EIM-91-4 | sulf-crb vein/cp,po,py | mtuf/ab schist | fr.nm.1.4A ;-200 | PY(acid leach) | db | 558.82 | 81.907 | 43.033 | 0.1466 | 0.0770 |
| 98B | SP-Cu/EIM-91-4 | sulf-crb vein/cp,po,py | mtuf/ab schist | fr.nm.1.4A ;-200 | PY(acid leach) | db | 539.50 | 79.118 | 41.614 | 0.1467 | 0.0771 |
| 78-ic | SP-Cu/EIM-91-4 | sulf-crb vein/cp,po,py | mtuf/ab schist | fr.nm.1.4A | RUTILE | | 1092.6 | 125.83 | 46.947 | 0.1152 | 0.0430 |
| 79-ic | SP-Cu/EIM-91-4 | sulf-crb vein/cp,po,py | mtuf/ab schist | fr.nm.+m.1.4A | MONAZITE | | 13685 | 1496.9 | 4712.2 | 0.1094 | 0.3443 |
| 117 | SP-Cu/EIM-91-5 | breccia/py,cp,aspy | phyllite | fr.nm.1.4A ;-200 | ASPY,CP(py) | IIb | 89.174 | 23.843 | 38.638 | 0.2674 | 0.4333 |
| 126 | SP-Cu/EIM-91-5 | breccia/py,cp,aspy | phyllite | fr.nm.1.4A | PY(cp) | IIb | 148.09 | 31.922 | 42.330 | 0.2156 | 0.2858 |
| 58-le | SP-Cu/EIM-91-5 | | phyllite | acid leach | LE | IIb | 276.11 | 40.583 | 55.440 | 0.1470 | 0.2008 |
| 58-wr | SP-Cu/EIM-91-5 | | phyllite | total dissolution | WR | - | 286.16 | 40.278 | 55.333 | 0.1408 | 0.1934 |

BV = Bidjovagge; HL = Hangaslampi; KU = Kuotko; LAM = Lammasvuoma; MA = Meurastuksenaho; PV = Pahtavaara; PVU = Pahtavuoma; SK = Suurikuusikko; SP(A,B,C) = Saattopora gold ore/ A-, B-, C-ores; SP-Cu = Saattopora Cu-mineralization; SV = Soretiavuoma; diss = dissemination; ab = albite; amph = amphibole; bar = barite; bt = biotite; ch = chlorite; crb = carbonate; qtz = quartz; se = sericite; sulf = sulfide; tlc = talc; tour = tourmaline; tre = tremolite; ASPY = arsenopyrite; CP = chalcopyrite; GA = galena; LE = acid leach of whole rock powder; MAGN = magnetite; PO = pyrrhotite; PY = pyrite; WR = total dissolution of whole rock powder; graph-schist = graphite-rich schist; mtuf = mafic tuffite; metased = metasedimentary; umr = ultramafic rock; d = density; fr.nm/fr.m. = non magnetic/magnetic fraction with a specific current; +200,-100 = size fractions; Pb* = the colour of the anode precipitation (- = colourless, IIb = brownish, Ib = light brown, b = brown, db = dark brown, bl = black).

**Appendix 4.** Continued 6/7.

| ANAL. NO. | DEPOSIT/ SAMPLE | MINERALIZATION TYPE/ ORE MINERALS | HOST ROCK | ANALYSED FRACTION | ANALYSED MINERAL | *Pb* | LEAD ISOTOPE RATIOS 206/204 | 207/204 | 208/204 | 207/206 | 208/206 |
|---|---|---|---|---|---|---|---|---|---|---|---|
| 66a | HL-R388/22.7-22.8 | magn brecciate py | metased/ab-ch-qtz rock | fr.nm.1.4A | PY | - | 56.087 | 21.647 | 82.315 | 0.3860 | 1.4676 |
| 66b | HL-R388/22.7-22.8 | magn brecciate py | metased/ab-ch-qtz rock | hand magnet | MAGN(bulk) | lb | 73.168 | 24.219 | 103.48 | 0.3310 | 1.4143 |
| 70A-le | HL-R388/23.7-23.8 | | metased/ab-ch-qtz rock | acid leach | LE | - | 291.04 | 39.383 | 65.495 | 0.1353 | 0.2250 |
| 70B-le | HL-R388/23.7-23.8 | | metased/ab-ch-qtz rock | acid leach | LE | - | 564.43 | 62.536 | 93.135 | 0.1108 | 0.1650 |
| 70B-wr | HL-R388/23.7-23.8 | | metased/ab-ch-qtz rock | total dissolution | WR | - | 360.57 | 47.438 | 62.172 | 0.1316 | 0.1724 |
| 120## | HL-R388/41.2-41.3 | diss/stripes/py,magn | metased/ab-se-qtz rock | fr.nm.1.4A | PY | IIb | 807.95 | 104.42 | 43.268 | 0.1292 | 0.0536 |
| 215 | HL-R388/41.2-41.3 | diss/stripes/py,magn | metased/ab-se-qtz rock | fr.nm.1.4A | PY | - | 1043.9 | 131.40 | 45.056 | 0.1259 | 0.0432 |
| 64##-le | HL-R388/57.9-58.0 | | metased/ab-ch-qtz rock | acid leach | LE | lb | 451.79 | 65.299 | 465.40 | 0.1445 | 1.0301 |
| 64-wr | HL-R388/57.9-58.0 | | metased/ab-ch-qtz rock | total dissolution | WR | - | 540.84 | 72.149 | 394.76 | 0.1334 | 0.7299 |
| 68## | HL-R388/66.8-66.9 | magn brecciate po | metased/ab-se-qtz rock | fr.nm.1.4A | PO | db | 2893.2 | 343.77 | 54.412 | 0.1188 | 0.0188 |
| 216-ic | HL-R388/66.8-66.9 | magn brecciate po | metased/ab-se-qtz rock | fr.nm.1.4A | PO | db | 15551 | 1745.8 | 138.35 | 0.1123 | 0.0089 |
| 107 | HL-R388/71.0-71.1 | sulf-crb vein/py | metased/ab-se-qtz rock | fr.nm.1.4A; coarse | PY | - | 108.01 | 28.003 | 47.072 | 0.2593 | 0.4358 |
| 131## | HL-R388/71.0-71.1 | sulf-crb vein/py | metased/ab-se-qtz rock | fr.m.1.4A; fine | PY | IIb | 109.10 | 27.510 | 43.660 | 0.2522 | 0.4002 |
| 106 | HL-R388/71.0-71.1 | sulf-crb vein/py | metased/ab-se-qtz rock | d<3.3 | CRB(inclusions) | - | 31.816 | 17.594 | 37.414 | 0.5530 | 1.1760 |
| 142 | HL-R388/71.0-71.1 | sulf-crb vein/py | metased/ab-se-qtz rock | fr.m.1.4A | CRB | - | 25.731 | 16.859 | 36.672 | 0.6552 | 1.4252 |
| 103## | MA-R332/179.6 | magn brecciate po | metased?/chl-amph rock | hand magnet | MAGN(bulk) | IIb | 130.32 | 27.567 | 44.387 | 0.2115 | 0.3406 |
| 104 | MA-R332/179.6 | magn brecciate po | metased?/chl-amph rock | fr.m.0.6A | PO | IIb | 166.45 | 32.055 | 47.348 | 0.1926 | 0.2845 |
| 105 | MA-R332/179.6 | magn brecciate po | metased?/ch-amph rock | fr.nm.0.6A | CP | IIb | 96.754 | 26.105 | 47.605 | 0.2698 | 0.4920 |
| 176-le | BV-N15P/20.2-20.3 | | metadiabase | acid leach | LE | - | 28.093 | 16.861 | 43.192 | 0.6002 | 1.5375 |
| 176-wr | BV-N15P/20.2-20.3 | | metadiabase | total dissolution | WR | - | 32.063 | 17.171 | 42.613 | 0.5356 | 1.3291 |
| 145## | BV-N20E/197.5-197.6 | diss/stripes/cp,po | mtuf?/ab-crb rock | fr.m.1.4A ;-200 | CP | b | 43.158 | 18.401 | 42.587 | 0.4264 | 0.9868 |
| 147 | BV-N20E/197.5-197.6 | diss/stripes/cp,po | mtuf?/ab-crb rock | fr.nm.1.4A; +200 | PY,CP | db | 46.813 | 19.007 | 42.597 | 0.4060 | 0.9099 |
| 166## | BV-N20E/203.5-203.6 | diss/stripes/cp,po | mtuf?/ab-crb rock | fr.nm.1.4A; +200 | PY | db | 32.263 | 17.532 | 46.373 | 0.5434 | 1.4373 |
| 167 | BV-N20E/203.5-203.6 | diss/stripes/cp,po | mtuf?/ab-crb rock | fr.m.1.4A; -200 | CP | b | 28.721 | 16.995 | 44.325 | 0.5917 | 1.5433 |
| 168 | BV-N20E/203.5-203.6 | diss/stripes/cp,po | mtuf?/ab-crb rock | fr.m.1.4A; +200 | CP | lb | 28.343 | 16.921 | 44.027 | 0.5970 | 1.5534 |
| 146 | BV-N20E/213.2-213.3 | diss/py,magn | metadiabase | fr.nm.0.6A | PY | IIb | 34.980 | 17.666 | 48.405 | 0.5050 | 1.3838 |
| 160b | BV-N95F/2.1-2.20 | sulf-crb vein/py | mtuf?/ab-crb rock | d<3.3; acid leach | CRB | - | 45.826 | 19.635 | 45.030 | 0.4285 | 0.9826 |
| 161A | BV-N95F/2.1-2.20 | sulf-crb vein/py | mtuf?/ab-crb rock | fr.nm.0.3A | PY | - | 72.032 | 23.057 | 53.474 | 0.3201 | 0.7424 |
| 161B | BV-N95F/2.1-2.20 | sulf-crb vein/py | mtuf?/ab-crb rock | fr.nm.0.3A | PY | - | 72.702 | 23.114 | 53.572 | 0.3179 | 0.7369 |
| 162 | BV-N95F/7.0-7.10 | diss/stripes/py | mtuf?/ab-crb rock | fr.nm.1.4A | PY | - | 113.94 | 27.977 | 77.501 | 0.2455 | 0.6802 |
| 157a | BV-N95F/14.1-14.2 | sulf-crb breccia/po,cp | mtuf?/ab-crb rock | d<3.3; acid leach | CRB | - | 35.059 | 17.737 | 42.388 | 0.5059 | 1.2091 |
| 157b | BV-N95F/14.1-14.2 | sulf-crb breccia/po,cp | mtuf?/ab-crb rock | d<3.3; acid leach | CRB | - | 32.827 | 17.637 | 41.491 | 0.5373 | 1.2639 |
| 169 | BV-N95F/14.1-14.2 | sulf-crb breccia/po,cp | mtuf?/ab-crb rock | fr.nm.1.4A ;-200 | PY | db | 49.315 | 19.534 | 45.355 | 0.3961 | 0.9197 |

BV = Bidjovagge; HL = Hangaslampi; KU = Kuotko; LAM = Lammasvuoma; MA = Meurastuksenaho; PV = Pahtavaara; PVU = Pahtavuoma; SK = Suurikuusikko; SP(A,B,C) = Saattopora gold ore/ A-, B-, C-ores; SP-Cu = Saattopora Cu-mineralization; SV = Soretiavuoma; diss = dissemination; ab = albite; amph = amphibole; bar = barite; bt = biotite; ch = chlorite; crb = carbonate; qtz = quartz; se = sericite; sulf = sulfide; tlc = talc; tour = tourmaline; tre = tremolite; ASPY = arsenopyrite; CP = chalcopyrite; GA = galena; LE = acid leach of whole rock powder; MAGN = magnetite; PO = pyrrhotite; PY = pyrite; WR = total dissolution of whole rock powder; graph-schist = graphite-rich schist; mtuf = mafic tuffite; metased = metasedimentary; umr = ultramafic rock; d = density; fr.nm/fr.m. = non magnetic/magnetic fraction with a specific current; +200,-100 = size fractions; Pb* = the colour of the anode precipitation (- = colourless, IIb = brownish, lb = light brown, b = brown, db = dark brown, bl = black).

**Appendix 4.** Continued 7/7.

| ANAL. NO. | DEPOSIT/ SAMPLE | MINERALIZATION TYPE/ ORE MINERALS | HOST ROCK | ANALYSED FRACTION | ANALYSED MINERAL | *Pb* | LEAD ISOTOPE RATIOS 206/204 | 207/204 | 208/204 | 207/206 | 208/206 |
|---|---|---|---|---|---|---|---|---|---|---|---|
| 170## | BV-N95F/14.1-14.2 | sulf-crb breccia/po,cp | mtuf?/ab-crb rock | fr.nm.1.4A; +100 | PY(cp) | db | 46.770 | 19.228 | 45.041 | 0.4111 | 0.9630 |
| 177-le | BV-N95F721.8-21.9 | | mtuf?/ab-crb rock | acid leach | LE | - | 340.66 | 39.662 | 169.24 | 0.1164 | 0.4968 |
| 177-wr | BV-N95F721.8-21.9 | | mtuf?/ab-crb rock | total dissolution | WR | - | 264.41 | 33.199 | 128.02 | 0.1305 | 0.5032 |
| 155 | BV-N95F/45.3-45.4 | sulf-crb vein/po,cp | mtuf?/ab-crb rock | fr.m.1.4A ;+200 | CP(py) | - | 188.93 | 34.720 | 90.309 | 0.1838 | 0.4780 |
| 156 | BV-N95F/45.3-45.4 | sulf-crb vein/po,cp | mtuf?/ab-crb rock | fr.nm.1.4A | PY | - | 100.08 | 26.520 | 63.616 | 0.2650 | 0.6357 |
| 158a | BV-N95F/46.7-46.8 | sulf-crb vein/cp | mtuf?/ab-crb rock | d<3.3; acid leach | CRB | - | 37.184 | 18.082 | 42.715 | 0.4863 | 1.1487 |
| 158b | BV-N95F/46.7-46.8 | sulf-crb vein/cp | mtuf?/ab-crb rock | d<3.3; acid leach | CRB | - | 34.648 | 18.062 | 41.588 | 0.5213 | 1.2003 |
| 148## | BV-N95F/46.7-46.8 | sulf-crb vein/cp | mtuf?/ab-crb rock | fr.m.1.4A; +100 | CP | b-db | 35.443 | 17.853 | 43.211 | 0.5037 | 1.2192 |
| 149 | BV-N95F/46.7-46.8 | sulf-crb vein/cp | mtuf?/ab-crb rock | fr.nm.1.4A; +100 | PY(porous) | db | 35.601 | 17.857 | 43.269 | 0.5016 | 1.2154 |
| 150 | BV-N95F/59.4-59.5 | sulf-crb-tre lens/py | mtuf?/ab-crb-tre rock | fr.nm.1.4A; +200 | PY | IIb | 780.83 | 111.98 | 362.07 | 0.1434 | 0.4637 |
| 163 | BV-S154B/81.4-81.5 | sulf networks/po | mtuf?/ab-crb rock | fr.nm.1.4A | PY | - | 48.936 | 18.956 | 43.721 | 0.3874 | 0.8934 |
| 181 | BV-S154B/81.4-81.5 | sulf networks/po | mtuf?/ab-crb rock | hand magnet | PO(bulk) | Ib | 33.896 | 17.522 | 43.361 | 0.5169 | 1.2792 |
| 171 | BV-S154B/96.2-96.3 | sulf-qtz-crb breccia/po,cp | black schist | d>4.0 | CP(py) | Ib | 28.394 | 16.825 | 42.782 | 0.5925 | 1.5067 |
| 182## | BV-S154B/96.2-96.3 | sulf-qtz-crb breccia/po,cp | black schist | hand magnet | PO(bulk) | b | 27.123 | 16.812 | 42.446 | 0.6198 | 1.5649 |
| 151## | BV-S154B/96.3-96.4 | sulf-crb vein/po,cp,py | black schist/ab-crb rock | fr.m.1.4A; -200 | CP | Ib-b | 26.399 | 16.650 | 42.191 | 0.6307 | 1.5982 |
| 152## | BV-S154B/96.3-96.4 | sulf-crb vein/po,cp,py | black schist/ab-crb rock | fr.em.1.4A | PY,CP | IIb | 26.917 | 16.724 | 42.205 | 0.6213 | 1.5679 |
| 183 | BV-S154B/96.3-96.4 | sulf-crb vein/po,cp,py | black schist/ab-crb rock | hand magnet | PO(bulk) | IIb | 26.328 | 16.726 | 42.083 | 0.6353 | 1.5984 |
| 153## | BV-S154B/102.4-102.5 | diss/cp,po | metadiabase | d>4.2; -200 | CP(acid leach) | Ib-b | 30.031 | 17.257 | 47.190 | 0.5746 | 1.5714 |
| 154a | BV-S154B/102.4-102.5 | diss/cp,po | metadiabase | fr.nm.1.4A; +200 | CP(acid leach) | Ib | 30.166 | 17.261 | 47.397 | 0.5722 | 1.5712 |
| 154b | BV-S154B/102.4-102.5 | diss/cp,po | metadiabase | d>4.0; fr.nm.1.4A | PY(acid leach) | - | 28.012 | 16.913 | 46.381 | 0.6038 | 1.6557 |
| 184 | BV-S154B/102.4-102.5 | diss/cp,po | metadiabase | hand magnet | PO(bulk) | - | 27.416 | 16.828 | 44.983 | 0.6138 | 1.6408 |
| 186-ic | BV-S154B/102.4-102.5 | diss/cp,po | metadiabase | d>4.2; -100 | RUTILE | | 143.74 | 28.171 | 67.476 | 0.1960 | 0.4694 |
| 159a | BV-S154B/124.6-124.7 | sulf-crb vein/po,cp,py | black schist | d<3.3; acid leach | CRB | - | 40.489 | 18.459 | 45.483 | 0.4559 | 1.1234 |
| 159b | BV-S154B/124.6-124.7 | sulf-crb vein/po,cp,py | black schist | d<3.3 | CRB | - | 43.524 | 18.895 | 41.983 | 0.4341 | 0.9646 |
| 172 | BV-S154B/124.6-124.7 | sulf-crb vein/po,cp,py | black schist | fr.nm.1.4A ;-200 | PY | db | 48.699 | 19.725 | 53.721 | 0.4050 | 1.1031 |
| 173 | BV-S154B/124.6-124.7 | sulf-crb vein/po,cp,py | black schist | fr.nm.1.4A; +200 | PY(dull) | db-bl | 46.645 | 19.454 | 52.775 | 0.4171 | 1.1314 |
| 174## | BV-S154B/124.6-124.7 | sulf-crb vein/po,cp,py | black schist | fr.m.1.4A; -100 | CP | b | 40.132 | 18.574 | 49.692 | 0.4628 | 1.2382 |
| 175 | BV-S154B/124.6-124.7 | sulf-crb vein/po,cp,py | black schist | fr.m.1.4A; +100 | CP(py) | b | 39.863 | 18.515 | 49.527 | 0.4645 | 1.2424 |
| 185 | BV-S154B/124.6-124.7 | sulf-crb vein/po,cp,py | black schist | hand magnet | PO(bulk) | IIb | 37.428 | 18.202 | 48.385 | 0.4863 | 1.2927 |
| 178-le | BV-S154B/139.8-139.9 | | black schist | acid leach | LE | - | 31.885 | 17.198 | 54.146 | 0.5394 | 1.6982 |
| 178-wr | BV-S154B/139.8-139.9 | | black schist | total dissolution | WR | - | 33.909 | 17.404 | 56.650 | 0.5133 | 1.6706 |
| 179-le | BV-S154B/143.0-143.1 | | black schist | acid leach | LE | - | 30.276 | 16.908 | 51.162 | 0.5584 | 1.6898 |
| 179-wr | BV-S154B/143.0-143.1 | | black schist | total dissolution | WR | - | 33.120 | 17.146 | 52.651 | 0.5177 | 1.5897 |
| 164 | BV-S154B/149.8-149.9 | sulf-qtz/stripes/py | black schist | fr.m.0.3A | PY(dull) | db | 36.893 | 18.349 | 57.416 | 0.4974 | 1.5563 |
| 208A## | BV-S186B/108.7-108.8 | sulf-crb vein/py,po,cp | mtuf?/ab-crb rock | | GA | | 21.791 | 16.125 | 41.394 | 0.7400 | 1.8996 |
| 208B## | BV-S186B/108.7-108.8 | sulf-crb vein/py,po,cp | mtuf?/ab-crb rock | | GA | | 21.801 | 16.116 | 41.415 | 0.7392 | 1.8997 |

BV = Bidjovagge; HL = Hangaslampi; KU = Kuotko; LAM = Lammasvuoma; MA = Meurastuksenaho; PV = Pahtavaara; PVU = Pahtavuoma; SK = Suurikuusikko; SP(A,B,C) = Saattopora gold ore/ A-, B-, C-ores; SP-Cu = Saattopora Cu-mineralization; SV = Soretiavuoma; diss = dissemination; ab = albite; amph = amphibole; bar = barite; bt = biotite; ch = chlorite; crb = carbonate; qtz = quartz; se = sericite; sulf = sulfide; tlc = talc; tour = tourmaline; tre = tremolite; ASPY = arsenopyrite; CP = chalcopyrite; GA = galena; LE = acid leach of whole rock powder; MAGN = magnetite; PO = pyrrhotite; PY = pyrite; WR = total dissolution of whole rock powder; graph-schist = graphite-rich schist; mtuf = mafic tuffite; metased = metasedimentary; umr = ultramafic rock; d = density; fr.nm/fr.m. = non magnetic/magnetic fraction with a specific current; +200,-100 = size fractions; Pb* = the colour of the anode precipitation (- = colourless, IIb = brownish, Ib = light brown, b = brown, db = dark brown, bl = black).

**Appendix 5.** Descripitions of sulfide and wall rock samples.

## STRATABOUND COPPER DEPOSITS

EIM-91-6-PAHTAVUOMA, Kittilä:
Sulfide and wall rock sample from a phyllite/black schist with ilmenite(±magnetite) dissemination. Chalcopyrite and arsenopyrite occur in fissures.

G202-HORMAKUMPU/R387/50.40, Kittilä:
Galena sample from a brecciated sericitic schist, with pyrite, chalcopyrite, and galena.

G127-ALAKYLÄ, Kittilä:
Galena sample from a schist brecciated by chalcopyrite, pyrite, and galena.

G178-RIIKONKOSKI, Kittilä:
Galena sample from a sericitic schist brecciated by pyrrhotite and galena.

G228-RIIKONKOSKI/R349/72.10-72.20, Kittilä:
Galena sample from a carbonate vein cutting a black schist.

## GOLD DEPOSITS

SORETIAVUOMA, Kittilä

R307/48.45-48.50:
Sulfide sample from a chalcopyrite rich quartz-carbonate vein. Quartz is coarse grained and invariably shows undulose extinction. Quartz mosaic occurs locally as overgrowths at the grain boundaries. Chalcopyrite has been at least partially mobilized into the microfractures. Accessory minerals are: albite, tourmaline, arsenopyrite, galena and locally, violarized Ni-sulfide(?).

R307/48.70-48.75:
Sulfide sample from an albite-carbonate-chlorite rock. Microfractured subhedral pyrites have commonly crystallized on the irregularly oriented chlorite veins and zones.

R307/55.35-55.45:
Wall rock sample from a fine grained carbonate-chlorite-talc rock (ultramafic volcanic rock) with coarser carbonate spots.

KUOTKO, Kittilä

R305/7.95:
Sulfide sample from a slightly cataclastic quartz-sulfide-carbonate vein. Pyrrhotite and chalcopyrite occur around coarse grained arsenopyrite. Three types of quartz are present: undeformed bright grains, overgrowths with undulose extinction, and granoblastic mosaics between the boundaries of the sulfide and carbonate grains. Carbonate is coarse grained and shows undulose extinction.

R443/18.60-19.60:
Sulfide sample from an ankerite-vein rich in gold, pyrite and arsenopyrite. Cross-cutting relations indicate that this vein is the latest in the area (Härkönen, oral com. 1991).

R436/21.35-21.45:
Wall rock sample from a carbonate-sericite-chlorite schist with thin quartz-carbonate veinlets and shear zones containing carbonate. Disseminated opaques are aligned parallel to the direction of schistosity.

R436/42.20-42.30:
Sulfide sample from a carbonate-sulfide breccia in which partially pyritized pyrrhotite brecciates carbonate. The host-rock is extremely fine grained chlorite-sericite-carbonate-albite rock. A carbonate-filled fracture cuts the breccia.

R436/73.40-73.50:
Wall rock sample from a fine grained (biotite)-chlorite-sericite-albite rock with coarse carbonate spots and weakly discernible plagioclase phenocrysts.

R436/76.30-76.40:
Wall rock sample, which is macroscopically analogous with the preceding sample.

R436/76.40-76.50:
Sulfide sample from a quartz-carbonate vein/breccia with coarse microfractured pyrite cubes, idiomorphic arsenopyrite, minor chalcopyrite, and relicts of idiomorphic coarse magnetite grains. Carbonate brecciates quartz, and both minerals show undulose extinction. Macroscopically, galena occurs as a thin seam.

R436/86.30-86.40:
Sulfide sample from a compact pyrrhotite vein. The wall rock is extremely fine grained albite-quartz-sericite schist. Some quartz veinlets older than the sulfide vein cut the rock. Pyrrhotite has locally altered to marcasite.

R436/87.85-87.96:
Sulfide sample from a coarse grained quartz-pyrite vein cutting the fine grained carbonate-albite-quartz-chlorite-sericite rock. The vein quartz shows undulose extinction and quartz overgrowths sometimes occur at grain boundaries. The schist contains disseminated ilmenite.

A1168-Kuotko (R308/22.50-22.80) + composite sample (R308 and R311):
Lamprophyre sample was initially delivered to GSF for U-Pb-dating, but apatite was not sufficiently radiogenic. The lamprophyre consists of subhedral phlogopite laths (flow-structure) in a fine grained groundmass. Idiomorphic pyrite has also been separated from the lamprophyre.

A1262-Kuotko:
Host-rock and sulfide sample from a felsic porphyry. The zircons were heterogeneous and the fraction sizes were too small for U-Pb dating. Lead isotope analysis was done from the acid-leach arsenopyrite-pyrite fraction. In thin section, the relationship between the sulfides (dissemination/vein?) and the host-rock was not discernible. The porphyry consists of sub-euhedral plagioclase laths in a fine grained groundmass with carbonate, sericite, and albite.

SUURIKUUSIKKO AND KIISTALA, Kittilä

R434/65.80:
Sulfide sample from a carbonate vein with arsenopyrite and pyrite.

R434/80.55-80.80:
Sulfide sample from a breccia with arsenopyrite and pyrite.

G347-Kiistala:
Galena sample from the Vuomajärvi galena- and arsenopyrite-rich vein. Visible gold has been recorded from the galena and vein carbonate. The wall rocks are graphite bearing schist and chlorite rich tuffite with intermediate lava intercalations.

PAHTAVAARA, Sodankylä

R508/87.30:
Sulfide sample from a fine grained amphibole-chlorite-carbonate schist with disseminated magnetite. Pyrite occurs mainly in felsic veins (albite, carbonate, quartz) which brecciate the wall rock.

R508/96.40-96.50:
Wall rock sample from a biotite-talc-carbonate schist (initially ultramafic volcanic rock). Subhedral biotite laths can be distinguished from the groundmass. Accessory minerals are cubic opaque (magnetite), zoisite, and zircon in biotite.

R508/111.55-111.70:
Sulfide sample from a coarse grained carbonate-tremolite rock with pyrite. Pyrite contains some carbonate and tremolite inclusions. A carbonate-filled fracture surrounded by abundant magnetite disseminations, cuts the rock.

R508/111.90:
Sulfide sample from a coarse grained amphibole-carbonate-chlorite rock with some disseminated pyrite and magnetite.

R508/117.30:
Sulfide sample from a fine grained magnetite-disseminated biotite-chlorite schist with a coarse grained talc-carbonate lens. Pyrite occurs in the felsic part.

R508/124.00-124.10:
Wall rock sample from a fine grained chlorite-talc-carbonate rock with coarser flow-structured amphibole laths and disseminated magnetite.

R509/110.90:
Sulfide sample from a coarse grained talc-carbonate-barite vein with abudant magnetite and minor pyrite.

4A:
Sulfide sample from a coarse grained amphibole rock with some spherulitic amphiboles and several pyrite grains.

EIM-91-1:
Wall rock sample from a chlorite-talc-amphibole rock, representing a moderately altered metakomatiite with macroscopically observable pillow lava structures.

LAMMASVUOMA, Kittilä

LAM-3/45.00-45.10:
Sulfide sample from a biotite-chlorite-albite-quartz schist comprising a granoblastic grain mass with bands rich in biotite and chlorite. Pyrite occurs partly as dissemination networks that are schistosity-controlled and partly as breccias. Tourmaline is an accessory mineral, and ilmenite and rutile (ilmenite=>rutile?) tend to be restricted to certain bands.

LAM-3/45.80-45.90:
Wall rock sample from a strongly carbonatized and sheared albite-carbonate rock with fine grained sericitic intercalations. Carbonate surrounds albite laths and replaces the transecting shear zones.

SAATTOPORA, Kittilä

A1205 (hand specimen/A-ore):
Sulfide sample from a sulfide-carbonate-quartz vein cutting albitic felsite (albite-carbonate-quartz schist/rock). Chalcopyrite brecciates carbonate and sometimes occurs as a grain mosaic at the margins of the coarse subhedral pyrrhotites. A broken chalcopyrite-filled fracture cuts the vein.

A-ore; R257/61.40-61.45:
Sulfide sample from a sulfide-carbonate vein in which sulfides brecciate carbonate. Chalcopyrite occurs as small separate grains and, like pentlandite, as inclusions in pyrrhotite. Gold occurs in pyrrhotite, in carbonate, and at thucolite grain boundaries. A younger carbonate filled fracture has formed inside the vein.

A-ore; R257/70.60-70.70:
Wall rock sample from a strongly sheared and carbonatized rock in which the albite laths occur in the carbonate groundmass. Additional minerals are apatite and opaques. The rock is cut by thin carbonate veinlets.

A-ore; R257/74.60-74.70:
Sulfide sample from an albite-rich and tourmaline-bearing, sheared fine grained albite-carbonate schist. Pyrrhotite-tourmaline breccias, older quartz veins, and pyrrhotite±chalcopyrite veins cut the schist. Marcasite is an alteration product after pyrrhotite. Accessory minerals are ilmenite and rutile.

A-ore; R257/82.20-82.30:
Sulfide sample from a quartz-sulfide(-albite-tourmaline-scheelite) vein cutting schistose and extremely fine grained albite-quartz-tourmaline rock. In the vein pyrrhotite and chalcopyrite occur between coarse quartz grains with undulose extinction. The gold in the sample is associated with chalcopyrite.

A-ore; EIM-91-2:
A vein carbonate sample.

B-ore; R208/109.10-109.15:
Wall rock sample from a fine to medium grained and schistose albite-carbonate schist, in which the fine grained carbonate surrounds albite laths or is confined to certain layers. The quartz is also related to certain layers. Additional minerals are tourmaline and oxides. A carbonate filled fracture cuts the rock.

B-ore; R208/112.65-112.70:
Wall rock sample from a quartz-albite-carbonate-tourmaline schist. The rock is fine grained but contains coarse grained flattened quartz-albite domains and carbonate spots. It is cut by quartz-albite veinlets, which in turn are cut by fine grained tourmaline veinlets. Accessory minerals are apatite, biotite, and opaques.

B-ore; R208/120.80-120.90:
Wall rock sample from a fine grained quartz-albite-carbonate-tourmaline schist. Fine albite-quartz-tourmaline±biotite±chlorite groundmass surrounds the coarser carbonate grains. Opaques with carbonate and chlorite form poorly preserved relicts after some minerals or rock fragments. Tourmaline is usually present in thin laminae.

B-ore; R208/124.45-124.55:
Sulfide sample from a carbonate-sulfide(-quartz) vein. The vein pyrite and pyrrhotite locally brecciate carbonate. Some sulfides occur poikilitically in quartz-albite-carbonate mass. Pyrite is found as inclusions in pyrrhotite or as separate medium to coarse sub-euhedral grains. The wall rock is banded schist with diffuse irregular rock fragments and abundant tourmaline and lesser biotite, chlorite, and albite. Several gold grains were found in the sulfide separates.

C-ore; EIM-91-3:
Sulfide and wall rock sample from the C-ore. The wall rock consists of albite laths, quartz, and carbonate with variable grain sizes. The coarse grained carbonate-albite portions traverse the wall rock with irregular contacts. Sulfides, mainly arsenopyrite with chalcopyrite and pyrrhotite inclusions, occur as patchy disseminations. Ilmenite is the major oxide mineral. In thin section, one gold grain was found within an arsenopyrite grain.

G443-concentrate:
Main minerals: pyrrhotite, chalcopyrite, pyrite, and rutile.
Accessories: monazite, ilmenite, scheelite, Fe-Co-Ni-sulfarsenides, pentlandite, cobaltite, tellurides, and gold.

Cu-mineralization; EIM-91-4:
Sulfide and wall rock sample from a mineralized, slightly carbonatized, fine to medium grained, albite-quartz schist. Coarser grained irregular quartz-carbonate-albite-chalcopyrite veinlets with some tourmaline occur in the schist, and are cut by coarse grained carbonate veins. Accessory minerals are pyrite, pyrrhotite, marcasite (an alteration product of pyrrhotite), thucolite, rutile, and ilmenite.

Cu-mineralization; EIM-91-5:
Sulfide and wall rock sample from the Cu-mineralization hosted by black schist/phyllite. The major sulfide minerals are pyrite, chalcopyrite, and arsenopyrite.

HANGASLAMPI, Kuusamo

R388/22.75-22.80:
Sulfide sample from pyrite, which occurs as poikilitic inclusions in a magnetite groundmass with some chlorite and biotite flakes.

R388/23.75-23.85:
Wall rock sample from a granoblastic (albite-)quartz rock, which is brecciated by chlorite veinlets.

R388/41.20-41.30:
Sulfide sample from a schistose and banded sericite-quartzite, which is brecciated by some irregular and diffuse quartz veinlets. Pyrite, occasionally with magnetite inclusions, forms a pronounced dissemination associated with bands cutting the graded bedding. Magnetite with ilmenite lamellae is concentrated in certain layers, and in addition ilmenite occurs as separate grains.

R388/57.90-57.95:
Wall rock sample from a schistose granoblastic (albite-)chlorite-quartz rock with carbonate grain-accumulations.

R388/66.85-66.90:
Sulfide sample from a compact magnetite-pyrrhotite rock. Pyrrhotite occurs poikilitically in magnetite and some inclusions of quartz and carbonate occur in both.

R388/71.05-71.10:
Sulfide sample from idiomorphic coarse grained pyrite in a carbonate vein. Sheared fine grained carbonate and quartz grains with undulose extinction occur at the margins of the coarse carbonate grains.

MEURASTUKSENAHO, Kuusamo

R332/179.60:
Sulfide sample from a compact magnetite-pyrrhotite-chalcopyrite rock containing some carbonate and chlorite.

BIDJOVAGGE, Finnmark, northern Norway

N95F/2.10-2.20:
Sulfide sample from a coarse grained carbonate vein/rock with pyrite spots hosted by albite-carbonate schist.

N95F/7.00-7.10:
Sulfide sample from a schistose albite-carbonate rock, which is cut by some carbonate veins and quartz veinlets. Pyrite occurs as flattened grains parallel to the direction of schistosity.

N95F/14.10-14.20:
Sulfide sample from an albite-carbonate rock brecciated or replaced by some irregularly bordered carbonate-sulfide veinlets. In the albite-carbonate rock, the sulfides are aligned parallel to the direction of schistosity. The main sulfide mineral is pyrrhotite. The minor sulfides consist of chalcopyrite, which occurs either in microfractures or at pyrrhotite grain boundaries, and pyrite cubes. Ilmenite is disseminated throughout the rock.

N95F/21.80-21.90:
Wall rock sample from a sulfide deficient albite-carbonate rock.

N95F/45.30-45.40:
Sulfide sample from a carbonate vein containing pyrrhotite, chalcopyrite, and rutile, and which cuts the metadiabase. High Au-contents have been obtained from this drill-core section (Lamberg & Toikkanen 1991).

N95F/46.70-46.80:
Sulfide sample from a chalcopyrite-rich carbonate vein cutting the metadiabase. Mackinawite occurs inside the chalcopyrite. This drill-core section is rich in copper (Lamberg & Toikkanen 1991).

N95F/59.45-59.55:
Sulfide sample from a sulfide-carbonate-tremolite part or vein in albite-carbonate schist. This skarn type also contains pyrite, titanite, and minor tourmaline.

S186B/108.70-108.80:
Galena sample from a carbonate vein. The vein sulfides are pyrrhotite, pyrite, and chalcopyrite. Minor secondary pyrite occurs in carbonate as thin veinlets, diffuse and irregular spots, and idiomorphic grains.

S154B/81.40-81.50:
Sulfide sample from a metadiabase with "network-like" disseminated pyrrhotite.

S154B/96.25-96.30:
Sulfide sample from a black schist in contact with a carbonate vein. In the schist the pyrrhotite occurs as thin veinlets or thicker patches. The cross-cutting fractures are filled with carbonate and/or chalcopyrite.

S154B/96.35-96.40:
Sulfide sample from a carbonate vein in contact with black schist. Pyrrhotite dominates, with minor chalcopyrite and pyrite also occuring in the vein.

S154B/102.45-102.55:
Sulfide sample from a metadiabase with chalcopyrite and pyrrhotite. High Au-contents have been obtained from this drill-core section (Lamberg & Toikkanen 1991). In thin section one chalcopyrite-hosted Au-grain was found. The sample also contains abudant ilmenite and rutile.

S154B/124.65-124.75:
Sulfide sample from a black schist, cut by a sulfide-carbonate vein containing pyrrhotite, chalcopyrite, and pyrite. Some of the pyrite has grown over the carbonates. The vein is cut by a thin carbonate-pyrite veinlet.

S154B/139.80-139.90:
Wall rock sample from a sulfide-poor black schist.

S154B/143.00-143.10:
Wall rock sample from a sulfide-poor black schist. Compared with the preceding sample this contains more graphite.

S154B/149.80-149.90:
Sulfide sample from a sheared black schist, in which pyrite is associated with sharply folded quartz rich layers. The schist contains diffuse chlorite-rich fragments.

N20E/197.50-197.65:
Sulfide sample from a graded albite-carbonate rock. Chalcopyrite occurs as flattened grains parallel to the schistosy direction. High Au-, U-, Pb- and Cu-contents have been obtained from this drill-core section (Lamberg & Toikkanen 1991). In thin section, one pyrrhotite-hosted Au-grain was found.

N20E/203.55-203.60:
Sulfide sample from a graded and folded albite-carbonate rock. The sulfides, mainly chalcopyrite, are mostly associated with the coarse grained quartz layers containing plagioclase laths. High Au-contents have been reported from this drill-core section (Lamberg & Toikkanen 1991).

N20E/213.25-213.35:
Sulfide sample from sub- to euhedral pyrite in a magnetite-disseminated metadiabase.

N15P/20.20-20.30:
Wall rock sample from a slightly altered metadiabase.

**Appendix 6.** Lead isotope data from the Porkonen-Pahtavaara iron fromation, Kittilä (A590, A591), and from the Toto-Oja volcanics, Kittilä (A874).

| ANAL. NO. | DRILL CORE DEPTH (m) | ROCK TYPE | LEAD ISOTOPE RATIOS 206/204 | 207/204 | 208/204 |
|---|---|---|---|---|---|
| PORKONEN-PAHTAVAARA, Kittilä[1)] | | | | | |
| A590* (Fig. 1) | | | | | |
| A | R1/22.80 | greenstone | 29.423 | 16.944 | 37.868 |
| B | R1/22.80 | banded greenstone | 59.431 | 19.600 | 46.193 |
| C | R1/102.50 | sulphide rich schist | 17.036 | 15.446 | 35.032 |
| D | R1/140.80 | sulphide rich schist | 31.311 | 16.870 | 39.159 |
| E | R1/150.00 | jasper, siderite | 37.790 | 17.514 | 38.326 |
| F | R1/169.30 | brecciated greenstone | 25.001 | 16.357 | 37.070 |
| G | R1/170.30 | magnetite breccia | 20.554 | 15.825 | 35.868 |
| H | R1 | siderite rich schist | 58.032 | 19.421 | 52.812 |
| I | R1 | banded tuffite | 68.583 | 21.115 | 58.439 |
| K | R1 | greenstone | 53.078 | 19.303 | 67.245 |
| A591** (Fig. 2) | | | | | |
| A | R2/8.50 | greenstone | 46.035 | 18.540 | 73.268 |
| B | R2/15.50 | tuffite | 59.621 | 19.649 | 46.254 |
| C | R2/17.60 | jaspilite(+siderite) | 20.392 | 15.768 | 35.627 |
| D | R2/20.50 | sulphide rich schist | 42.845 | 17.611 | 38.039 |
| E | R2/149.70 | greenstone, jaspilite | 61.056 | 19.646 | 49.537 |
| F | R2/207.80 | sulphide rich schist | 19.918 | 15.844 | 35.344 |
| G | R2/212.60 | sulphide rich schist | 21.532 | 16.024 | 35.738 |
| H | R2/212.60 | jaspilite | 21.412 | 15.847 | 35.327 |
| I | R2/297.00 | sulphide rich schist (CP) | 28.587 | 16.593 | 36.821 |
| TOTO-OJA, Kittilä[2)] | | | | | |
| A874*** (Fig. 3) | | | | | |
| A | R3/9.80 | felsic volcanic rock (biotite) | 57.357 | 19.432 | 69.219 |
| B | R3/16.30 | tuffitic band/felsic volcanic rock | 39.014 | 17.721 | 44.769 |
| C | R3/21.50 | porphyritic felsic volcanic rock | 74.047 | 21.135 | 80.141 |
| D | R3/28.55 | tuffite | 36.873 | 17.543 | 41.044 |
| E | R3/58.90 | porphyritic felsic volcanic rock | 62.333 | 19.907 | 80.417 |
| F | R3/65.90 | porphyritic felsic volcanic rock | 93.990 | 23.014 | 107.78 |
| G | R3/79.80 | felsic volcanic rock | 90.173 | 22.913 | 109.36 |
| H | R3/83.20 | felsic volcanic rock | 51.605 | 19.566 | 135.45 |

[1)] Source of samples: Pentti Rastas, GSF. Analyses: Matti Sakko, GSF.
*) R1: x=7517.94, y=446.46; **) R2: x=7517.95, y=446.40;
[2)] Source of samples: Rautaruukki Oy. Analyses: Matti Sakko, GSF.
***) R3: x=7507.28, y=524.93

**Appendix 6.** Continued.

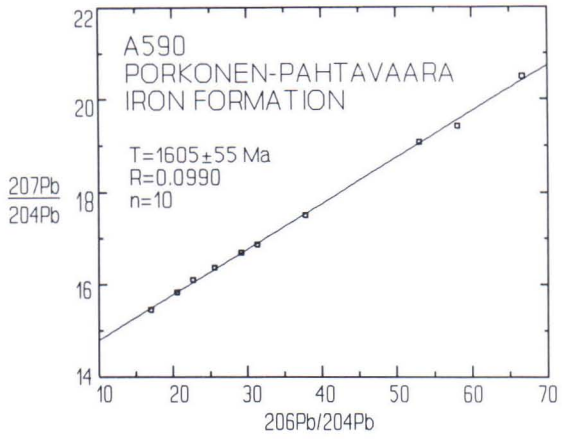


Fig. 1. $^{206}Pb/^{204}Pb$ vs. $^{207}Pb/^{204}Pb$ diagram, A590 Porkonen-Pahtavaara, drill core R1.

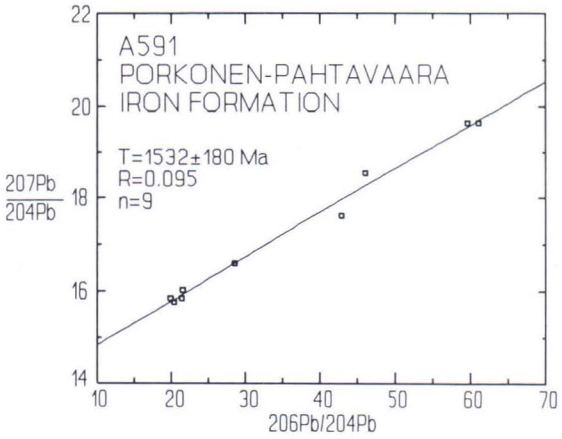


Fig. 2. $^{206}Pb/^{204}Pb$ vs. $^{207}Pb/^{204}Pb$ diagram, A591 Porkonen-Pahtavaara, drill core R2.

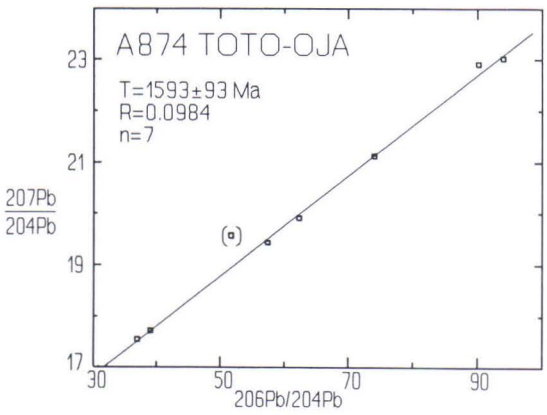


Fig. 3. $^{206}Pb/^{204}Pb$ vs. $^{207}Pb/^{204}Pb$ diagram, A874 Toto-Oja, drill core R3.

Tätä julkaisua myy

GEOLOGIAN
TUTKIMUSKESKUS (GTK)
Julkaisumyynti
02150 Espoo

☎ (90) 46 931

Teleksi: 123185 geolo fi
Telekopio: (90) 462 205

GTK, Väli-Suomen
aluetoimisto
Kirjasto
PL 1237
70211 Kuopio

☎ (971) 205 111

Telekopio: (971) 205 215

GTK, Pohjois-Suomen
aluetoimisto
Kirjasto
PL 77
96101 Rovaniemi

☎ (960) 3297 111

Teleksi: 37295 geolo fi
Telekopio: (960) 3297 289

Denna publikation säljes av

GEOLOGISKA
FORSKNINGSCENTRALEN (GFC)
Publikationsförsäljning
02150 Esbo

☎ (90) 46 931

Telex: 123185 geolo fi
Telefax: (90) 462 205

GFC, Distriktsbyrån för
Mellersta Finland
Biblioteket
PB 1237
70211 Kuopio

☎ (971) 205 111

Telefax: (971) 205 215

GFC, Distriktsbyrån för
Norra Finland
Biblioteket
PB 77
96101 Rovaniemi

☎ (960) 3297 111

Telex: 37295 geolo fi
Telefax: (960) 3297 289

This publication can be
obtained from
GEOLOGICAL SURVEY
OF FINLAND (GSF)
Publication sales
FIN-02150 Espoo, Finland

☎ +358 0 46 931

Telex: 123185 geolo fi
Telefax: +358 0 462 205

GSF, Regional office for
Mid-Finland
Library
P.O. Box 1237
FIN-70211 Kuopio, Finland

☎ +358 71 205 111

Telefax: +358 71 205 215

GSF, Regional office for
Northern Finland
Library
P.O. Box 77
FIN-96101 Rovaniemi, Finland

☎ +358 60 3297 111

Telex: 37295 geolo fi
Telefax: +358 60 3297 289

ISBN 951-690-593-5
ISSN 0367-522X